AIT

Asian Institute of Technology
Thailand

thesis

SUPPORT VECTOR MACHINE BASED-IMAGE CLASSIFICATION FOR AN INDIVIDUAL TREE CROWN DETECTION AND DELINEATION

Poonsak Miphokasap

T551001

SUPPORT VECTOR MACHINE BASED-IMAGE CLASSIFICATION FOR AN INDIVIDUAL TREE CROWN DETECTION AND DELINEATION

By

Poonsak Miphokasap

A thesis submitted in partial fulfillment of the requirements for the degree of Master of Science

Examination Committee: Prof. Seishiro Kibe (Chairperson)
Dr. Vivarad Phonekeo
Dr. Wataru Takeuchi

Nationality: Thai
Previous Degree: Bachelor of Art in Geography
Kasetsart University
Bangkok, Thailand

Scholarship Donor: Royal Thai Government

Asian Institute of Technology
School of Engineering and Technology
Thailand
May 2008

ACKNOWLEDGEMENTS

The accomplishment of this thesis would have not been feasible without the support and cooperation of many individuals and institutions. Initially, I wish to convey my deeply gratitude and sincere appreciation to Prof. Seishiro Kibe who facilitate and offer an opportunity to decide the thesis topic by myself. During the entire course of my study, he was very understanding and ready to provide constructive suggestions to my research.

I am very grateful to Dr. Dr. Vivarad Phonekeo and Dr. Wataru Takeuchi for accepting to supervise my research and provide me with the meaningful advices that led my thesis to accomplish.

I highly appreciate the generous financial support extended to me from the Royal Thai Government and my organization, BIOTEC as well as BRT.

I wish to thank khun Siriporn, khun Sunthorn, Bamae, Bala staffs who support me for data collection in the study area as well as younger monkey. In addition, many thanks go to khun Apichart, khun Manop, khun Yottanut and other friends for their kind supports.

Especially, I would like to express my hearfelt appreciation to khun wasinee for her spiritual, moral, assistance and material support. Thankful go to myself for my concentration and endeavor.

Last but not least, I wish express my strong and sincere appreciation to my family, my mother and my farther who give me a life and future. Without them, I could not stand at here.

ABSTRACT

Tropical rain forests (TRF) now cover only 6% of the Earth's terrestrial surface yet they maintain a large proportion of the world's biotic diversity. In fact, our understanding, monitoring, conservation and management of TRF are greatly hindered by a lack of spatially and temporally extensive information of tree composition, species richness and forest structure mainly due to prohibitive costs and inaccessibility. The emergence of the sophisticated technology, Remote Sensing makes it feasible to achieve the reliable and updating information either in the landscape or individual scales. Individual tree crown classification is one of the challenging tasks especially in the TRF. In this research, not only concentrate on the spectral reflectance derived from RS image, but the texture features obtained by running Gray Level Co-occurrence Matrix (GLCM) are deemed. Support Vector Machine Classifier based on the concept of machine learning was evaluated for tree crown detection and delineation into tree genus and species. At this point, the high spatial resolution image, QuickBird, was utilized. Subsequently, the kernel functions, parameter configurations as well as texture features that returning the best performance were evaluated. Also, the minimum spatial resolution of image to serve the research targets was examined. As the results of thesis experiments, non-tree crown were effectively eliminated from the image to avoid misclassification and reduce some noises. By taking the advantages of Laplaciane filtering, edge boundary of each tree crown can be possible detected. Subsequently lower edge threshold filtering play the significant role to segment the combined crown into an individual shape. However, it's accepted that the large continuous crowns were impossible to disconnect without the changes of crown shapes.

SVM source code, namely SVM^{light} that is available on the Internet, is the powerful learning machine. When applying SVM model to the live dataset, linear kernel provides the best performance when considering the precision rate and error assessment. Linear kernel with the penalty parameter (C=100) give the accuracy rate at 60.63 %. The number of support vectors and their status determined by the SVM learning algorithm influence to the precision and error rate of models when applying to the unseen data. After included the texture feature, the overall performance of SVM algorithm were lightly adjusted. The combination of four spectral bands and argument second moment texture returns the best probability score with accuracy 70.67% and kappa coefficient 0.44. Variance, second moment and correlation texture were ranked the best in the linear kernel. While homogeneity, correlation and contrast give the sound performance for polynomial kernel. On the other hand, mean, contrast and variance were interested. However, the integration of spectral and groups of the best texture cannot improve the classification accuracy.

TABLE OF CONTENTS

LIST OF TABLES

LIST OF FIGURE

LIST OF FIGURE (contd.)

LIST OF TERMS AND ABBREVIATIONS

SVMs	Support Vector Machine
GPS	Global Positioning System
GLCM	Grey Level Co-occurrence Matrix
QB	QuickBird imagery
DBH	Diameter at Breast Height
TRF	Tropical Rain forest
DN	Digital Value
RED	Red channel of wavelength
NIR	Near-infrared of wavelength
VI	Vegetation Index
NDVI	Normalized Difference Vegetation Index
nm	nanometer
ROI	Region of Interest
GCPs	Ground Control Point
PCA	Principle Component Analysis
MEA	Mean texture
VAR	Variance texture
HOM	Homogeneity texture
CON	Contrast texture
DIS	Dissimilarity texture
ENT	Entropy texture
ASM	Angular Second moment texture
COR	Correlation texture

NOMENCLATURE FOR SVMs

The lowercase bold letters to denote vectors and uppercase italic letters to denote matrices are used. The following list shows the symbols utilized for Support Vector Machine.

ε_i:	slack variable associated with x_i
C:	Margin Parameter
F:	Feature Space
d:	Degree of a polynomial kernel
γ:	Gamma parameter for a radial basis function kernel
M:	Number of training data
m;	Number of input variables
r:	bias term in the kernel function for the polynomial and sigmoid kernels
$K(x_i, x_j)$:	Kernel function
Φ	Mapping Function
w:	weight vector
b:	bias term of the i^{th} hyper-plane
α	Lagrange multiplier for x_i
$\|x\|$	Euclidean norm of Vector x
Sgn	sign function
r	Bias parameter in polynomial and sigmoid kernel

CHAPTER I

INTRODUCTION

1.1 Background

The degradation of forest is the critical issue in region and global. Tropical rain forests (TRF) now cover only 6% of the Earth's terrestrial surface yet they maintain a large proportion of the world's biotic diversity (Thomas et al. 2004). TRF biodiversity is imperiled by wide-spread deforestation, logging and landscape-scale. At individual crown to landscape scales, tropical trees have the dominant role in maintaining the rich biota because they define the horizontal and vertical substrate, moisture and climate. In fact, our understanding, monitoring, conservation and management of TRF are greatly hindered by a lack of spatially and temporally extensive information of tree composition, species richness and structure. Mainly due to prohibitive costs and inaccessibility, most available data comes from relatively small field plots (Clark et al. 2005). In order to evaluate and monitor the condition, properties and trend of changes, the reliable and updated tree attributes must be periodically acquired usually consisting of forest type, estimation of forest stand parameters (stem biomass, density of trees, basal density and mean height), canopy properties (average canopy diameter, canopy coverage area, canopy closure density) and other relevant tree attributes. In addition, the diversity and distribution of tree species is the meaningful information for the diversity assessment. In the last a few decades, such information is usually obtained through field surveying investigation, which is labor intensive, costly, low frequency and low accuracy (Wu and Zhang 2004).

In the tropical rain forest, the capabilities of identifying and mapping are the limited conjunction with the slope complex landscape type reducing the accessibility of the area. Instead mapping tree species by intensive field sampling, another advance technique should be concerned. Remote Sensing, which concerns the reflectance value of the objects varying in the wavelength of the spectrum is adopted as the high potential technique to derive the land surface information. In parallel with a requirement of adaptation are ongoing advancements in remote sensing technology and associated interpretation tools that provide new opportunities to meet the information demands of forest and resource management. With growing requirements of information, remotely sensed data become increasingly valuable sources of information for assisting forest management decisions. In remote sensing task, there are several processes to achieve the meaningful information; radiometric correction, geometric correction, image enhancement, image filtering, image transformation and the most important step namely image classification. It's the process of converting remotely sensed data to information products which concern the difference in the interaction of electromagnetic radiation in different wavelength and various objects. Because satellite image is recorded in the digital formats, therefore, digital image processing is essential for data analysis. Hence, digital number (DN) or spectral data plays the significant role for clustering similar pixels into a unique datasets based on the statistical characteristics of DN value.

Forest management regimes are also becoming more flexible due to the new knowledge, and can be possible to integrate with the advance technologies in forest science. Various applications can be widely done. For instance, tree species identification (Meyer et al.1996; Key et al.2001; Gougeon 1995a), forest type classification (Bliss et al. 1980), tree counting (Lowel 1998, Moe 1998), estimation of tree spatial distribution (Uuttera et al.

1998) and canopy structure determination for damage assessment (Dralle and Rudemo 1996; Kasischke et al. 1997). In the remote sensing domain, spatial, spectral, radiometric and temporal resolutions are the attributes often used in defining image classification approach (Hall 2003). So, to segment genus or species of tree, the suitable spatial resolution for image classification approach must be determined. In addition, the environment of information needed to extract play the main role to define the image classification. In order to identify tree species, the high spatial resolution image that comes with the fine spatial resolution smaller than the interest objects must be available (Woodcock and Strahler 1987). Concomitantly, the development of high potential algorithms for image processing must be constructed.

1.2 Statement of Problems

In any remote sensing application, the choices of spatial resolution of the sensing device are the fundamental factors requiring consideration of the environment being studied and the types of information requirements (Woodcock and Strahler 1987). High spatial resolution remotely sensed data offers the potential to improve the accuracy of forest inventory attributes. The availability of high spatial resolution with the pixel size less than one meter enlarges the possibilities to obtain more details of forest inventory information. The advantage is that individual trees are often visible, especially when the forest is mature and not too dense. However, analysis of high resolution imagery poses a number of challenges that require specific image interpretation procedures. How to extract information from the high spatial resolution images and how to implement the appropriate algorithm for forest inventory analysis are the key issues in the studies of tree species identification.

Broadly, image classification algorithms vary both in the concepts and methods depending on the objectives, forest types, tree species, location, temporal and spatial resolution of input image (Fournier and Maily 2003). In the forestry studies, identification of vegetation focused on the examination of the chlorophyll absorption feature is even more complex. Unfortunately, the spectral signatures are similar in each tree species, time period and environmental conditions and vary over a wide range of spatial frequencies from m to km (Gemmel 1998). Likewise surface reflectance differs from another due to the stage of growth and the light conditions when the images are taken (Franz and Gebhardt 1991). Moreover, the influence of crown structure on reflectance generally occurs at different scales within the crown, ranging from individual leaves and stems, to internal crown structure and the interaction of light between the neighbouring crowns. In dense forest, neighbouring trees will shade and obscure the edges of their co-neighbours, resulting in characteristically darker image values at tree boundaries (Li and Strahler 1992). The combined effects of illumination angle, view angle, tree geometry and bidirectional reflectance cause large variation in pixel intensity at different positions within the crown resulting in a non-uniform crown reflectance profile (Leckie et al. 1992). In particular, simple per-pixel spectral classifiers commonly applied to low spatial resolution data are not suitable due to the spectrally heterogeneous nature of the data (Townshend and Justice 1981; Woodcock and Strahler 1987; Dikshit 1996). Therefore, only reflectance value (DN) cannot be used to discriminate various vegetation types or tree species in the nature condition. In fact, it is unfeasible to derive the exactly surface reflectance because of the atmospheric errors such as the aerosol density, pressure, temperature etc. (Lin 2001). Misclassification results are always found in the methods that group the DN value regardless the spatial pattern or texture feature. Texture describes the spatial relationship

among neighboring pixels within a pre-defined window area (Chan and Laporte 2003). For our eye-brain vision, the spatial properties of context, texture data are almost certainly more significant in the discrimination of objects than the spectral property of color (Warner et al. 1998). Fortunately, the accuracy of land cover or vegetation type classification may be increased through the combination of spectral and texture data (Berberoglu et al., 2000; De Jong et al.2001). Texture analysis offers interesting possibilities to characterize the structural heterogeneity of classes. Extraction of texture features from the satellite image provides a complementary source of data for those applications in which the spectral information is not sufficient for identification or classification of spectrally heterogeneous landscape units.

Indeed, not only the texture feature, but also the classification approach must be concerned to achieve the best performances. The conventional classifiers such as K-Means, Maximum Likelihood or Minimum Distance return the poor performance when working directly to the multi-spectral image because of the high dimensionality of the image data. Therefore, more sophisticated machine learning classifiers should be considered such as Decision Tree, Neural Network or Support Vector Machine (SVM) etc. Especially, SVM method can avoid such problem (Cristianini and Taylor 2000). SVM technique is the hot topic in the current research, being used in a variety of research to solve a multitude of different learning and classification problems (S. Chapman 2004) such as land cover classification, forest fire detection (Lafarge and Descombes 2004) leaf area index estimation (Durbha and King 2007) handwriting recognition (Bahlmann and Haasdonk, 2002), speech recognition (Ma and Randolph, 2001) protein sequence transitions (Zien and Ratsch 2000) and so on. Moreover, the applications of SVM in remote sensing field of study are rather scarce compared to the other methods particularly in the tree attribute extraction (Huang and Davis 2000). Hence, the investigations of the effectiveness and limitations of SVM for detecting the tree crown boundaries and delineating them into species by concerning the integration of spectral and spatial data are the challenging tasks.

1.3 Research Problems

(1) Which textures can improve the accuracy of tree crown classification by applying SVM algorithm?

(2) How does the boundary of individual tree crowns in the tropical rain forest can be segmented and delineated into tree genus and species?

(3) What is the minimum spatial resolution for tree genus and species identification in the dense forest?

1.4 Research Objectives

The main objectives of this thesis are:

(1) To apply SVMs classifier for individual tree crown detection and delineation into genus and species from the high spatial resolution image.

(2) To evaluate the SVMs kernel functions that returning the best performance when classifying satellite image to the tree genus and species in the intense tree crowns.

(3) To explore the texture features possible to improve the classification capacities of SVMs.

(4) To decide the minimum spatial resolution of satellite image for an individual tree crown detection and delineation in the tropical rain forest.

1.5 Scope and Limitation

The optimum goals of this algorithm are to segment the spatial extent of tree crowns in the tropical rain forest by utilizing the combination of spectral and spatial data, and classify them to the tree genus and species. QuickBird imagery is the main source of spectral data. In contrast, texture features are directly extracted from the panchromatic image by GLCM algorithm with the constant window size 3 x 3. SVM technique is applied to be the main classifier. Free source code of SVM in C code is already available turns into the main algorithm in this research. To meet the objectives, source code must be modified to match the image processing requirements. Image file must be transformed to the text file. Tree crown delineations are done by SVM classifier with the different kernel configurations and functions. Spatially, Hala-Bala, the southernmost of wildlife sanctuary in Thailand is defined as the study site with the total areas of 0.5 sq.km. Only the most dominant tree genus in our study area is investigated namely "*shorea*", the member of *Dipterocarpaceae* family. The conceptual of research can be summarized following.

For the first scenario, an analysis is focused on the application of SVM for tree genus classification exploiting only the spectral data (Blue Green Red and Near-Infrared). Classifications are performed with the three types of kernel function and the different parameters (C, γ, d). Subsequently, the comparisons of three kernel performances are conducted. The goals of this scenario are to find the appropriate kernels and the best value of parameters for tree crown delineation. In the second scenario, spectral data and eight texture features computed by GLCM are incorporated one by one into the SVM algorithm to explore the possibility to improve the genus classification. The best parameter values from the first experiment are determined for four types of kernel function. Afterward, texture feature which take the first, second and third ranking of accuracy performance are integrated with the four dimensions of spectral data. So, seven bands of image become the input data for the further analysis. The target of this scenario is to find the best texture that can improve the potential of SVM.

In the last scenario, the minimum of spatial resolution that possibly returns the sound performances for genus classification is investigated. To do so, up-scaling and down-scaling methods are applied. The original of spatial resolution is degraded from 0.6 m to 1.2 m and 1.8 m respectively. Similarly in each resolution level, three of the optimal textures from the second experiment and four spectral bands are integrated and then SVM classification is performed. In this case, only the best parameter configuration for each kernel type from the second steps is applied. The minimum of spatial resolution suitable for tree crown analysis is obtained concerning to the accuracy of image classification. At the end, applicability and limitations of SVM algorithm for tree crown detection and delineation in the tropical rain forest are discussed.

1.6 Expected outputs

(1) Modified SVM algorithm for image classification.
(2) Texture features that can improve the capacities of SVM classifier in each of kernel function.
(3) The prototype of tree genus classification in the tropical rain forest which is possible to be adapted to another genus or other sites.
(4) Minimum of spatial resolution of satellite image for tree crown delineation
(5) Map of *shorea* genus and species members in the study area

1.7 Study Area

Under the control of Department of National Park, Wildlife and Plant Conservation, the Hala-Bala wildlife sanctuary is selected to examine the tree crown classification algorithm based on Support Vector Machine. This forest is legally divided into two separated forests, Hala and Bala, which are respectively situated in the Yala and Narathiwat province at the southernmost part of Thailand (latitude 5° 37′– 6° 14′ North and longitude 101° 8′ – 101° 52′ East) shown in figure 1.1. Combining both parts and the northern forest area of Malaysia namely Balum forest, this region is considered as the third ranking of the tropical rain forest of the world with the total area about 300 sq. km. (BIOTEC 2006). But this research is focused only on the east side, Bala forest.

Average annual rainfall in this area is about 2,098 mm and average temperature is approximately 28 °C. Most areas are the steep mountain with the elevation ranging from 100 to 945 m. Furthermore, this area is the upstream of three main rivers. All biome are covered with the diversity of dominant flora and fauna species ranging from the ground to the top within the specific ecological system.

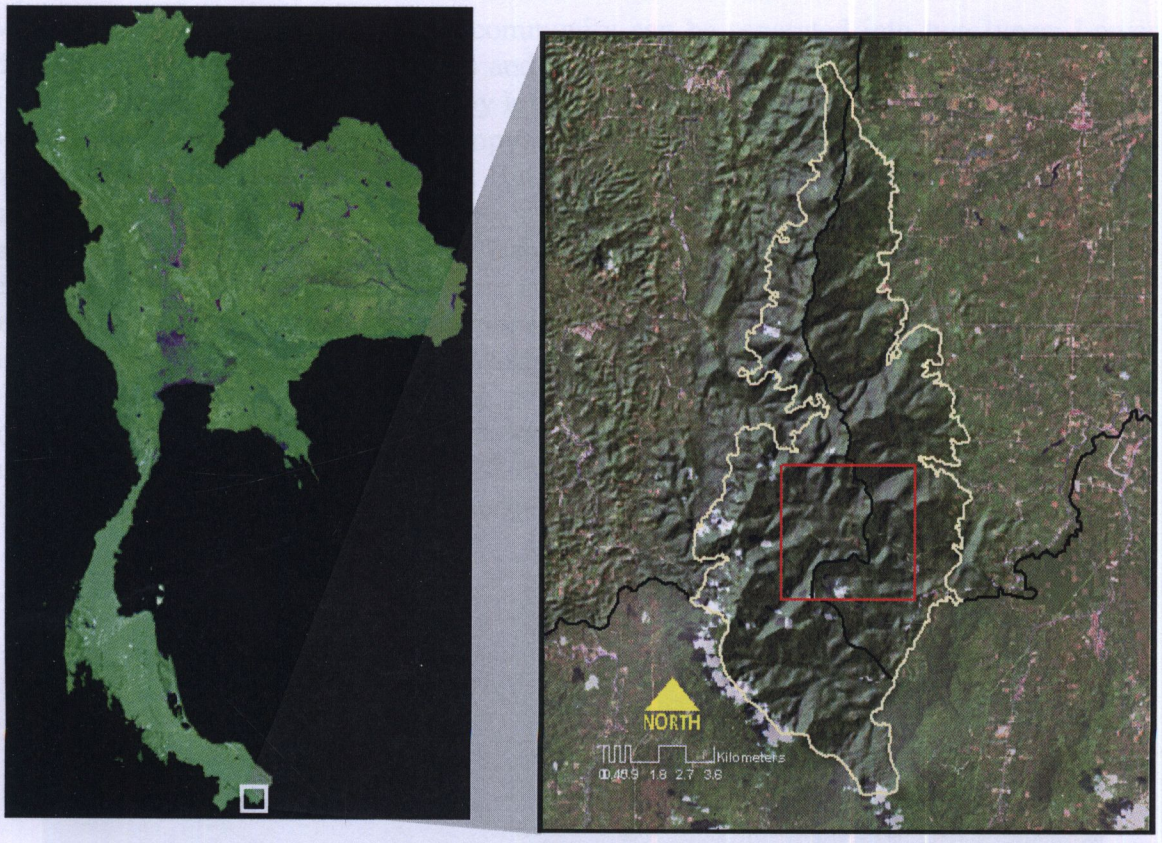

Figure 1.1 Map of the study area: Bala Forest, Narathiwat Province

As being tropical rainforest, this sanctuary is called as Indo-Malaysian Rainforest as it has many rare tree species differenting from the other ecosystems that are important to eco-biodiversity of Thailand. More than 600 tree species already were found in the Bala forest and plant database was implemented (BIOTEC 2006).

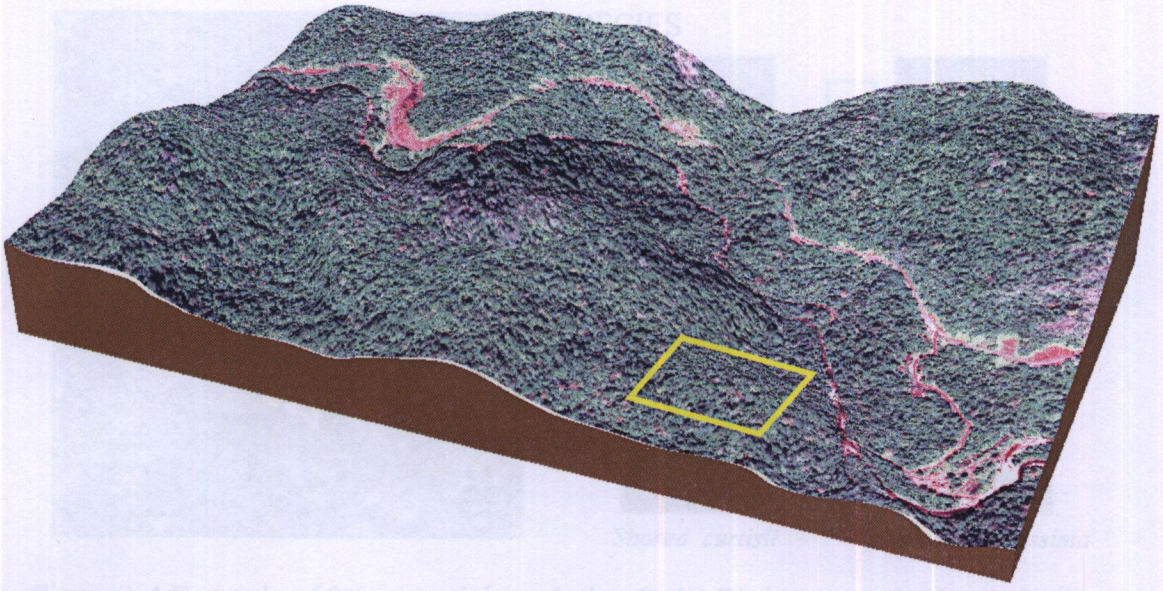

Figure 1.2 Terrain surface of the study plot (Yellow frame) for machine training

When concerning the elevation, tree community can be separated into two types: Lower Mountain Rain Forest (1200-1400 m) and Tropical Rain Forest (40-1200 m) (Niyomtam 2000). At the upper canopy and canopy level, *Dipterocarpaceae* is the most dominant tree family, and covers 50 % of entire canopy. In Thailand, 8 genera and 62 species belonging to the *Dipterocarpaceae* can be found. But, 7 genera and 43 species were already explored in this area (Poopath 2007). Therefore, it can be concluded that this area has the most various species of *Dipterocarpaceae*. Furthermore, 16 of 43 species are classified as a new record of Thailand. In this study, *Shorea* is promoted when considering the most dispersal genus. According to the research of Poopath, 14 species of *shorea* can be explored in the Hala-Bala forest. All of them can be classified into 2 groups. In the low land (<600 msl), *Shorea leprosura*, *Shorea assamica, Shorea parvifolia* and *Shorea faguetiana* are dominant. In contrast, *Parashorea stelata, Shorea gratissima and Shorea curtiii* are outstanding in the high land (600-1000 msl). Remarkably, *Shorea* genus usually can be found in the ridge of a mountain and steep slope area.

Figure 1.3 *Shorea* species (black circle), the dominant stand tree in the study area

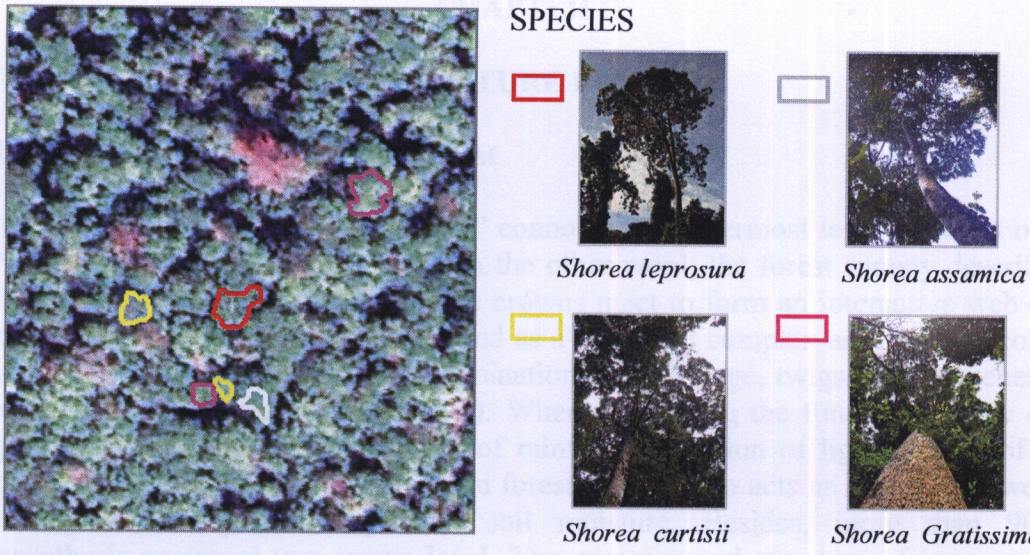

Figure 1.4 Example of 0.6 m spatial resolution QuickBird imagery in the study site overlaid with the individual tree crown vectors

For the diversity of fauna, four rare species can be found. According to the report of the Royal Department of Forestry, 217 species of bird, 114 species of mammal, 30 species of reptile and 23 species of amphibian are explored. All of information above can guarantee that this biome is one of the most abundant zones of the world. Figure 1.5 depicts the example of tree crown that is covered by the continuous layer. Due to the limitation of time and cost, only 0.5 sq. km. (~ 312 rai) was defined as the study site for making the training data and 0.09 sq. km. (~55.30 rai) for validating model to unseen data.

Figure 1.5 Study site covered by tree crown layers

CHAPTER II

LITERATURE REVIEW

2.1 Tree crown in the tropical rain forest

The term "forest canopy" or "tree crown" connotes the uppermost level of forest or outer layer of trees leaves (Richards 1954). On the other word, the forest canopy describes the area above the forest floor where the tree crowns meet to form an interactive web of life. Moreover, forest canopy is now considered as a structural complex and critical ecosystem of the forest, and is defined as "the combination of all foliage, twigs, fine branches, their attending flora and fauna" (Parker 1995). When concerning the functions, many critical canopy functions including interception of rainfall, absorption of light, uptake of gases, and provision of wildlife habitat. Also the forest canopy also acts as a buffer between the soil and the atmosphere to prevent soil moisture. Besides, more than 90% of photosynthesis occurs at tree crown level. The presence and structure of canopy exert a major influence on the temperature, vapor concentration, and radiation regime in the plant environment. Hence, canopy structure can therefore be important in determining the physical environment of other organisms within the plant community. The recent development of canopy access systems has lead to many new discoveries about the complexity and importance of canopies.

Tropical forest is found near the equator (within 23.5° latitude) where the temperature varies little from approximately 23°C. Tropical rain forest is used here to refer to those ecosystems where trees form a continuous canopy over the soil surface (Golley 1983). The canopy of a rainforest is typically 10m in thick, 10-20 m in width, and intercepts around 95% of sunlight. Rain forest canopy usually is categorized into three levels depicted in figure 1. This includes a high level that averages 50 – 60 m above ground, a middle level from 20 to 40 m and lower level from 5 to 15 m. For more details, lower level is composed of small seedlings, ferns, bamboo and the litter-strewn ground level in deep shade and fairly open. Middle canopy is the most continuous, with its broad leaves blocking much of the light and creating a darkened forest floor. In contrast, the upper level is not continuous but features tall trees whose high crowns rise above the middle canopy. (Christopherson 1994).

Figure 2.1 Forest composition (Courtesy of Encyclopedia Britannice, Inc.)

With respect to the information needed for forest management, the complete and accurate descriptions of a canopy would require the specification of the position, size and orientation of each element of surface in the canopy. Also canopy properties are generally described statistically as appropriate space or time averages. In addition, canopy varies on spatial scales ranging from millimeters to kilometers, and on time scales ranging from milliseconds to decades (Campbell and Norman 1989). Structural characteristics of forest canopies help us better understand the co-evolution among its inhabitants. Forest canopy structure is defined differently according to the objectives and spatio-temporal scales adopted. In order to address the data requirements and management objectives in forest, the vertical and horizontal structures are described, in inventories, by variables meaningful to the management unit. For example, horizontal structure is described with continuous or categorical variables such as species composition, spatial distribution of trees, stands, crown cover, height class, etc. On the other hand, the vertical structure is often referred to as the social hierarchy of the overstorey composed of, starting from the top of the canopy, dominance, inter-mediate and suppressed trees (Fournier et al. 2003).

2.2 Remote Sensing Technology

2.2.1 Definition and Concept

So, what exactly is remote sensing? For the purpose of this research, we will use the following "Remote Sensing is defined as the science and art of acquiring information by which the characteristics of objects of interest can be identified, measured or analyzed without direct contact (Lillesand and Kiefer 2000). Electromagnetic radiation which is reflected or emitted from an object is the usual sources of remote sensing data. In other word, remote sensing is the measurement of electromagnetic radiation that is emitted or reflected from the earth surface. The reflected electromagnetic waves may be emitted by sun (visible and infrared remote sensing) or by artificial sources (radar). A device to detect the electromagnetic radiation is called a remote sensor. A vehicle to carry the sensor is called a platform. Aircrafts or satellites are used as platforms. The object characteristics can be determined using reflectance or emitted electromagnetic radiation. This concept is illustrated in figure 2.

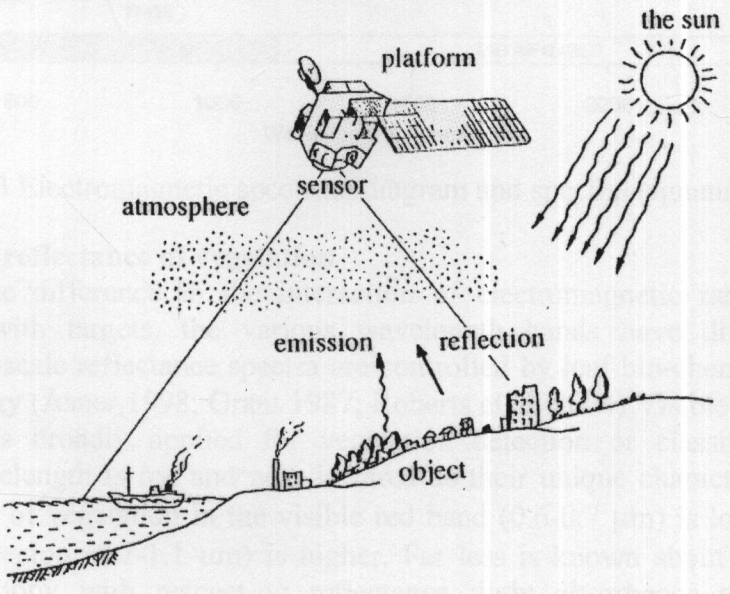

Figure 2.2 Data Collection by Remote Sensing (Lillesand and Kiefer, 2000)

2.2.2 Spectral reflectance

Electromagnetic radiation coming from an object is being measured and translated into information about the object or into processes related to the object. We restrict ourselves to the use of electromagnetic radiation as a characteristic of numerous physical processes. All materials with a temperature above have the power to emit electromagnetic energy. Objects on or near the earth's surface are able to reflect or scatter incident electromagnetic radiation emitted by a source, which may be artificial, e.g., flash light, laser or microwave radiation, or natural, such as the sun. Wavelength regions of electromagnetic radiation have different names ranging from γray, X-ray, ultraviolet (UV), visible light, infrared (IR) to radio wave. The shorter the wavelength is, the more the electro-magnetic radiation is characterized as particle motion with more linearity and directivity. In the visible, near-infrared (NIR) and middle-infrared (MIR) part of the electromagnetic spectrum, we are measuring solar radiation reflected by objects at the earth's surface. In the thermal-infrared (TIR) part, particularly in the atmospheric window at about 10 um, we are measuring emitted radiation by objects at earth's surface, this radiation is originating from the sun. In the microwave part of the spectrum, both reflection of solar light and emission occur at very low energy rates. As a result, radiation mostly is transmitted to the earth's surface by an antenna on board the remote sensing system and, subsequently we measure the amount of radiation that is reflected (backscattered) towards the same antenna. Figure 2.3 displays the electromagnetic spectrum and spectral signature of some surface objects.

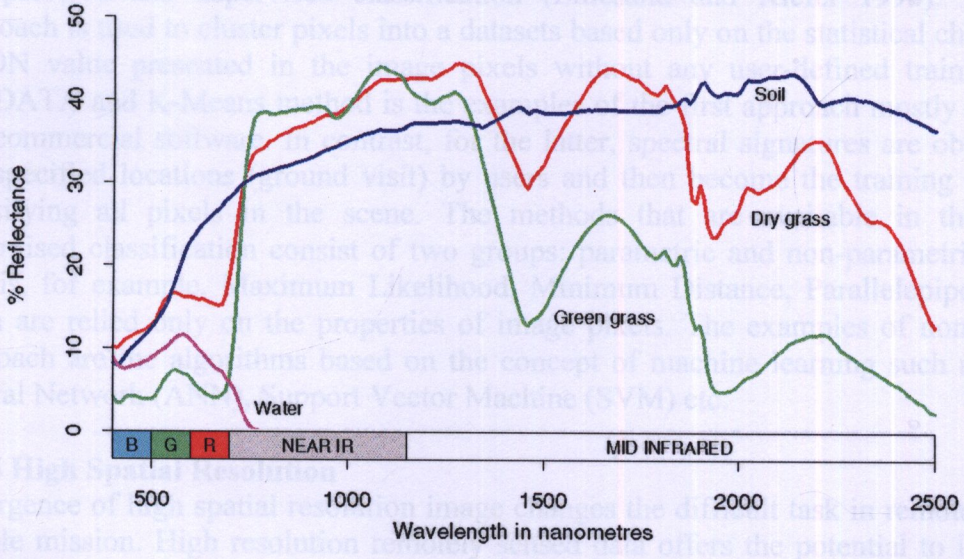

Figure 2.3 Electromagnetic spectrum diagram and spectral signature (Culvenor 2000)

2.2.3 Spectral reflectance of vegetation

Because of the difference in the interaction of electromagnetic radiation of different wavelengths with targets, the various wavelength bands have different information contents. Leaf-scale reflectance spectra are controlled by leaf bio-chemical properties and leaf morphology (Asner 1998; Grant 1987; Roberts et al. 2004) Visible and infrared region of spectrum is broadly applied for vegetation detection or classification. The most important wavelength is red and near infrared as their unique characteristics. In general, the reflectance of vegetation in the visible red band (0.6-0.7 μm) is lower and that in the near infrared region (0.7-1.1 μm) is higher. Far less is known about the behavior of an entire tree canopy with respect to reflectance, light absorbance and photosynthesis. Photosynthesis is based on conversion of radiation absorbed in blue and red parts of electromagnetic spectrum to energy. Three features of leaves have an important effect on

the reflectance properties of leaves: pigmentation, physiological structure and water content.

The major bottleneck of tree crown classification is how to measure the surface reflectance from satellite imagery. Usually the reflectance value obtain from the satellite is top of atmospheric (TOA) reflectance. In fact amount of RED and NIR radiation reflected from a tree canopy reaching a satellite sensor varies with solar irradiance, atmospheric conditions, canopy background, canopy structure, forest type and tree species. So, atmospheric correction must be performed to remove the effect of aerosol scattering, water vapor and other atmospheric gases. From the surface reflectance, various vegetation indices can be calculated such as normalized differential vegetation index (NDVI), Simple Ratio Index (RI), Enhance Vegetation Index (EVI) and so forth. In fact, VIs spectral variability among species is low due to the strong absorption by chlorophyll (Cochrane 2000; Poorter et al. 1995)

2.2.4 Algorithms for image classification

Digital image classification is the process of making quantitative decisions from image data based on the radiometric value or digital value (DN), or grouping the homogeneous pixels into the classes intended to represent the different physical objects or types (Rees 2001). Typically, the digital image classification procedures are categorized as unsupervised and supervised classification (Lillesand and Kiefer 1994). The former approach is used to cluster pixels into a datasets based only on the statistical characteristics of DN value presented in the image pixels without any user-defined training classes. ISODATA and K-Means method is the examples of the first approach mostly available in the commercial software. In contrast, for the latter, spectral signatures are obtained from the specified locations (ground visit) by users and then become the training data set for classifying all pixels in the scene. The methods that are available in the frame of supervised classification consist of two groups: parametric and non-parametric. The first one is, for example, Maximum Likelihood, Minimum Distance, Parallelepiped. Most of them are relied only on the properties of image pixels. The examples of non-parametric approach are the algorithms based on the concept of machine learning such as Artificial Neural Network (ANN), Support Vector Machine (SVM) etc.

2.2.5 High Spatial Resolution

Emergence of high spatial resolution image changes the difficult task in remote sensing to simple mission. High resolution remotely sensed data offers the potential to improve the accuracy of traditional forest inventory attributes while retrieving important information relating to the structural diversity of forests. Moreover it can be applied in various fields such as urban management, agriculture monitoring or damage assessment. In addition this information provides the opportunities to monitor tree attributes at an individual tree crown level. Each tree crown consists of several pixels. The size of spatial resolution of the imagery is higher than the size of the crown in the scene. IKONOS and QuickBird are the examples of the fine spatial resolution of satellite imagery. IKONOS provides multi-spectral bands with 4 m and panchromatic with 1 m. QB offers the largest swath width and highest resolution of any currently available or planned commercial satellite 2.44 m for four multi-spectral bands and 0.6 m for gray scale image. As such data becomes more widely accessible the potential exists for quantitative spatial forest assessment to be economically applied over broad areas at the individual tree scale. However, analysis of high resolution imagery poses a number of challenges that require specific image

interpretation procedures. The most important specifications of QB are illustrated in table 2.1.

Table 2.1 Specifications of QuickBird satellite

Features	Descriptions
Orbit Altitude	450 km
Sensor Resolution at nadir	Panchromatic: 0.60 cm (nadir) to 72 cm (25°off-nadir) Multi-spectral: 2.44 m (nadir) to 2.88 m (25°off-nadir)
Panchromatic Bandwidth	445 - 900 nm
Multi-spectral Bandwidth	Blue 450 – 520 nm Green 520 - 600 nm Red 630 - 690 nm Near-infrared 760 - 900 nm
Metric Accuracy	23-meter circular and 17-meter linear error (without ground control)
Revisit Frequency	1 to 3.5 days depending on latitude
Nominal Swath Width	16.5 km at nadir
Single Area Size	16.5 km x 16.5 km

Source: Digital Globe.

2.2.6 Laplacian Edge Detector

Image edges are the most important information for image segmentation and the foundation of image texture. Edge detection treats the localization of significant variations of a gray level image and the identification of physical and geometrical properties of objects of the scene (Argialas 2004). Most recent edge detectors are autonomous and multi-scale and include three main processing steps: smoothing, differentiation and labeling. In general, edge detection algorithms are available in convolution filter. This produces output images in which the brightness value at a given pixel is a function of some weighted average of the brightness of the surrounding pixels. The examples of edge detector are Sobel, Laplacian, Directional, Gaussian, Roberts etc.

The Laplacian edge detector generates sharp edge definition of an image. A second derivative edge enhancement filter that operates without regard to edge direction. Laplacian filtering emphasizes maximum values within the image by using a kernel with a high central value typically surrounded by negative weights in the north-south and east-west directions and zero values at the kernel corners. This filter can be used to highlight edges having both positive and negative brightness slopes. The two Laplacian filters have different weight arrangements as display below:

0	1	0
1	-4	1
0	1	0

-1	-1	-1
-1	8	-1
-1	-1	-1

1	-2	1
-2	4	-2
1	-2	1

Figure 2.4 Three commonly used discrete approximations to the Laplacian filter, where sum of all the weights = 0

The Laplacian L(x,y) of an image with pixel intensity values I(x,y) is given by:

$$L(x,y) = \frac{\partial^2 I}{\partial x^2} + \frac{\partial^2 I}{\partial y^2}$$

Using one of these kernels, the Laplacian can be calculated using standard convolution methods. Convolution provides a way of multiplying together two arrays of numbers, generally of different sizes, but of the same dimension, to produce a third array of numbers of the same dimensionality. The convolution is performed by sliding the kernel over the image, generally starting at the top left corner, so as to move the kernel through all the positions where the kernel fits entirely within the boundaries of the image.

I_{11}	I_{12}	I_{13}	I_{14}	I_{15}	I_{16}
I_{21}	I_{22}	I_{23}	I_{24}	I_{25}	I_{26}
I_{31}	I_{32}	I_{33}	I_{34}	I_{35}	I_{36}
I_{41}	I_{42}	I_{43}	I_{44}	I_{45}	I_{46}
I_{51}	I_{52}	I_{53}	I_{54}	I_{55}	I_{56}

K_{12}	K_{12}	K_{13}
K_{21}	K_{22}	K_{23}

Figure 2.5 example small image (left) and kernel (right) to illustrate convolution. The labels within each grid square are used to identify each square.

2.3 Tree crown delineation Algorithm

Recently, a variety of algorithms exist for the purpose of tree crown identification and delineation. An automated approach to tree delineation may facilitate the implementation of efficient, consistent and reliable tree scale inventories across the whole landscape (Culvenor 2002). To achieve the sound results, the assumptions implicit in automated tree crown delineation should be considered prior to done an automated tree crown delineation. A fundamental assumption inherent in crown delineation algorithms is that the centre of a crown is brighter than the edge of the crown, or more particularly, the boundary between crowns. The assumption is somewhat intuitive, but can also be explained theoretically (Culvenor, 2003). In general, full individual tree crown delineation are image processing algorithms either following valleys of shade between tree crowns in an intensity image or following edges created by gradient operator and analyzing their curvature (Gougeon, 1995b).

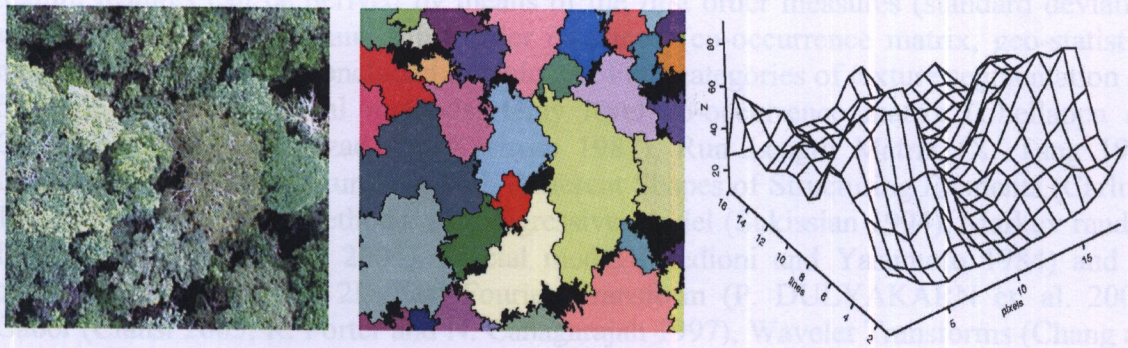

Figure 2.6 The procees of tree crown delineation (Gougeon)

Figure 2.6 represents the process of tree crown classification (a) Example of tree crown, (b) the results from tree crown extraction and (c) a three-dimensional view of image showing the brighter tree crowns as mountains. Techniques for finding tree locations and crown dimensions are based on finding local maxima and then finding the edge of the crown (Pinz 1991; Uuttera et al. 1998). Such approaches can lead to stem counts, species classifications and crown area estimations. Tree crown algorithms may be broadly categorized as either "bottom-up", "top-down" or "template matching" algorithm (Culvenor 2003). The first group focuses on the valleys of shadow between trees as a means of isolating crown boundaries. "Valley-following" method developed by Gougeon is the example of this group. The algorithm exploits the bands of shadow that often occur between trees in dense forest. These bands of shadow are termed "valleys" meaning "radiometric valleys". For the second group, it involves initially estimating the location of tree crowns from radiometric maxima, and subsequently locating the boundary using the characteristic decrease in brightness from the centre of a crown to its edge. Multiple scale edge segments, Threshold-based spatial clustering, Double-aspect method and Vision expert system are the instant of the second group. For the final, the algorithms are based on the use of pre-defined a three-dimensional templates of tree crowns defined by geometric and radiometric parameters. Moreover, another sophisticated algorithms are available such as Tree Identification and Delineation Algorithm: TIDA (Culvenor 2001), Tree speices classification based on support vector machine (Kulikova et al. 2007), Algortihm using the point of maximum rate of change in the transect data (Pouliot et al 2002), algorithm based on colour information, the shape of the segmented tree crowns (Erikson 2003b), ANN application for tree crown classification (Kanellopoulos et al. 1992). The following aspects must be considered to select the appropriated algorithm to meet the required objectives: spatial and spectral characteristics as well as view angle, sun angle and atmospheric effects.

2.4 Texture Analysis by Grey Level Co-Occurrence Matrix

Although a precise definition of image texture is rather difficult to formulate, it can be loosely defined as structure in the spatial variation of the pixel values (Tso and Mather 2001). Texture data is a statistical feature used mainly for image segmentation and region characterization. (Chan and Laporte 2003) summarized that texture or pattern of data describes the spatial relationship among neighboring pixels within a pre-defined window area. Presumably the image is characterized by a small number of various pixel-neighborhoods that differ according to specific texture measures (Christoulas and Tsagaris 2007). The classification of the central pixel in this neighbourhood is reassigned to

whichever image class is most strongly represented in the neighbourhood. In general, texture features can be derived by means of the first order measures (standard deviation, variance, mean), second and third order measures (co-occurrence matrix, geo-statistical measures or variogram) concluded in table 2.2. Four categories of texture segmentation can be defined: (1) Statistical methods: Gray level co-occurrence matrix (Chellappa and Chatterjee 1985; Khotanzad and Kashyap 1987), Run Length Matrix (X. Tang 1998; Galloway 1975) (2) Structural method: Different Shapes of Structuring Elements (Carlucci 1972) (3) model-based methods: Autoregressive Model (Sukissian 1994), Markov random fields (G. Cuozzo et al., 2004), Fractal model (Medioni and Yasumoto 1984) and (4) transform-based method: 2D Fast Fourier Transform (P. DULYAKARN et. al. 2000), Gabor (Clausi 2005; R. Porter and N. Canagarajah 1997), Wavelet Transforms (Chang and kuo 1992; Hill et. al. 2000; Z. Lscan et al. 2006). In recent times, all of them are applied to decrease errors of image classification algorithms.

Table 2.2 texture analysis techniques used in remote sensing

Texture measures in remote sensing	Advantages	Disadvantages
1. First order statistics : Standard deviation, Variance, Mean	• Simple to calculate • Indicates local variance	• No directionality • No distance function • Sensitive to noise
2. Second order statistics by co-occurrence matrix : Contrast, Angular second moment, Correlation, Entropy, Dissimilarity, Homogeneity, Sum average, Sum variance, Sum entropy, Difference variance, Difference entropy	• Describe relation between different pixels • Sensitive to directionality • Insensitive to noise • Does not over-emphasis field boundaries	• Computationally intensive • Similarity among the statistics derived from co-occurrence matrix
3. Geostatistics : Variogram, Correlogram, Covariance function, General relative variogram, Rodogram, madogram, Pairwise relative variogram	• Provides different scene measures • Insensitive to noise • Robust • Mathematically simple • Requires mean be weakly stationary • Easy to interpret	• Computationally intensive • Large data set required to fit a variogram model • One unusual DN value causes misquantification of all surrounding pixels

Source: S. Berbeoglu 2000

One of the commonest approaches to the quantification of image texture is through the use of grey-level co-occurrence matrix (GLCM), also know as the grey-tone spatial dependency matrix (W. G. Rees 2001). The fundamental concept of GLCM is that the texture information contained in an image is defined by the adjacency relationships that the grey tones in an image have to one another. In other word, it is assumed that the texture information is specified by values p_{ij} within the GLCM. A GLCM is a matrix where each cell i, j contains the number of times a point having intensity i occurs in a position j located at an angle θ and a distance d. Values of p_{ij} can be calculated for any feasible direction and

distance *d*. Only the first quadrant of that neighbourhood needs to be explored. Generally, only four directions corresponding to angle of 0° (Horizontal), 45° (Right diagonal), 90° (Vertical) and 135° (Left diagonal) are used (Tso and Mather, 2001). The GLCM of an image is an estimation of the second-order joint probability, P(i,j) of the intensity values of two pixels (i and j), a distance apart along a given direction θ. This joint probability takes the form of a square array P with row and column dimensions equal to the number of discrete gray levels (intensities) in the image being examined. If an intensity image are entirely flat (i.e. contained no texture), the resulting GLCM would be completely diagonal. As the image texture increases (i.e. as the local pixel intensity variations increase), the off-diagonal values in the GLCM become larger.

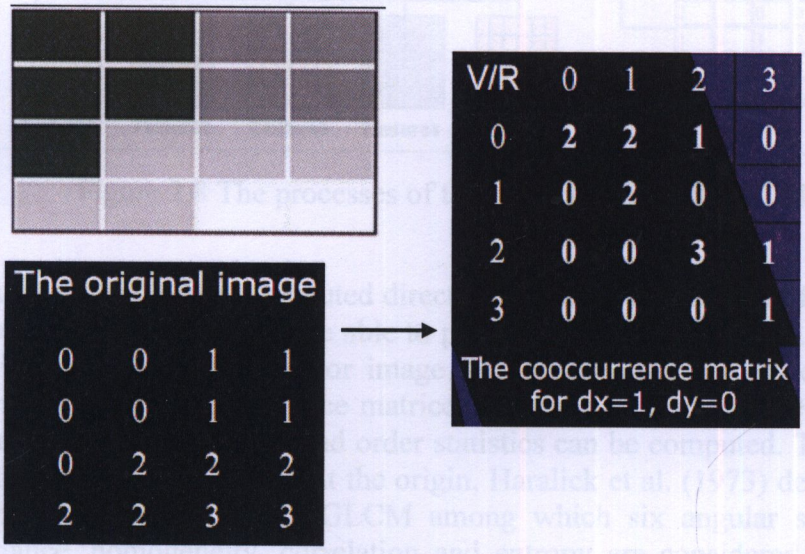

Figure 2.7 The Gray Level Co-occurrence Matrix process

GLCM texture considers the relation between two pixels at a time, called the reference and the neighbouring pixel. In the illustration of figure 2.7, the neighbouring pixel is chosen to be the one to the east of each reference pixel. This can also be expressed as a (1, 0) relation: 1 pixel in the x direction, 0 pixels in the y direction. Each pixel within the window becomes the reference pixel in turn, starting in the upper left corner and proceeding to the lower right. Pixels along the right edge have no right hand neighbour, so they are not used for this count. The top left cell represents the number of times the combination of 0, 0 (i, j) occurs. Texture measurement usually require the window size (neighbour), direction of offset (θ), offset distance (d), channel to run (the number of bands) and measure to use (texture feature). The GLCM described here is used for a series of texture calculations. Each of order is described below: (1) First order texture measures are statistics calculated from the original image values, like variance, and do not consider pixel relationships. (2) Second order means they consider the relationship between groups of two pixels in the original image. (3) Third and higher order textures (considering the relationships among three or more pixels) are theoretically possible but not implemented due to calculation time and interpretation difficulty.

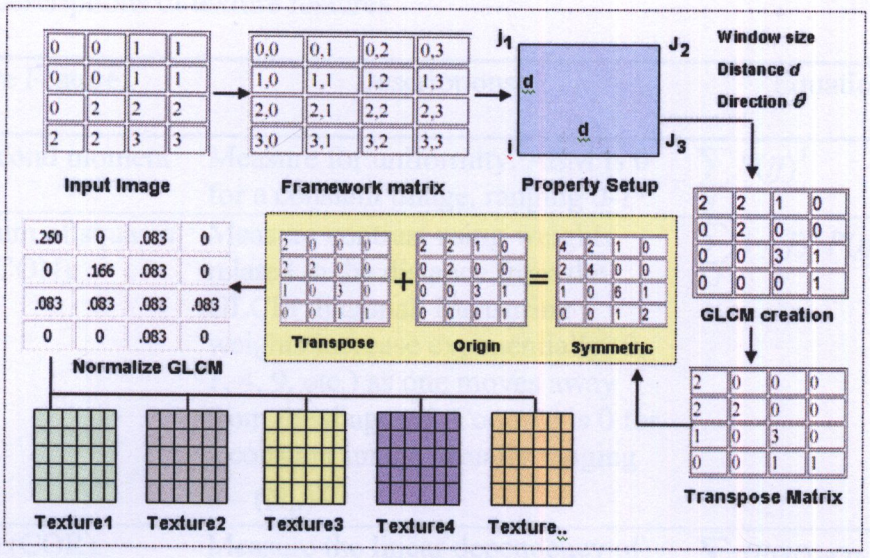

Figure 2.8 The processes of texture extraction by GLCM

Obviously, a GLCM cannot be computed directly from a color image but from a grayscale one, so a modification is needed to be able to process that kind of images. There are three ways for doing this: convert the color image to monochrome, process each RGB band separately and use cross-co-occurrence matrices (Muniz and Corrales, 2006). From a co-occurrence matrix, a number of second order statistics can be computed. Textural features can be extracted only from GLCM. At the origin, Haralick et al. (1973) defined 14 texture features that are derived from the GLCM among which six angular second moment, contrast, variance, homogeneity, correlation and entropy are considered to be the most relevant for remote sensing imagery analysis. Some of the commonest are described in table 2.3.

The texture parameter associated with a particular pixel is calculated from the pixel values in a "window" of the image center on that pixel, and this has the effects of degrading the spatial resolution. The moving window size of the GLCM is a key parameter in texture analysis. Choosing the appropriate window size is not straightforward: if it is too small, too few pixels will be available to give a statistically meaningful measure of texture, whereas if it is too large, the resolution of the "texture image" will be unnecessarily degraded. If the pixel values in the image are drawn from a set of N integer (e.g. N = 256 for 8-bit data), the GLCM is an N x N square matrix P. GLCM can be used as a powerful tool for texture analysis, classification, segmentation, and synthesis. The disadvantage of GLCM is that they contain only the co-occurrence information between two pixels, and thus cannot capture the spatial relationship between three or more pixels in the image (Rees 2001).

Table 2.3 Descriptions of texture features

Texture Feature	Descriptions	Equation
Angular second moment (ASM)	Measure for uniformity. ASM is 0 for a constant image, ranging 0-1	$\sum_{ij} P(ij)^2$
Contrast (sum of squares variance) (CON)	Measure contrast using weights related to the distance from the GLCM diagonal. Measuring weights increase exponentially (0, 1, 4, 9, etc.) as one moves away from the diagonal. Contrast is 0 for a constant image ,usually ranging $0-(N_g)^2$	$\sum_{i,j}(i-j)^2 P(ij)$
Correlation (COR)	Measure the linear dependency of grey levels on those of neighbouring pixels. 0 is uncorrelated, 1 is perfectly correlated.	$\frac{\sum_{ij} ijP(ij) - \mu_i\mu_j}{\sigma_i\sigma_j}$
Dissimilarity (DIS)	Measure weight which increase linearly (0, 1, 2, 3 etc.)	$\sum_{i,j=0}^{N-1} P_{ij}\lvert i-j\rvert$
Entropy (ENT)	Measure the level of spatial disorder of gray levels in the GLCM. Low value for smooth image. The maximum value of ENT is 0.5 Range: ≥ 0	$\sum_{ij} P(ij)\log P(ij)$
Homogeneity (HOM)	Return a value that measures the closeness of the distribution of elements in the GLCM to the GLCM diagonal. Homogeneity weights values by the inverse of the Contrast weight, with weights decreasing exponentially away from the diagonal 1 for a diagonal GLCM ranging 0-1	$\sum_{i,j=0}^{N-1} \frac{(p_{i,j})}{1+(i-j)^2}$
Mean (MEA)	Measures the mean of the probability values from the GLCM. It measures how many times that reference value occurs in a specific combination with a neighbour pixel.	$\mu_i = \sum_{i,j=0}^{N-1} i(p_{ij})$ $\mu_j = \sum_{i,j=0}^{N-1} j(p_{ij})$
Variance (VAR)	measure of the dispersion of the values around the mean of combinations of reference and neighbor pixels in the GLCM	$\sum_{i,j}(i-\mu)^2 P(ij)$

Source: Haralick 1973

2.5 Integration of spectral and textural information

In some cases, only the spectral data is not sufficient for identification or classification of spectrally heterogeneous landscape units from others due to the atmospheric errors such as the aerosol density, pressure and temperature etc. (Lin 2001). To obtain the more detail of related information from satellite image, spatial or textural information must be considered to include to the classification procedure. There is assumption that the combination of texture methods and spectral information can improve the results of classification. High spatial resolution embodied in IKONOS and QuickBird images provides a unique ability to incorporate small-scale textural information in the classification process. Small-scale spatial variability would help discriminate those canopy types that were hard to distinguish from spectral information alone.

2.6 Support Vector Machine

2.6.1 SVM Concept

Support Vector Machine (SVM) is the novel machine learning that be used as the hypothesis space of linear functions in a high dimensional feature space to classify the pattern of dataset based on statistical learning theory (Cristianini and Taylor 2000). In the other word, SVM is a set of supervised learning methods of classification and regression to find the maximum separation hyper-plane (Margin) in the high dimension space (such as satellite imagery) between classes using a set of observations called the "training data" usually represented as input/output pairs (Vapik 1995).

2.6.2 SVM Procedures

SVM performs classification by constructing an N-dimensional hyper-plane that optimally separates the dataset into two categories, the positive and the negative sides within the high dimension space usually known as "optimal separating hyper-plane". In the parlance of SVM literature, a predictor variable is called an "attribute", and a transformed attribute that is used to define the hyper-plane is called a "feature". The task of choosing the most suitable representation is known as "feature selection". A set of features that describes one case (i.e., a row of predictor values) is called a "vector". So the goal of SVM modeling is to find the linearly optimal hyper-plane that separates clusters of vector in such a way that cases with one category of the target variable are on one side of the plane and cases with the other category are on the other size of the plane. The vectors closest to the optimal hyper-plane are the "support vectors" (See figure 2.9). An assumption is made that the larger the margin or distance between these parallel hyper-planes, the better the generalization error of the classifier will be (Vapnik 1995).

However, in practice, the data is often not linearly separable. In order to enhance the feasibility of linear separation, one may transform the input space via a non-linear mapping into a higher dimensional dot product feature space. This transformation is done by using a kernel function. The kernel function plays a major role in locating complex decision boundaries between classes. This separation of the input and feature space allows a variety of kernels to be employed (Chapman 2004).

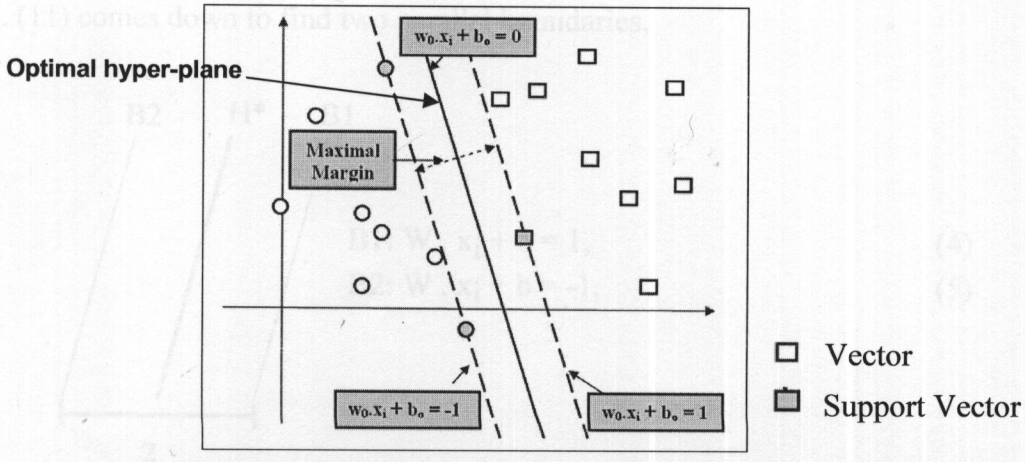

Figure 2.9 Support vector and optimal hyper-plane (Chapman 2004)

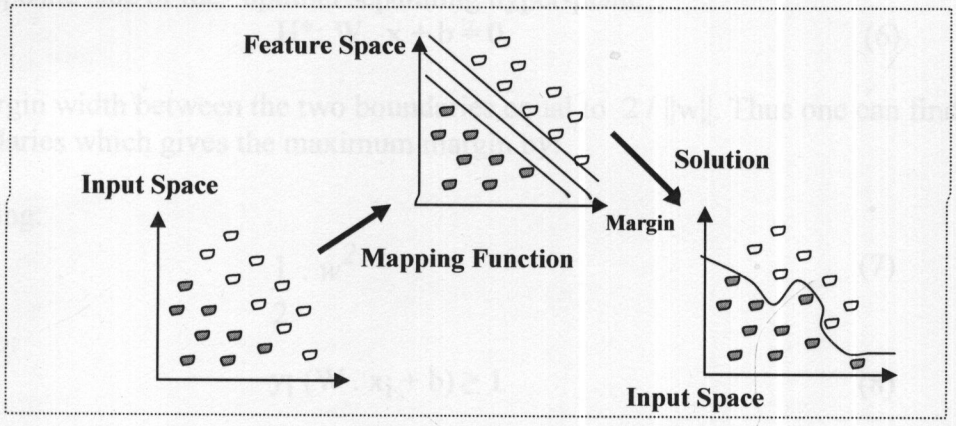

Figure 2.10 The SVM algorithm process (DTREG)

Below, a general overview of SVMs for a binary classification problem (2 classes) is briefly explained by referring to the tutorial of Burges, 1998.

Given a set of labeled training examples $\{x_i, y_i\}$ with $i = 1, 2, 3, \ldots, N$ where $x_i \in R^m$ (m: the dimension of input space), and $y_i \in \{-1, 1\}$ (y: class label. Suppose that the training data is linearly separable, there exists a weight vector "w" and a bias "b" such that the inequalities

$$W \cdot x_i + b \geq 1 \text{ when } y_i = 1, \quad (1)$$

$$W \cdot x_i + b \leq 1 \text{ when } y_i = -1, \quad (2)$$

are valid for all elements of the training set. As such, we can rewrite these inequalities in the form:

$$y_i (W \cdot x_i + b) \geq 1 \text{ with } i = 1, 2, 3, \ldots, N. \quad (3)$$

Eq. (11) comes down to find two parallel boundaries,

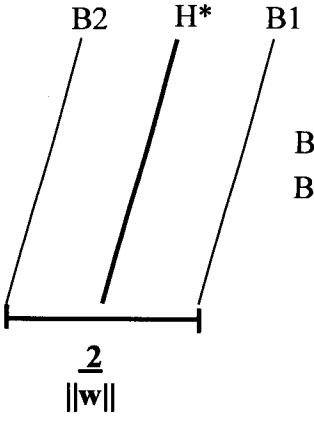

$$B1: W \cdot x_i + b = 1, \quad (4)$$

$$B2: W \cdot x_i + b = -1, \quad (5)$$

at the opposite side of the "optimal separating hyper-plane",

$$H^*: W \cdot x + b = 0, \quad (6)$$

with margin width between the two boundaries equal to $2 / \|w\|$. Thus one can find the pair of boundaries which gives the maximum margin by:

minimizing:

$$\frac{1}{2} \cdot w^2 \quad (7)$$

subject to:

$$y_i (W \cdot x_i + b) \geq 1 \quad (8)$$

This constrained optimization problem can be solved using the characteristics of the Lagrange multipliers (α) by
maximizing:

$$w(\alpha) = \sum_i \alpha_i \quad -\frac{1}{2} \sum_i \sum_j \alpha_i \alpha_j y_i y_j x_i x_j \quad (9)$$

subject to:

$$\alpha_i \geq 0 \text{ with } i = 1, 2, 3, \ldots, N \text{ and } \sum_i \alpha_i y_i = 0 \quad (10)$$

The weight vector could be stated as follows:

$$W = \sum_i \alpha_i y_i x_i \quad (11)$$

The decision function $f(x)$ can be written as

$$f(x) = \text{sgn}(W \cdot x + b) = \text{sgn}[\sum_i \alpha_i y_i (x \cdot x_i) + b] \quad (12)$$

Where sgn is a sign function. In practice, the input data will often not be linearly separable. However, one can still implement a linear model by introducing a higher dimensional feature space to which an input vector is mapped via a non-linear transformation:

$$\Phi: X \dashrightarrow X' \quad (13)$$

$$X_i \dashrightarrow \Phi(x_i) \quad (14)$$

Where X is the input space, Φ is the non-linear transformation and $\Phi(x_i)$ represents the value of x_i mapped into the higher dimensional feature space X'.

Therefore Equation (9) can be transformed to

minimizing:

$$w(\alpha) = \sum_j \alpha_i - \frac{1}{2} \sum_i \sum_i \alpha_i \alpha_j y_i y_j \Phi(x_i)\, \Phi(x_j) \quad (15)$$

subject to:

$$\alpha_i \geq 0 \text{ with } i = 1, 2, 3, \ldots, N \text{ and } \sum_i \alpha_i y_i = 0 \quad (16)$$

By mapping the input space to the higher dimensional feature space, the problem of high dimensionality and implementation complexity occurs. One can introduce the concept of inner product kernels. Consequently, there is no more need to know the exact value of $\Phi(x_i)$, only the dot inner product is considered which facilitates the implementation. Input data are displayed in the form of "dot product" of two vectors to be easily integrated into the support vector machine.

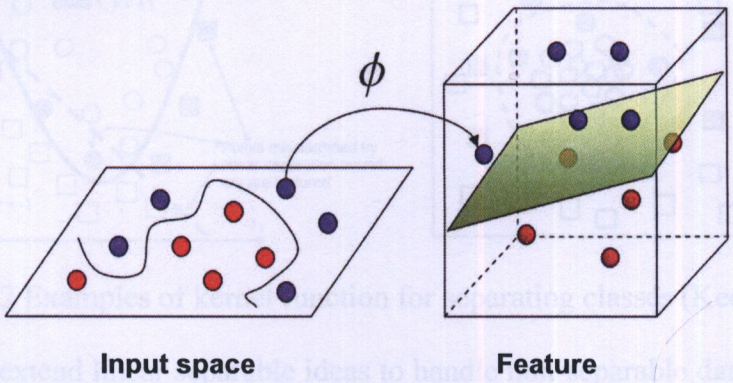

Figure 2.11 Data transformation to higher dimension space (Chapman 2004)

According to above picture, there are two predictor variables (attribute). If we plot the data point using the value of one predictor on the X-axis and the other on the Y-axis, SVM analysis attempts to find a 1-dimensional hyper-plane (i.e. a line) that separates the cases based on their target categories. In this case, we add a third predictor variable, then, we can use its value for a third dimension and plot the points in a 3-dimensional cube. Points in a 3-dimensional cube can be separated by a 2-dimensional plane.

Kernel function:

$$K(x_i, x_j) = \Phi(x_i).\, \Phi(x_j) \quad (17)$$

Therefore the decision function becomes

$$f(x) = \text{sgn}[\sum_i \alpha_i y_i\ \Phi(x).\, \Phi(.x_i) + b] = \text{sgn}[\sum_i \alpha_i y_i\, k(x.x_i) + b] \quad (18)$$

For resolving this decision function, several types of kernel functions are available as given in table 2.4.

Table 2.4 Overview of the different kernel functions

Kernel Function	Mathematical Form*
Linear Kernel	$K(x, x_i) = (x.x_i)$
Polynomial Kernel of degree d	$K(x, x_i) = (\gamma x. x_i + r)^d, \gamma > 0$
Radial Basis Function	$K(x, x_i) = \exp(-\gamma \|x-x_i\|^2), \gamma > 0$
Sigmoid Kernel with r ∈ N	$K(x, x_i) = \tanh(\gamma x. x_i + r)$

* $d, r \in N; \gamma \in R^+$

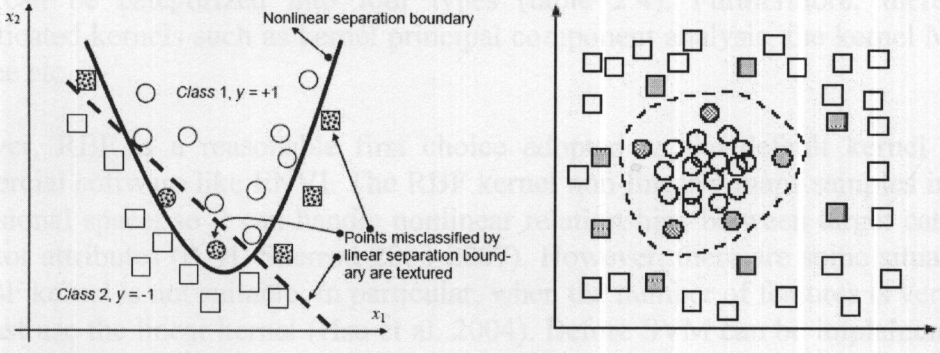

Figure 2.12 Examples of kernel function for separating classes (Kecman 2004)

It is possible to extend linear separable ideas to handle non-separable data. In this case, the margin will become very small and it will be impossible to separate the data without any misclassification. To solve this problem, we relax the constraints (9) (10) by introducing positive slack variables (ε_i) (Cortes et al. 1995)

Equations (9) (10) become

$$W . x_i + b \geq 1 - \varepsilon_i \text{ when } y_i = 1, \quad (19)$$

$$W . x_i + b \leq 1 + \varepsilon_i \text{ when } y_i = -1, \quad (20)$$

With $\varepsilon_i \geq 0$.

Equations (27) (28) can be rewritten as

$$y_i (W . x_i + b) \geq 1 - \varepsilon_i \text{ with I} = 1, 2, 3, \ldots, N. \quad (21)$$

The goal of the optimization process is to find the hyper-plane that maximizes the margin and minimizes the probability of misclassification:

minimize

$$\frac{1}{2} . w^2 + C \sum_i \varepsilon_i \quad (22)$$

subject to

$$y_i(W . x_i + b) \geq 1 - \varepsilon_i \quad (23)$$

with *C*, the cost, the penalty parameter for the error term. The larger *C*, the higher the penalty to errors.

Adapting equation (23) to the non-separable case, one receives the following optimization problem:

maximizing

$$\sum_j \quad \frac{1}{2} \sum_i \sum_i$$

$$w(\alpha) = \alpha_i - \alpha i \alpha j y i y j k(xi,xj) \quad (24)$$

subject to

$$0 \leq \alpha_i \leq C \text{ with } I = 1, 2, 3, \ldots, N \text{ and } \sum_i \alpha_i y_i = 0 \quad (25)$$

2.6.3 Model selection for SVM

In training a support vector machine, we need to select an appropriate kernel and set a value to the margin parameter *C*. The accuracy of SVM models depend on the selecting suitable parameter values. Thus to develop the optimal classifier, we need to determine the optimal kernel parameter and the optimal value of *C* (margin) called model selection (Abe 2005). The kernel function converts non-linear boundaries in the original data space into linear ones in the high-dimensional feature space. In general, kernels that widely used in SVM can be categorized into four types (table 2.4). Furthermore, there are other sophisticated kernels such as kernel principal component analysis, the kernel Mahalanobis distance etc.

However, RBF is a reasonable first choice adopted as the default kernel function in commercial software like ENVI. The RBF kernel non-linearly maps samples into a higher dimensional space, so it can handle nonlinear relationships between target categories and predictor attributes (P. H. Sherrod 2003-2007). However, there are some situations where the RBF kernel is not suitable. In particular, when the number of features is very large, one may just use the linear kernel (Hsu et al. 2004). Before SVM can be implemented, several parameters have to be optimized to construct the first-class classifier. The RBF kernel needs two parameters to be set; *C* and γ, with *C* the penalty parameter for the error tern and γ as the kernel parameter. Both parameters play a crucial role in the performance of SVM. Beforehand it is impossible to know which combination of (C, γ) will result in the highest performance when validating the trained SVM to unseen data. Some kinds of parameter selection procedure have to be done.

(Hsu and Chang et al. 2004) proposed a "grid search" on *C* and γ and a "v-fold cross validation" on the training data. The goal of this procedure is to identify the optimal *C* and γ, so that the classifier can accurately predict unseen data. A common way to accomplish this is 2-fold cross-validation, where the training set is divided into two parts of which one is unseen in training the classifier. This performance better reflects the capabilities of the classifier in validating unknown data. More generally, in a v-fold cross-validation, the training data is split into v subsets of equal size. Iteratively, one part is left out for validation, while the other remaining (v-1) parts are used for training. Finally, each case in the training set is predicted once. The cross-validation performance will better reflect the true performance as when validating the classifier to unseen data, while the validation set stays untouched.

In order to identify which parameter pair performs best, one can repeat this procedure with several pairs of (C,γ). As such it is possible to calculate a cross-validated evaluation measure for every parameter pair. In the end, it is possible to select these parameters based on the best cross-validation performance. A grid search on *C* and γ is performed on the training set using a v-fold cross-validation. The grid search is realized by evaluating exponential sequences of *C* and γ (i.e. $C = 2^{-5}, 2^{-3}, .., 2^{13}$; $\gamma = 2^{3}, 2^{1}, .., 2^{-15}$). All combinations of ($C$,$\gamma$) are tried and two pairs of parameters are restrained: (1) the one with the best cross-validated accuracy (2) the one with the biggest cross-validated area under the receiver operating curve. Two samples of sufficient size are randomly selected; the

training set is used to estimate the model with the most cross-validated accuracy, while the test set is used to validate the model.

2.6.4 Advantages and Disadvantages

Today the full classes of SVM are used extensively in a variety of complex fields not only for pattern classification, however, SVMs are primarily applied for classification regression and density estimation problems (Chapman 2004). The advantages and disadvantages of this technique can be summarized following:

(1) SVMs have an additional advantage to other vector space separation techniques as the probability of making an error is dependent upon support vectors rather than the full dimensionality of the initial feature space (Chapman 2004).

(2) SVMs are considered as a good approach because of its high generalization performance without the need to add a priori knowledge, even when the dimension of the input space is very high (O. Chapelle, P. Haffner 1999).

(3) The optimization method of a support vector machine is quadratic programming, which is a well-studied and understood mathematical programming technique (Sebald, Bucklew 2000)

Here, the disadvantages of this technique also briefly explained below

(1) Long training time: Because training of a support vector machine is done by solving the associated dual problem, the number of variable is equal to the number of training data (Abe 2005).

2.7 Relevant Researchs

Segmentation of tree crowns in the high spatial resolution images to an individual tree species has been an ongoing research field for several years. Various techniques already were applied. Related researches are summarized. Template matching, valley following, local maximum filtering, edge detection, spatial clustering and machine learning are utilized by the many algorithms. The combinations of all techniques give the results rather good for tree crown detection (Brandtberg & Walter 1998; culvenor 2002; Erikson 2003a; Erikson 2003b; Gouge 1995; Pinz 1989; Pollock 1996 and Pouliot et al. 2002). In contrast, classification of tree crowns into genus or species, less research has been done. Crown delineation is based on the colour information as well as the shape of the segmented tree crowns extracted from the colour infrared aerial images with pixel size corresponding to 3 – 10 cm. The overall classification result is about 71 %. (Erikson 2003). Other methods are utilized for classifying image pixels into species class including fuzzy sets classification (Brandtberg 2002; F. Hajek 2006), spectral signatures (Gougeon et al. 1998), double-aspect technique (Walsworth and King 1999b), template matching designed base on species characteristics (Larsen et al. 1998; Pollock 1996), the individual tree crown algorithm (ITC) based on the valley following approach (Leckie et al., 2005; Clark et al. 2005), algorithm utilized the k-nearest neighbour classification (Groesz an Kstdalen, 2007). Airborne laser range scanning is also applied to classify tree species (Orka et al. 2007). In the research of (Kulikova et al 2007), Support Vector Machine was employed for tree species classification by the integration of radiometry, texture and crown shapes. Tree crown shapes can improve classification performance. Signature Generation Process where for every crown extracted, a class of signatures is created from the multi-spectral data of initial image.

CHAPTER III

MATERIALS AND RESEARCH METHODOLOGY

3.1 Materials and equipments

3.1.1 Materials

(1) Satellite Image Data

- QuickBird satellite image is very high resolution so the visual interpretation of tree crown can be carried out. Panchromatic mode with 0.6 m and multi-spectral mode with 2.4 m. stored in 16 bit unsign integer were obtained over the study site. The image was recorded on 9th January 2008 GMT 04.00.42 with the maximum sun elevation 56.1°, maximum sun azimuth 146.1°, 14° off nadir angle and cloud cover 0.056%.

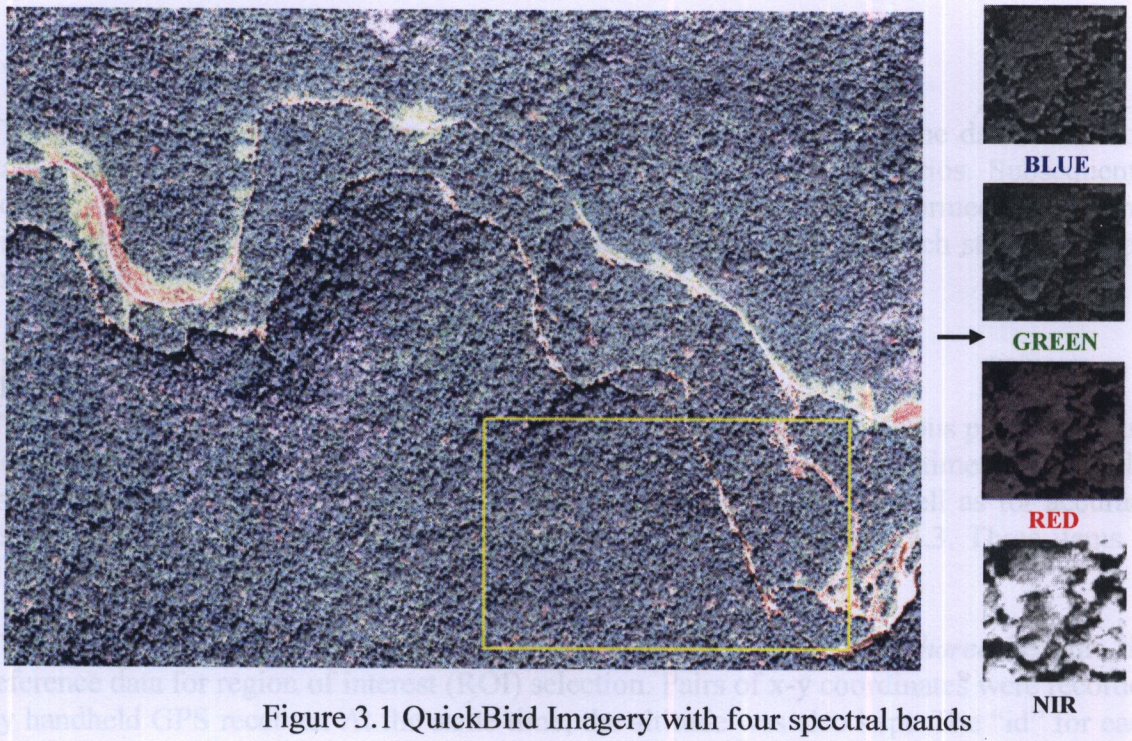

Figure 3.1 QuickBird Imagery with four spectral bands

(2) Ancillary data

- ESRI vector layer consisting of wildlife sanctuary boundary, line transect.
- Contour line with interval 20 m, scale 1:50000.
- Descriptions of tree species in the study area.

(3) Field data

- Approximately 100 sampling points (*shorea*) along the survey routes within the study site were collected by field visit. Several information and geo-coordinates were recorded by the handheld GPS. The spatial accuracy of GPS varies from 4 m to 10 m.
- Relevant information is noticed (altitude, crown diameter, crown shape)
- Specimens consisting of leaf, flower and fruit were collected from the field for further species identification by taxonomists.
- Pictures of specimen and stand tree.

3.1.2 Equipments

- Notebook computer (Linux and window operating system)
- Handheld GPS (Garmin 60CSx)
- Tape Rule
- Digital Camera
- Compass
- Aluminum tag with the number (0101, 0201, 0301, 0102, 0102, ...), the first two digits represent species name and the last two digits represent the number of tree.
- Equipments for specimen collecting
- Microsoft visual C++
- ENVI version 4.3
- ERDAS version 9.1
- ArcGIS version 9.0
- ArcView version 3.3

3.2 Methodology

This sub-chapter describes the research methodology beginning with the data collection, data preparation and image classification including three main scenarios. Subsequently accuracy assessment, ground truth and tree genus map creation are performed. The overall methodologies can be summarized in the figure 3.2. The details for each step are deeply explained below.

3.2.1 Data Collection

(1) Field data collection

The field data was collected by visiting sites in the field, describing various parameters and determining the coordinates with GPS. The field surveys were done two times. All samples tree locations were provided for training and test SVM classifier as well as for accuracy assessment. The processes of data collection were displayes in figure 3.3. Three items of field data were discussed following.

- Tree location

The spatial locations of 10 species of *shorea* and 1 species of *parashorea* become the reference data for region of interest (ROI) selection. Pairs of x-y coordinates were recorded by handheld GPS receiver. At the same time, the altitude was also kept. The "id" for each point was determined by the aluminum tags with the specific codes. By concerning the accessibility and spatial distribution, the sampling points were selected along the survey routes in examined plot with the total areas of 0.5 sq. km. The details of field data collection were summarized in table 3.1.

- Tree descriptions

In addition, descriptions of tree species consisting of crown diameter, diameter at breast height (DBH), bark color, tree height were gathered. Table 3.2 gives the general information of each species.

- Tree specimens

If some tree species cannot be identified at the field, tree specimens must be kept. With the assistance of the local monkey (*Macaca nemestrina*), the specimens of leaf, flower and fruit were easily collected. Subsequently, all specimens were identified into tree genus or species by taxonomists. Some tree species pictures are illustrated in the figure 3.4.

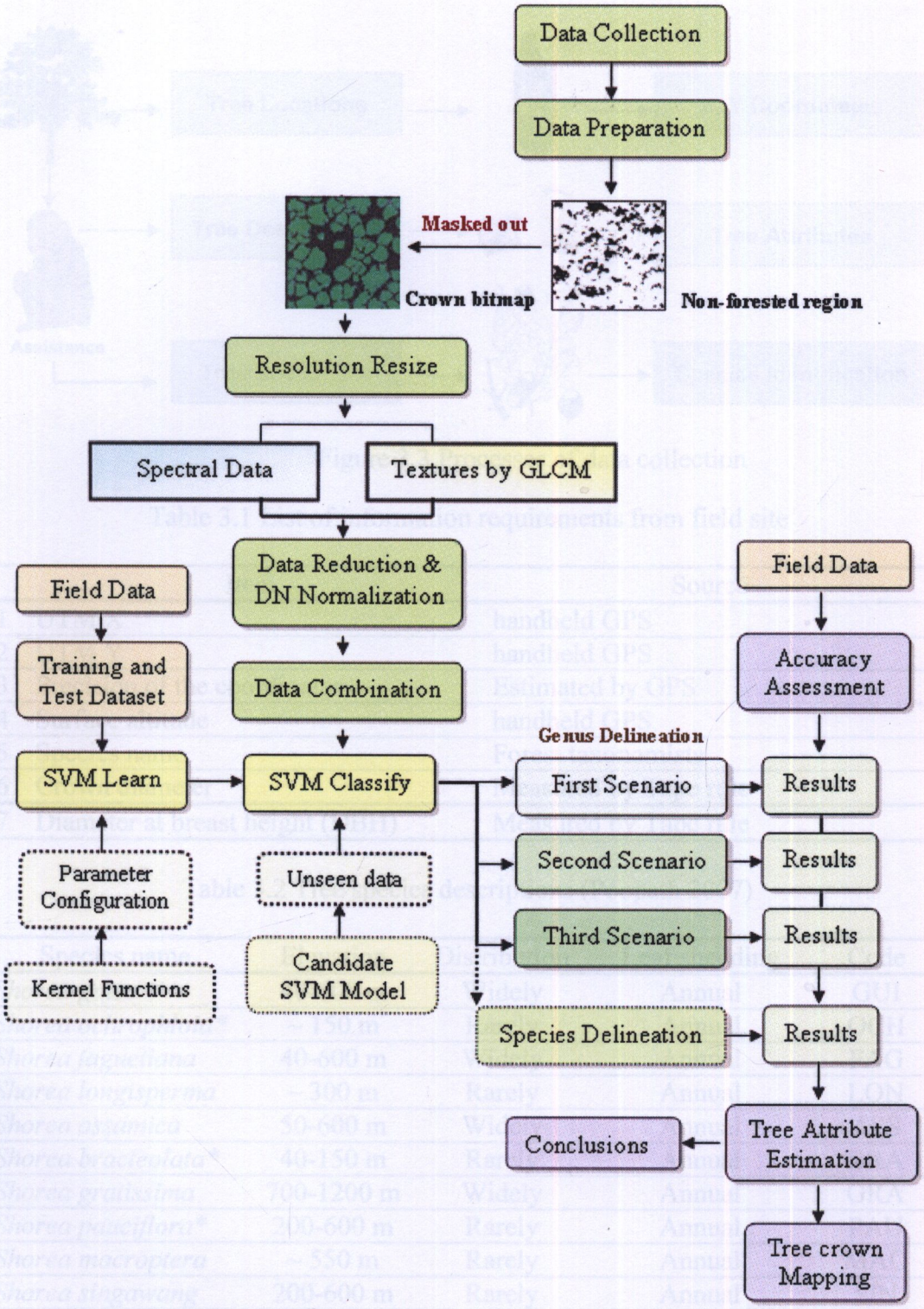

Figure 3.2 Overviews of procedure for an individual tree crown detection and delineation

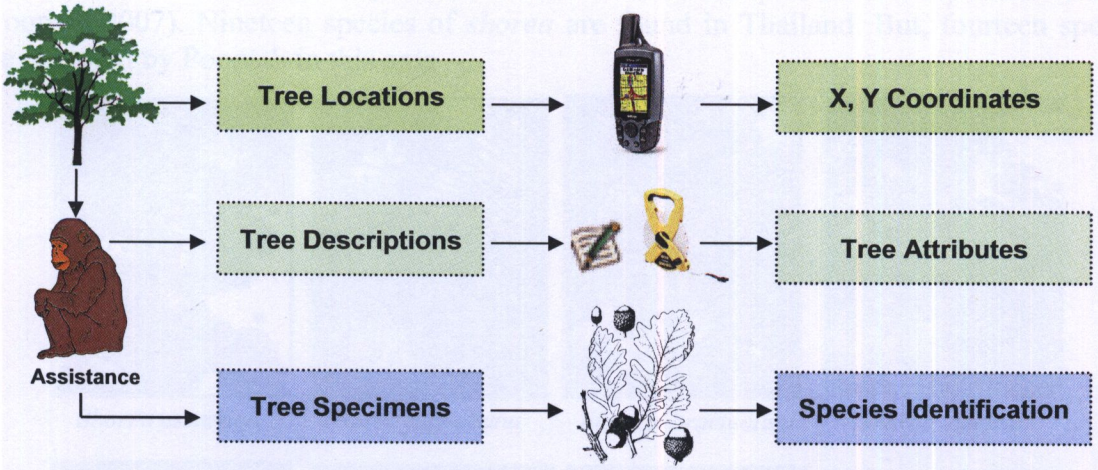

Figure 3.3 Processes of data collection

Table 3.1 List of information requirements from field site

	Item	Source
1	UTM X	handheld GPS
2	UTM Y	handheld GPS
3	Precision of the coordinates	Estimated by GPS
4	Surface altitude	handheld GPS
5	Species name	Forest taxonomists
6	Crown diameter	Measured by Tape rule
7	Diameter at breast height (DBH)	Measured by Tape rule

Table 3.2 Tree species descriptions (Poopath 2007)

Species name	Elevation	Distribution	Leaf shedding	Code
Shorea guiso	40-600 m	Widely	Annual	GUI
*Shorea ochrophloia**	~ 150 m	Rarely	Annual	OCH
Shorea faguetiana	40-600 m	Widely	Annual	FAG
Shorea longisperma	~ 300 m	Rarely	Annual	LON
Shorea assamica	50-600 m	Widely	Annual	ASS
*Shorea bracteolata**	40-150 m	Rarely	Annual	BRA
Shorea gratissima	700-1200 m	Widely	Annual	GRA
*Shorea pauciflora**	200-600 m	Rarely	Annual	PAU
Shorea macroptera	~ 550 m	Rarely	Annual	MAC
Shorea singawang	200-600 m	Rarely	Annual	SIN
Shorea leprosura	40-1000 m	Widely	Annual	LEP
Shorea curtisii	250-1000 m	Widely	Annual	CUR
Shroea ovata	500-900 m	Rarely	Annual	OVA
Shorea parvifolia	~ 700 m	Widely	Annual	PAR
Parashorea stelata	250-1000 m	Widely	Annual	STE

* New Record of Thailand

Mostly, members of *shorea* genus are categorized as the moderate or big tree. So, it can be possibly to detect from the top of view. Tree crown usually is circle shape and cylinder (Poopath 2007). Nineteen species of *shorea* are found in Thailand. But, fourteen species are explored by Poopath in this area.

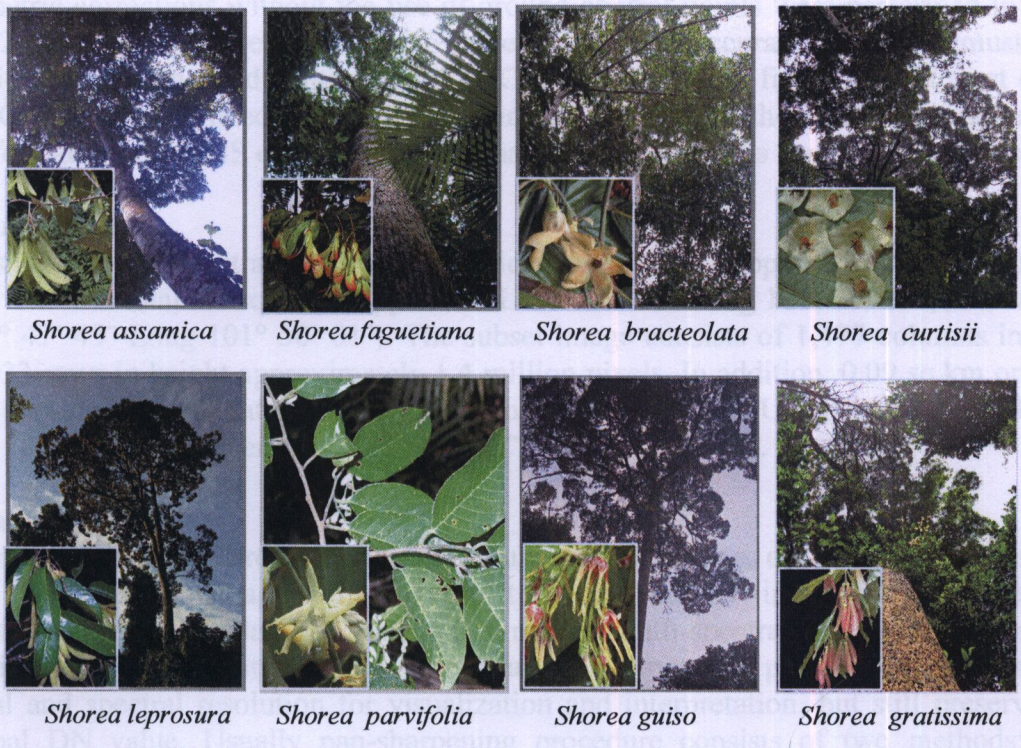

Figure 3.4 Examples of tree species, member of *shorea* (Poopath 2007)

However, some rare species can not be found in the study plot. Therefore, only 9 of 14 species becomes the training areas including *guiso, ochrophloia, faguetiana, longisperma, assamica, bracteolate, leprosura, curtisii and parvifolia.* Moreover, there is one species identified as a member of another genus that almost similar to *shorea*, namely *parashorea stelata*. Approximately 70 % of *stelata* concerning its crown shape, leat shape and size are similar to that of *shorea* members. So, this species must be included in the study.

3.2.2 Data Preparation

3.2.2.1 Image pre-processing

(1) Creation of training data

All X-Y coordinates collected from the field were plotted on the satellite image, and vector layers were constructed. In addition, the relevant field-work information such as tree height, DBH, crown diameter, family name, species name etc. were inputted in the layer attribute.

(2) Atmospheric Correction

Due to the effects of aerosol, water content, gases, digital number (DN) in remotely sensed data was considered as the reflectance at Top of Atmospheric level (TOA). So, atmospheric correction must be done to achieve the reflectance value at the surface. QuickBird satellite images level 2A which some data preprocessing were made are recorded in unsigned 16 bit integer. DN values were converted to radiance based on the gain and offset value. Afterward, physical model MODTRAN available in ENVI software is the main process. The average water content was approximately 3.41511 gm/cm^2. Four

bands and one band of multi-spectral and panchromatic image respectively were obtained based on the surface reflectance.

(3) Geometric Correction

Geometric corrections without the use of ground control points were performed in image level 2A by Digital Globe. However, to achieve the higher accuracy, the image must be re-rectified by using ground control points (GCP) collected from field visit. At least clearly five GCPs were utilized to rectify the image. By using the first-order polynomial transformation, the RMS error was approximately 1.1 m which is equal only 2 pixels.

(4) Subset image

Full size of multi-spectral and panchromatic images were clipped with the boundary of study site with total 0.5 sq. km. (Upper left: Lat 5° 48′ 01″ Long 101° 49′ 33″, Lower right: Lat 5° 47′ 43″ Long 101° 50′ 01″). The subset image consists of 1,477 columns in width and 933 rows in height approximately 1.4 million pixels. In addition, 0.09 sq.km or 55 rai were provided for validate model by applying to unseen data (Upper left: Lat 5° 48′ 12″ Long 101° 48′ 56″, Lower right: Lat 5° 48′ 3″ Long 101° 49′ 6″).

(5) Pan-sharpening

To improve the spatial resolution of the multi-spectral image, each band was sharpened with panchromatic image utilizing the transform model in ENVI software. The combination of the panchromatic image (0.6 m) and multi-spectral images (2.4 m) produce the higher spatial resolution of multi-spectral. This process is performed to enhance the spatial and spectral resolution for visualization and interpretation, but still preserves the original DN value. Usually pan-sharpening procedure consists of two methods: HSV sharpening and Color Normalized (Brovey). In this study, Brovey technique was adopted and Cubic Convolution (CC) was defined as the resampling method. Each band of the color image was multiplied by a ratio of the high resolution data divided by the sum of the color bands. Four bands of QuickBird (R G B NIR) were sharpened. The details of the output images were improved more than the original data equally the panchromatic 0.6 m.

The formula for Brovey transformation technique:

$$DN\_fused = \frac{DN\_b1}{DN\_b1 + DN\_b2 + DN\_b3 + DN\_b4} * DN\_pan \qquad (26)$$

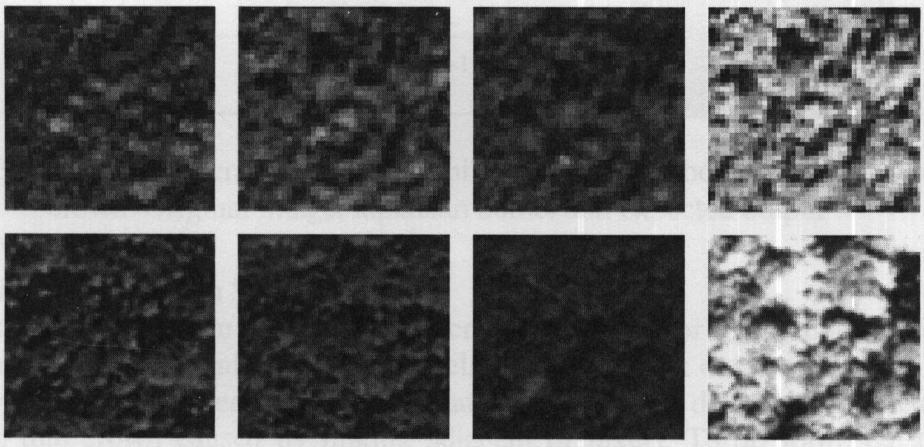

Figure 3.5 Comparison of spatial resolution before (upper) and after (lower) pan-sharpened transformation in band blue, green, red and nir (left to right)

3.2.2.2 Non tree crown elimination and segmentation

(1) Non tree-crown Elimination

In order to segment an individual tree crown boundary, it is necessary to detect non-tree crown and mask out them from satellite image beforehand. In this viewpoint, Remote sensing techniques were applied. For water area, Normalized Differential Vegetation Index (NDVI) indicating the ratio of reflectance values in the visible and near-infrared region of the spectrum becomes the main method to remove pixels that represent water area. Masking areas were generated over the pixel that NDVI less than zero. For another non tree-crown region, the training signatures obtained from field visit were constructed including tree shadow, cloud, crown gap, road, bare land, building, shrub. To do that, edge detection technique, LAPLACIAN convolution, with 3x3 kernels with a value of 8 for the center pixel and values of -1 for the north-south, east-west and both diagonal pixels, was applied to detect the boundary of each segment. Subsequently, supervised classification algorithm using maximum likelihood decision rules are performed to detect the non tree-crown pixels. Remaining pixels in this procedure were referred to as a tree-crown image.

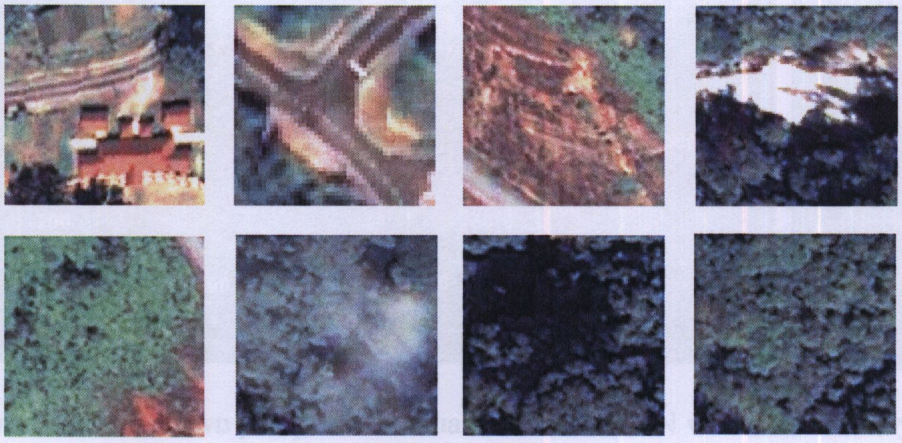

Figure 3.6 Training data set for non-tree crown masking procedure: building, road, bare land, stone, shrub, cloud, tree gap and tree crown (left to right, up to down)

1	1	1
1	1	1
1	1	1

-1	-1	-1
-1	8	-1
-1	-1	-1

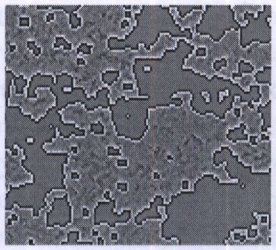

Figure 3.7 Laplacian operator with 3x3 applied to detect the boundary of non tree-crown. Original image, laplacian kernel and expected output

(2) Individual Tree Crown Segmentation

After obtaining tree crown image, another critical problem for tree genus classification is the overlap of crown boundaries. These pixels should be mask out to achieve an individual tree crown boundary earlier. Image segmentation procedure is done to solve the continuous and large tree crown caused by linking adjacent of pixels. To do forth, the changes of crown shape, size and texture must be considered. Therefore, tree crown segmentation must be carried out by lightly altering in the original pixels.

In this study, delineation of crown boundary by the local minimum brightness filtering was concentrated. From the borders of the non tree-crown areas and initial lower threshold in the tree-crown regions, pixels with the lower DN were recognized based on the threshold value. In this viewpoint, near-infrared band typically used for vegetation analysis was considered to determine the lower threshold region. Using geographical analogy, the bright individual tree crowns in an image appear like mountains (high pixel values). The darker areas surrounding them, the shaded lower branches and understorey, appear like valleys (low pixel values). In figure 3.8, QuickBird image covering the study plot was illustrated in 3d perspective view which the spatial information is represented in the x and y dimensions, while the brightness (DN) of pixels was depicted in the vertical dimension.

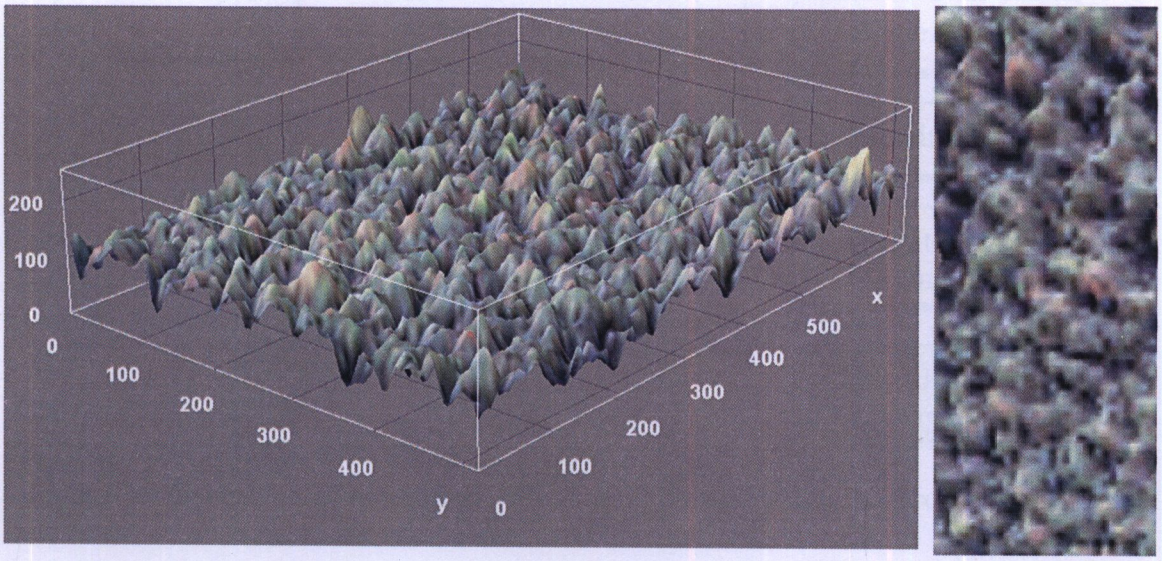

Figure 3.8 Tree crown perspective visualization with DN value in the study area

The threshold referred to as the lower threshold was used as a simple threshold throughout the image. This threshold value was defined to find out the pixels (the darker pixels of shade between tree crowns) in the remaining tree crown areas of the image. If this threshold was determined too high, the shaded parts of tree crowns may also get masked out. In contrast, if setting too low, some separation of crowns within tree clusters may be hindered (Gougeon 1999). An appropriate threshold value was assigned by checking the image section which DN can distinguish between tree crowns and shade surrounding areas. View angle, forest density, species composition, forest type affect to the lower threshold. However, the upper threshold value, in this case, was not defined because the non-forest areas already mask out. Subsequently, border pixels from lower threshold filtering were removed to derive an individual tree crown. However, it does not always fully separate them from their neighbours especially in the dense tree crown. That should be accepted as the limitation.

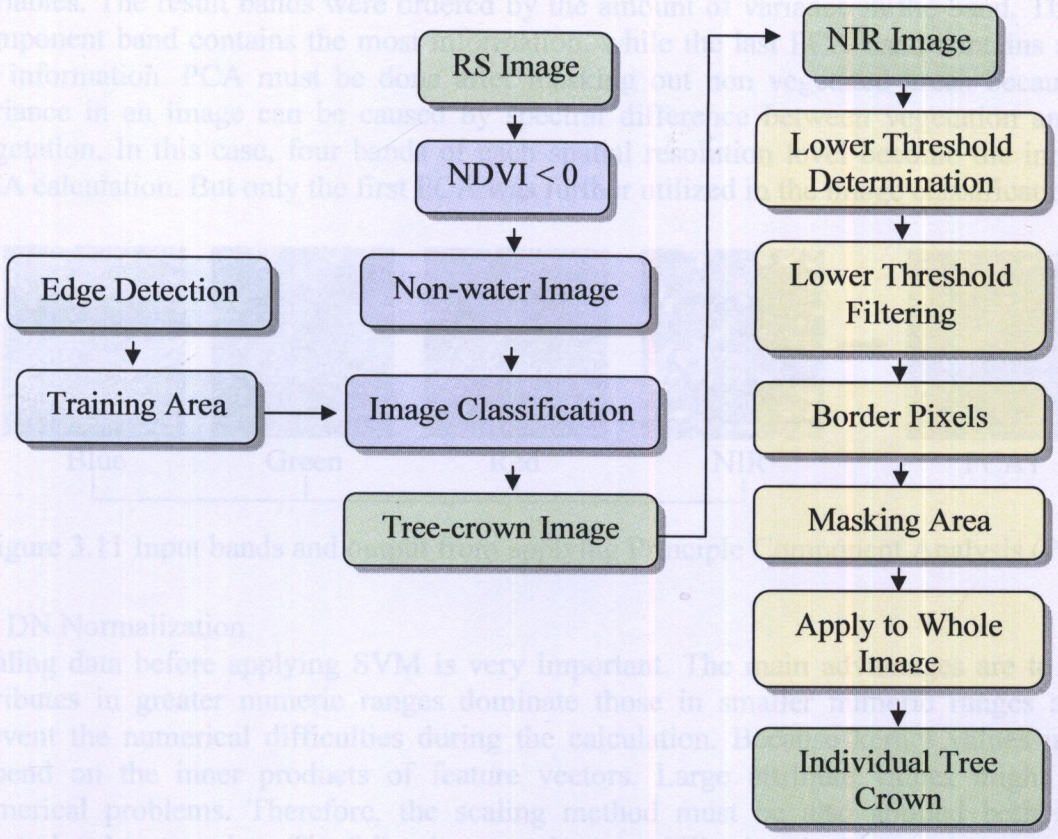

Figure 3.9 Overviews of non-tree crown elimination and individual crown segmentation

3.2.2.3 Data reduction and VI Calculation

(1) Spatial resolution upscaling

To serve the objectives of this research, original pan-sharped images with spatial resolution, 0.6 m, were upscaled two and three times respectively by nearest neighbor resampling method. According to figure 3.10, left image represents tree crown 0.6 m, while the middle shows resolution 1.2 m and right hand illustrates 1.8 m. The gradient resolutions of image are evaluated to find out the minimum resolution for tree crown delineation in the tropical rain forest.

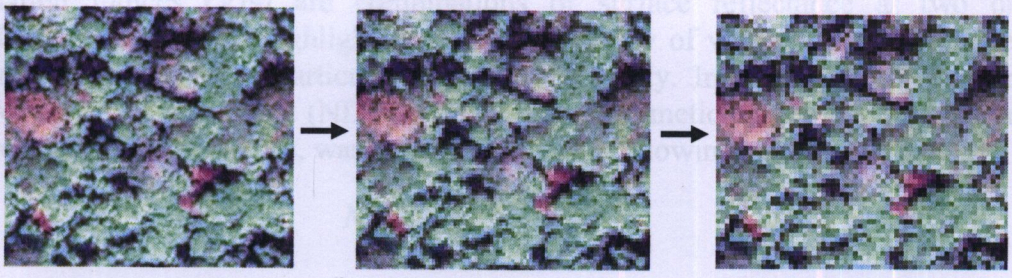

Figure 3.10 Different spatial resolution of multi-spectral image: 0.6, 1.2 and 1.8 m from left to right

(2) Principle Component Analysis

PCA is a procedure for transforming a set of correlated variables into a new set of uncorrelated variables. This transformation is a rotation of the original axes to new orientations that are orthogonal to each other and therefore there is no correlation between

variables. The result bands were ordered by the amount of variance in the band. The first component band contains the most information, while the last PCA band contains almost no information. PCA must be done after masking out non vegetated areas because the variance in an image can be caused by spectral difference between vegetation and non vegetation. In this case, four bands of each spatial resolution level become the input for PCA calculation. But only the first PCA was further utilized in the image classification.

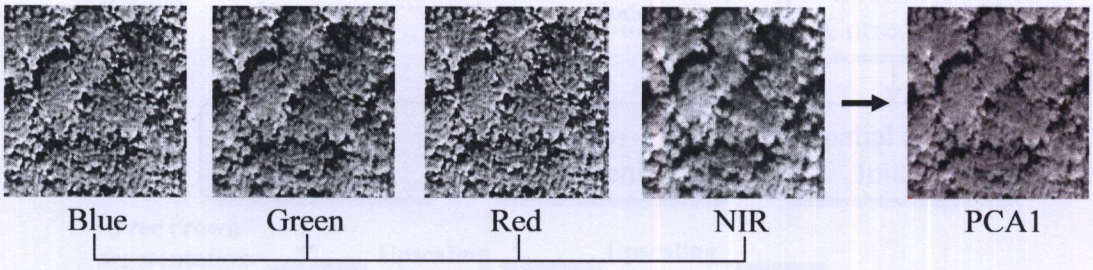

Figure 3.11 Input bands and output from applying Principle Component Analysis (PCA)

(3) DN Normalization

Scaling data before applying SVM is very important. The main advantages are to avoid attributes in greater numeric ranges dominate those in smaller numeric ranges and to prevent the numerical difficulties during the calculation. Because kernel values usually depend on the inner products of feature vectors. Large attribute values might cause numerical problems. Therefore, the scaling method must be also applied both to the spectral and texture data. The following equation was utilized to do that.

$$\frac{(DN - MIN_{image}) * (\max - \min)}{(MAX_{image} - MIN_{image}) + \min} \qquad (27)$$

MIN_{image} : minimum DN of image
MAX_{image} : maximum DN of image
max : maximum range of new scale
min : minimum range of new scale

4) Vegetation Index extraction

Vegetation Indices (VIs) are combinations of surface reflectance at two or more wavelengths designed to highlight a particular property of vegetation. Each of the VIs is designed to accentuate a particular vegetation property. In this study, only normalized differential vegetation index (NDVI) which is the arithmetic combination of red and near infrared spectral band values, was concentrated. The following equation is applied

$$NDVI = \frac{P_{NIR} - P_{RED}}{P_{NIR} + P_{RED}} \qquad (28)$$

The value of this index ranges from –1 to 1. The common range for green vegetation is 0.2 to 0.8.

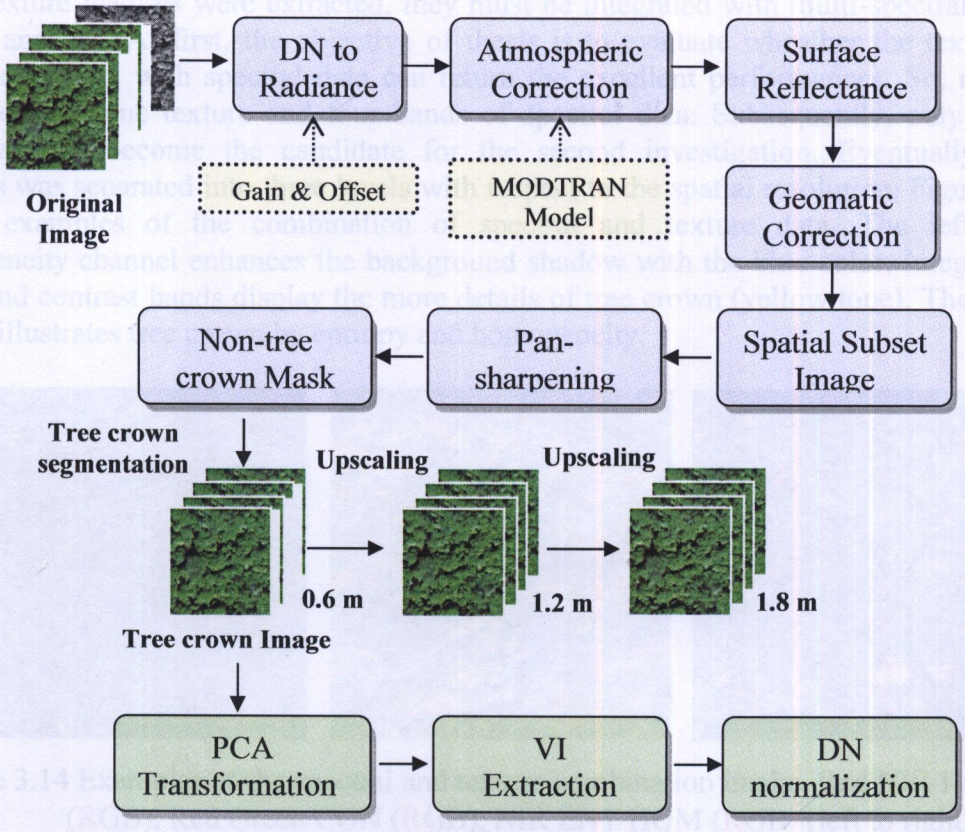

Figure 3.12 Overview of data preparation

3.2.3 Texture feature extraction

Gray Level Co-occurrence Matrix (GLCM) was used to derive the texture descriptors. First, GLCM was created with a square matrix N x N. Second, transpose matrix of GLCM was constructed to make the matrix symmetric because texture extractions are the best performed on a symmetrical matrix. In our case we apply co-occurrence measures texture filter with window size 3 x 3 and shift 1 pixel both in horizontal and vertical direction which is refers like best from previous experiences for extraction more features of image. ENVI software has eight different texture features including mean, variance, homogeneity, contrast, dissimilarity, entropy, second moment, and correlation. Three parameters were considered in this study. Values of the moving window size, distance d and direction θ were determined. Finally, values of texture data were normalized into the same intervale of spectral data (0-100).

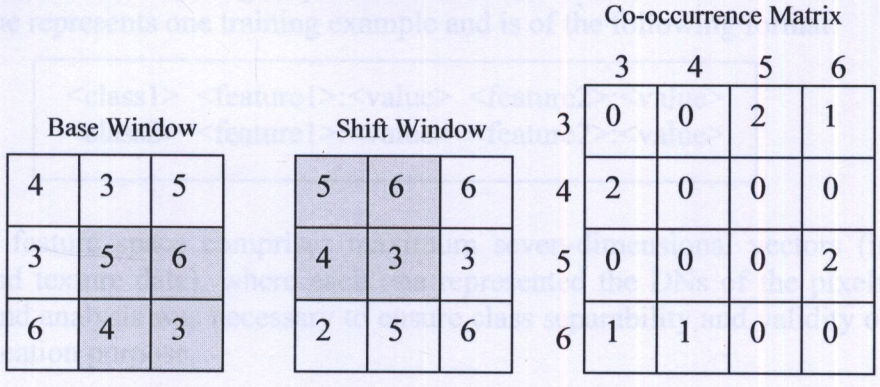

Figure 3.13 GLCM with shift window 1, 1 in vertical and horizontal direction

3.2.4 Integration of spectral and spatial data

After texture features were extracted, they must be integrated with multi-spectral data for further analysis. At first, the objective of thesis is to evaluate wheather the texture data when combining with spectral data can return the excellent performances. So, randomly stack between one texture and four bands of spectral data. Subsequently, only the best three textures become the candidate for the second investigation. Eventually, image analysis was separated into three levels with respect to the spatial resolution. Figure below is the examples of the combination of spectral and texture data. The left picture homogeneity channel enhances the background shadow with the blue color. Integration of green and contrast bands display the more details of tree crown (yellow tone). The last one clearly illustrates tree crown by entropy and homogeneity.

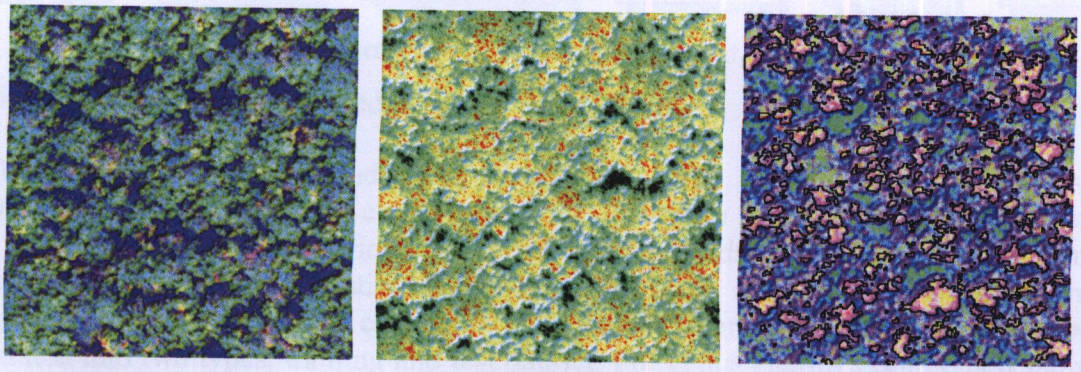

Figure 3.14 Examples of the spectral and texture combination image. Red NIR HOM (RGB), Red Green CON (RGB), NIR ENT HOM (RGB) (left to right)

3.2.5 Generating genus & species Signature

Spectral and textures signatures were acquired to be representatives of genus and species. The exact locations from GPS were overlaid on the tree crown image. Afterward, the manual digitizing was carried out on the screen to create ROI files (Region of Interest). Approximately 60 points were selected for the training and test data.

3.2.6 Image Classification by SVM

Tree genus classification was delineated by free source code in C. SVM^{light} version 6.0 was an implementation of Vapnik's SVM for the problem of pattern recognition based on the binary classification (-1, +1). SVM^{light} consists of a learning module (SVM_learn) and classification module (SVM_classify). With this software, user can determine the parameter configurations such as learning options, performance estimation, kernel types. To meet the requirement of software, image input must be converted to ASCII file format. The input file contains the represents one training example and is of the following format:

```
<class1> <feature1>:<value> <feature2>:<value>
<class2> <feature1>:<value> <feature2>:<value>
```

The input feature space comprises maximum seven-dimensional vectors (integration of spectral and texture data), where each one represented the DNs of the pixels. Initial data statistics and analysis was necessary to ensure class separability and validity of traiing sites for classification purpose.

For example: +1 1:235 2:123 3:24 ----> Positive class
-1 1:34 2:64 3:56 ----> Necgative class
0 1:434 2:64 3:98 ----> Unseen data

The class value belonging to the target and non-target class and each of the feature number were separated by a space character. Feature value indicates the number of band. Specially, feature/value must be ordered by increasing feature number. The value targets were possible three values: positive (+1), necgative (-1) and unseen data (0). This code is available from http://download.joachims.or/svm_light/current/.

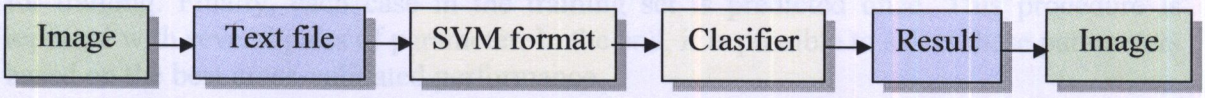

Figure.3.15 Overall processess for file format conversion

Following issues were performed in SVM source code.

(1) Determination of training and tested dataset

In order to make a decision for classification, it is necessary to know the spectral signature and texture feature characteristics of the training and test dataset. The number of sample observations has a direct relationship to the confidence interval of the estimation of classification accuracy and the estimation of statistical parameters. Then this dataset were separated into two types, training and test dataset. For genus classification, 6,000 samples were reserved for training and remaining 4,412 for decision model evaluation. Training signatures is based on DN values and independent of trainingsite location. So, x and y coordinate field not includes in the traing dataset.

(2) Mapping input data into the high dimension feature space

Due to the nonlinear decision function, the original data in term of x, y and z values were transformed into the higher dimensional dot product feature space by the function of Φ. In this case, five and seven dimensions of input data were considered (spectral and texture features).

(3) Kernel model selection

By mapping the input data to the high-dimensional space, the kernel function converts non-linear boundaries in the original data space into the linear ones in the high-dimensional space, which can then be located using an optimization algorithm. Kernel functions have to be chosen carefully since an inappropriate kernel can lead to poor performance. There is a kernel function K such that

$$K(x_i, x_j) = \Phi(x_i) \cdot \Phi(x_j) \qquad (29)$$

(4) Determination of kernel configuration

The accuracy of an SVM model is largely dependent on the selection of kernel parameters. SVM include *C* penalty parameter that allows a certain degree of misclassification which is particularly important for non-separable training sets. The penalty parameter controls the trade-off between allowing training errors and forcing rigid margins. It creates a soft margin that permits some misclassifications, such as it allows some training points on the wrong side of the hyper-plane. Increasing the value of *C*, increases the cost of misclassifying points and forces the creation of a more accurate model that may not generalize well. Usually *C* and γ parameter must be expressed in exponential value such as $C = 2^{-5}, 2^{-3}, .., 2^{13}$; $\gamma = 2^{3}, 2^{1}, .., 2^{-15}$.

(5) Tested Data
Beforehand it is impossible to know which combination penalty parameter and kernel parameter will result in the highest performance when validating the trained SVM to unseen data. Grid search on C, γ, d and a v-fold cross-validation on the training data. Cross-validation was a widely used technique to estimate the generalization error of a classifier for a limited number of gathered data. The goal of this procedure is to identify the optimal parameters, so that the classifier can accurately predict unseen data (entire data). In a v-fold cross-validation, the training data is split into v subsets of equal size. Iteratively, one part is left out for validation, while the other remaining (v-1) parts are used for training. Finally, each case in the training set is predicted once. This procedure is repeated with several pairs of parameter. In the end, it is possible to select these parameters based on the best cross-validated performance.

(6) Kernel Adjustment
If the test output is not the optimal solution, the selection of the kernel must be adjusted and the support vector machine may be retrained and retested. For RBF kernel, C and γ can be adjusted. For polynomial kernel, C, γ, r (bias term) and degree (d) can also be developed. When it is determined that the optimal solution has been identified, the entire datasets are inputted into the learning machine for processing.

(7) SVM classification through unseen data
After achieving the solution with the optimal separating hyper-plane from test SVM, unseen data were transferred into the SVM classifier by the kernel that produced the optimal solution. SVM classification output is the decision values of each pixel for each class, which are used for probability estimates. The probability values fall in the range of 1- to 1. Subsequently the class segmentation was conducted.

3.2.7 Image processing for tree crown delineation

3.2.7.1 Tree genus classification

The conceptual framework for tree crown classification into tree genus can be divided into 3 scenarios.

(1) The first scenario: Classification based on spectral information

SVM Classifier utilizes only spectral data for tree crown classification with the different four types of kernel function and different combinations of kernel configuration (C, γ, d). In this concept, only multi-spectral data are examined. The optimal separating hyper-plane for each kernel will be constructed with the different combination of kernel configuration (C, γ, d). The threshold value for each parameter is determined and increased equally in next iteration. Subsequently, the comparisons of three kernel performances were conducted. The goals of this scenario are to find the appropriate kernel and the best parameter values for tree crown classification into tree genus.

(2) The second scenario: Classification with spectral and texture information

The combinations of spectral and texture data were the input data. Eight texture features derived from GLCM method were incorporated in the analysis to explore the possibility to improve the genus classification capacities by the SVM algorithm. For the first round, one by one texture selection was done to be integrated with the spectral data. Subsequently, SVM classification was applied, and the performances were summarized. For the second round, only texture feature which take the performance ranking of the first, second and third become the input data for the next SVM classification. Three texture and four spectral data were combined together and SVM classification was repeated. The best parameter values from the first scenario were assigned for the kernel functions. The targets for this scenario are to find the best texture that can improve the classification power of SVM. At the same time, the capacities of kernel functions were tested.

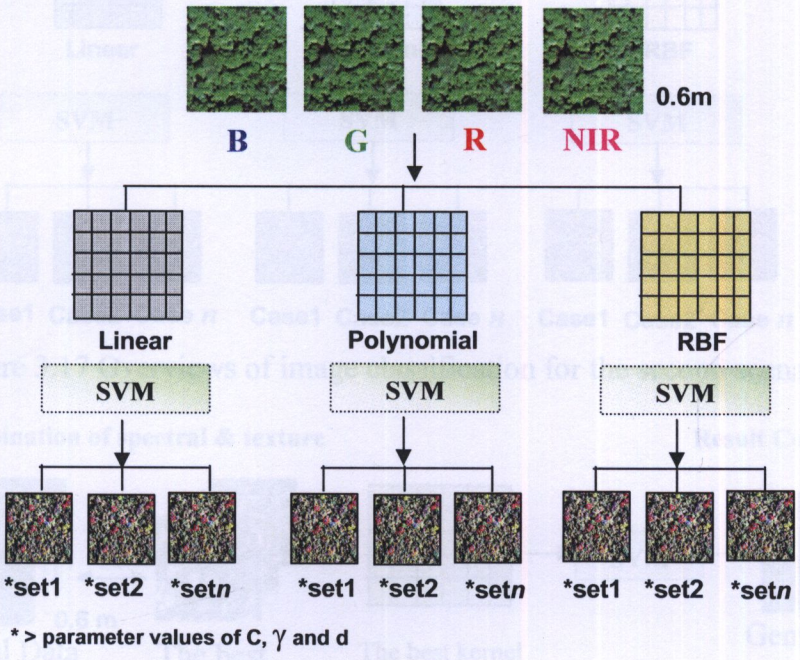

Figure 3.16 Overviews of image classification for the first scenario

(3) The third scenario: The minimum spatial resolution for tree crown delineation

To examine the minimum spatial resolution that can support tree crown delineation to specific genus, the imagery with the different pixel size needs to be compared the capacities. Upscaling and downscaling are the method to decrease and increase the spatial resolution. In this concept, the original panchromatic resolution and pan-sharpening resolution with 0.6m were increased. Two and three times in the pixel size of original resolution were applied for the whole image. Therefore, the input data in this concept comprises the three different spatial resolutions of 0.6, 1.2 and 1.8m. Similarly, three of the optimal textures from previous experiment were integrated with four of multi-spectral bands. SVM classification processes were repeated at three times for each pixel size image. At the end, the spatial resolution of image that suitable for tree crown analysis in the tropical rain forest was obtained when concerning an accuracy of image classification. In this scenario, only the best kernel obtained from the first scenario was applied and the optimum of parameter value sets were utilized.

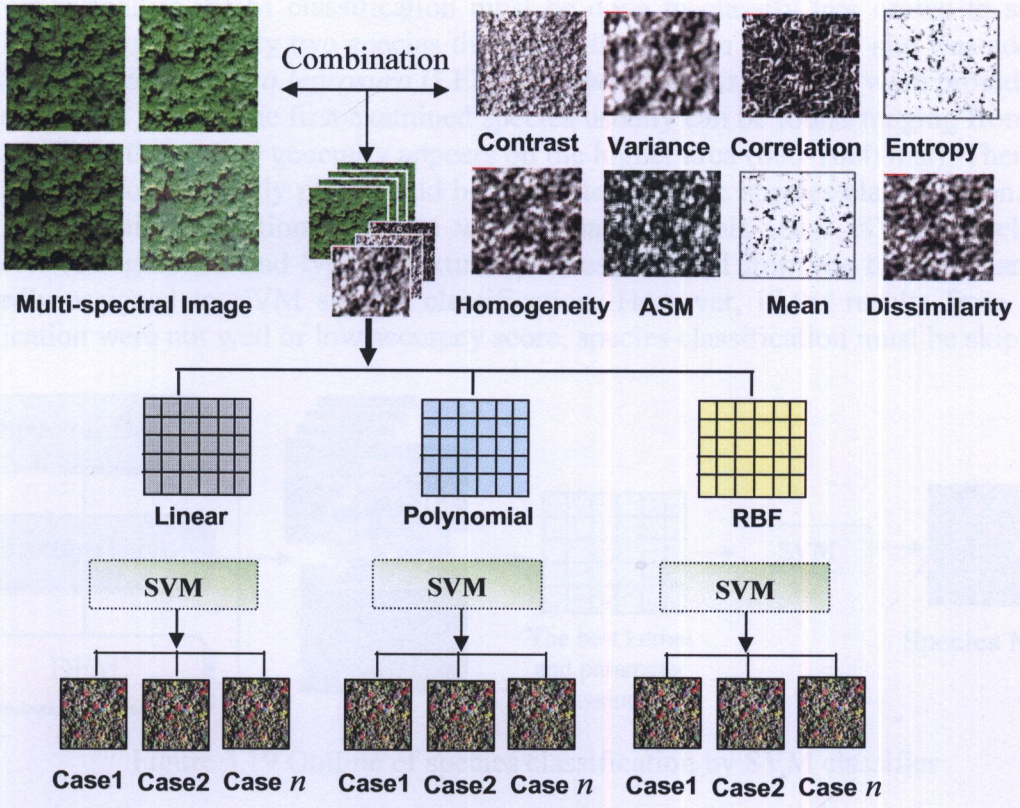

Figure 3.17 Overviews of image classification for the second scenario

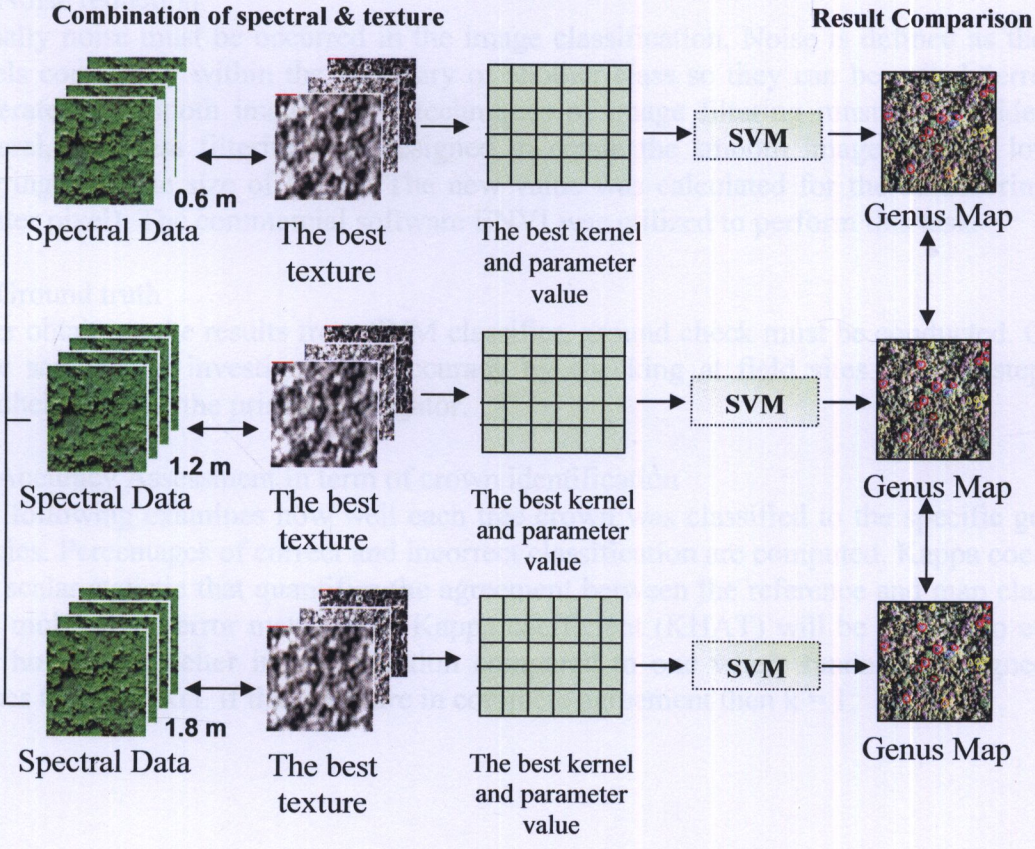

Figure 3.18 Overall processes of the third scenario analysis

3.2.7.2 Tree species classification

To advance analyze, SVM classification must be done to classify tree crown to species level. In this situation, only two species that were dispersal in the study site was adopted. The training data of *Shorea leprosura* (LEP) and *Shorea curtisii* (CUR) were provided for species analysis. In fact, the first examined species usually can be found ranging from 200-600 msl. While the second generally appears on the higher area (600-1000 msl). Therefore, DEM available on the study plot should be integrated into the species classification. Only image with spatial resolution of 0.6 m was evaluated. In this sense, SVM kernel type, parameter configuration and type of texture features obtained from the third scenario are repeatedly assigned to SVM species classification. However, if the results from genus classification were not well or low accuracy score, species classification must be skipped.

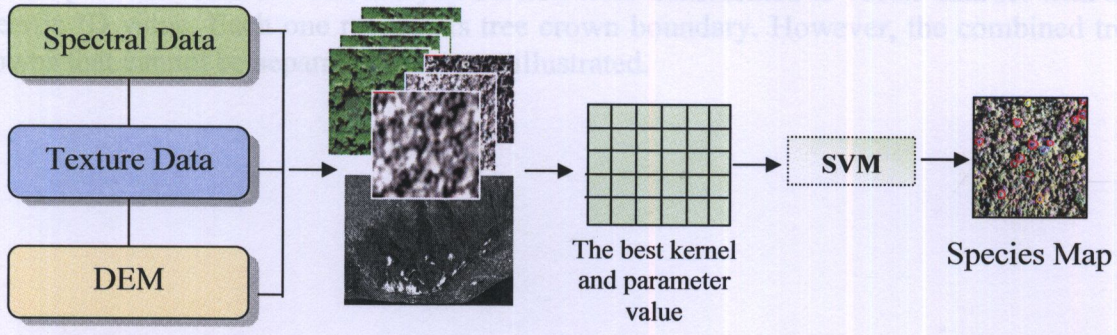

Figure 3.19 Outline of species classification by SVM classifier

3.2.8 Post classification

(1) Noise reduction

Usually noise must be occurred in the image classification. Noise is defined as the small pixels completely within the boundary of another class so they can be called "error". To generate the smooth image, some techniques of image filtering must be considered. In general, low pass filtering was designed to create the smooth image. Hence, low pass filtering with the size of kernel. The new value was calculated for the considering pixel (center pixel). The commercial software ENVI was utilized to perform this task.

(2) Ground truth

After obtaining the results from SVM classifier, ground check must be conducted. Outputs were sampled to investigate the accuracy by checking at field sites. In this step, GPS handheld become the primary navigator.

(3) Accuracy Assessment in term of crown identification

The following examines how well each tree crown was classified to the specific genus or species. Percentages of correct and incorrect classification are computed. Kappa coefficient is a scalar statistic that quantifies the agreement between the reference and map classifiers in a multivariate error matrix. The Kappa coefficient (KHAT) will be applied to evaluate that how much better in classification compared to one where randomly assigned class values to each pixel. If the raters are in complete agreement then $k = 1$.

If there is no agreement among the raters (other than what would be expected by chance) ,then $k \leq 0$. Values of kappa exceeding 0.6 were considered good (Czaplewski, 1994). The equation used for this assessment is following:

$$K = \frac{Pr(a) - Pr(e),}{1 - Pr(e)} \tag{30}$$

or Kappa = (Observed agreement - Chance agreement) / (1 - Chance agreement)
Where Pr(a): the relative observed agreement among raters
Pr(e): the probability that agreement is due to chance

(4) Output Vectorization
The outputs derived from data analysis session were transformed to vector data set with the specific ID value. Each one represents tree crown boundary. However, the combined tree crowns that cannot be separated also were illustrated.

CHAPTER IV

RESULTS AND DISCUSSIONS

4.1 Non tree-crown Elimination

Recent progress in RS makes it feasible to extract non-tree crown regions. Laplacian edge detection is very useful for image segmentation. Supervised classification based on the maximum likelihood rule can effectively separate non tree-crown from the tree crown image using training signatures. Masking image was created to be used to eliminate pixels corresponding to masked zone. Tree crown bitmaps were obtained. The total non tree-crown areas in the study plot were approximately 64.024 % or 0.318 sq.km. So, it means that tree crown segments remain only 0.17 sq.km. Figure 4.1 and 4.2 display the results after running the process to detect non tree crown.

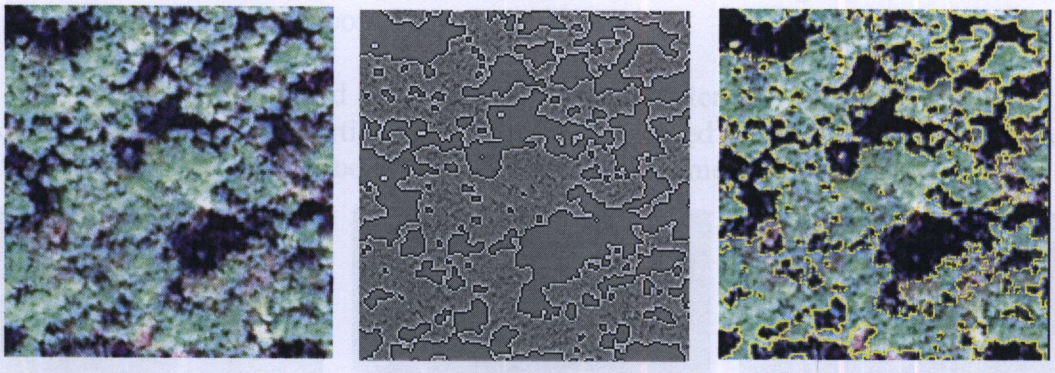

Figure 4.1 Laplacian Edge detection for non tree-crown segmentation. Original image (Left), output image (middle), edge boundary overlaid on an original image (Right)

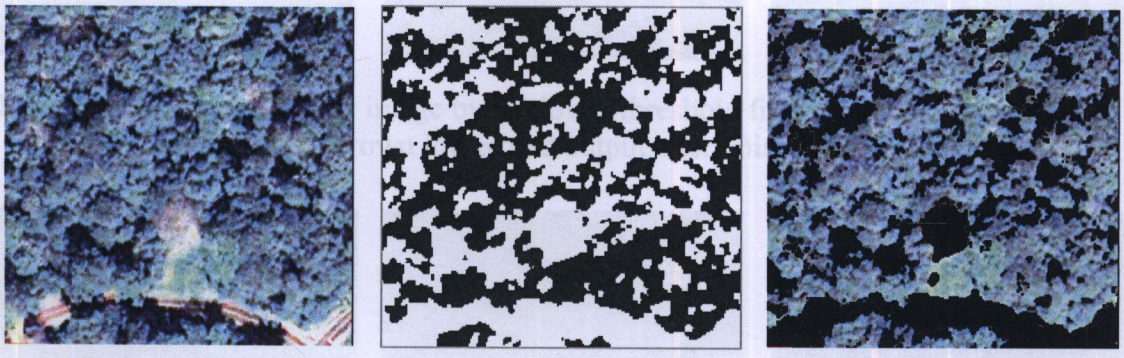

Figure 4.2 RGB image (left), non tree-crown area detection (middle) and masked out image (right)

4.2 Individual Tree Crown Segmentation

The DN manual checking and histogram frequency distribution were performed on the near-infrared image. This process was repeated until the low threshold value that can separate tree crown was obtained. In this experiment, the lowest threshold value assigned for further segmentation equal 180. Figure 4.3 shows the histogram of DN mean value of NIR image indicating the initial low DN. With the following threshold, the individual tree crown was possible to obtain.

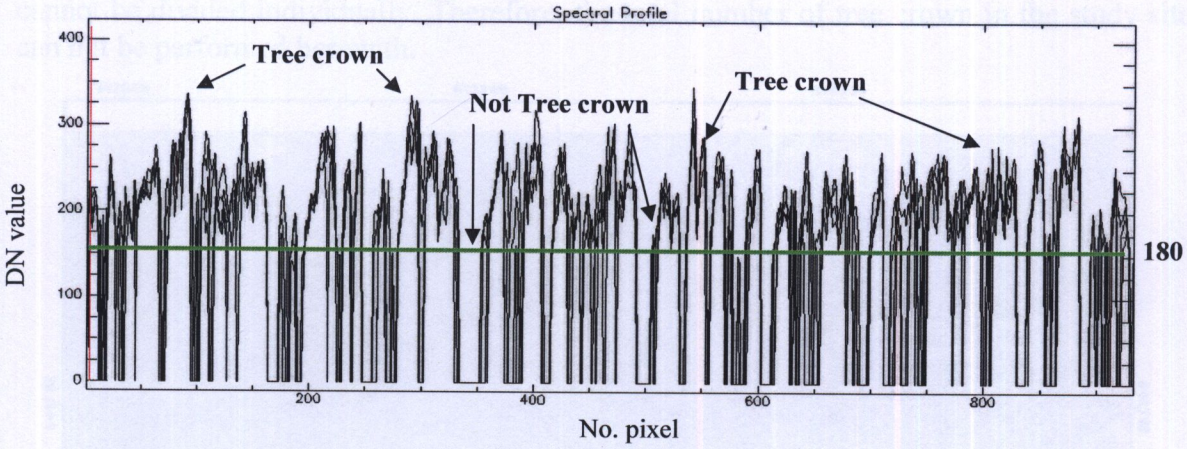

Figure 4.3 Spectral Profile of near-infrared band in one line using to determine the low threshold value, pointing out at DN 180

The image segmentation based on the lower threshold filtering was rather well to separate the continuous tree crown particularly for the tiny-merged pitches (figure 4.4). However, the dense tree crowns can not be split to an individual segment (figure 4.5).

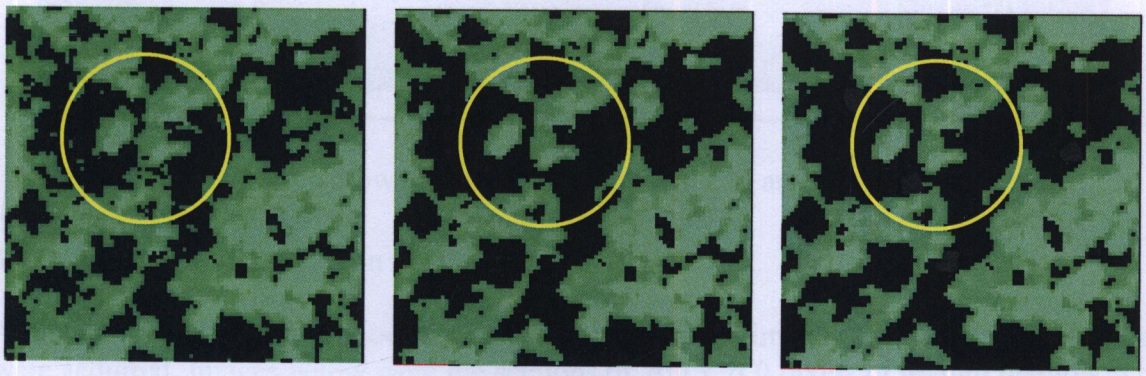

Figure 4.4 Section of output image by the lower threshold filtering. The original image, individual tree crown image and output after noise filtering (left to right)

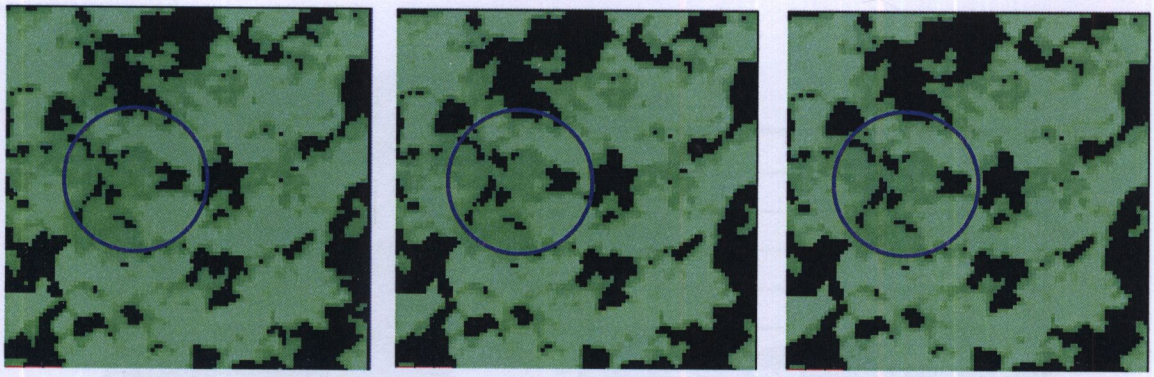

Figure 4.5 Section of tree crown that can not be divided by the lower threshold filtering. The original image, individual tree crown and filtered image (left to right)

Figure 4.6 indicates the tree crown in the study site. It notices that the some polygons cannot be divided individually. Therefore, the total number of tree crown in the study site can not be performed herewith.

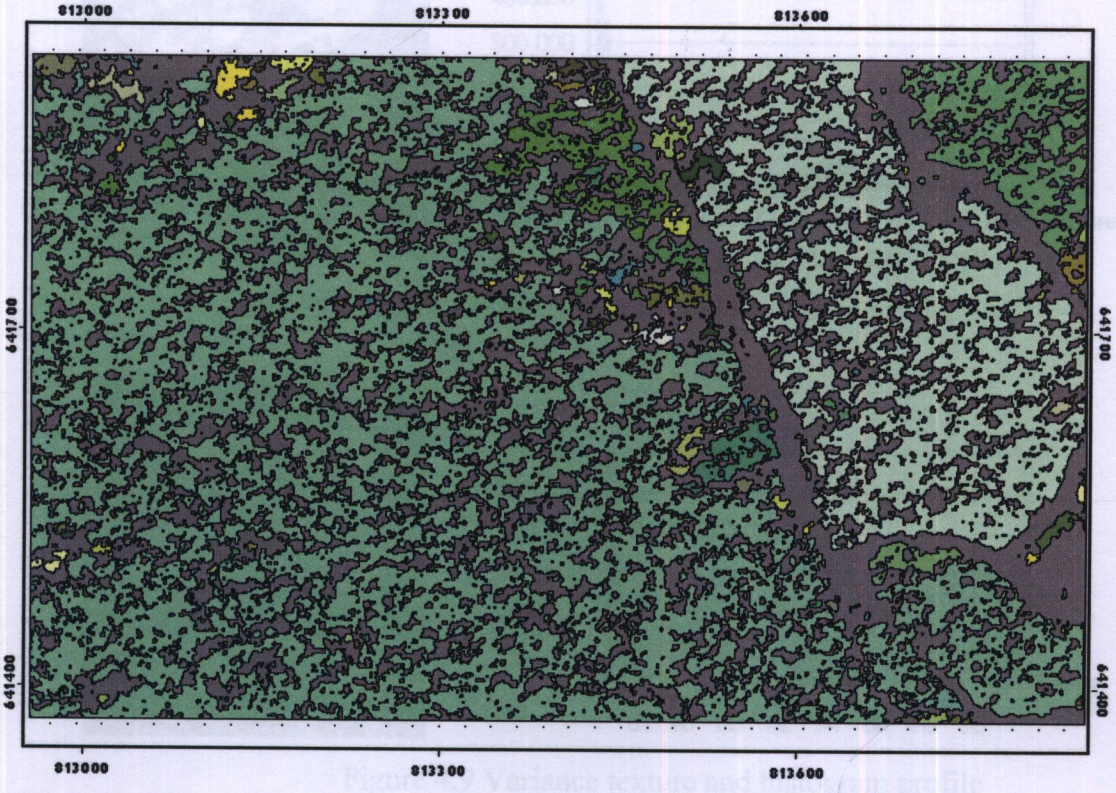

Figure 4.6 Map of tree crown after segmenting image to an individual tree crown

4.3 Texture Feature Extraction

After applying GLCM method to the segmented-crown image, various texture features were acquired. Images below were the sections of 200 x 200 pixels of texture features. The result images were calculated from panchromatic band using GLCM with kernel 3x3 shift 1, 1 pixel in both directions. Finally, the results were normalized to the same scale 0-100 to avoid the effects of the data scale. Frequency distribution histogram for each texture data was compared.

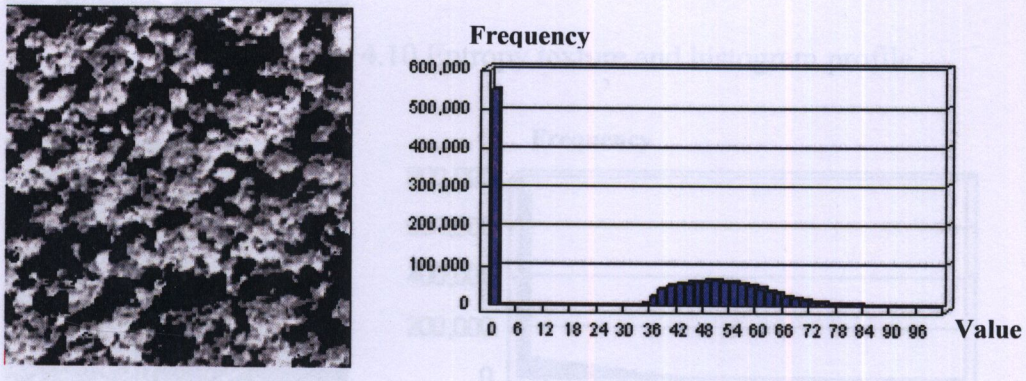

Figure 4.7 Original panchromatic image and histogram profile

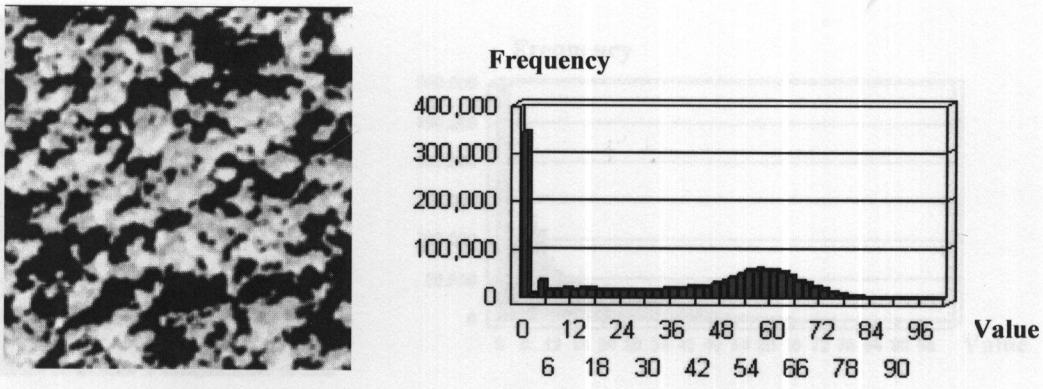

Figure 4.8 Mean texture and histogram profile

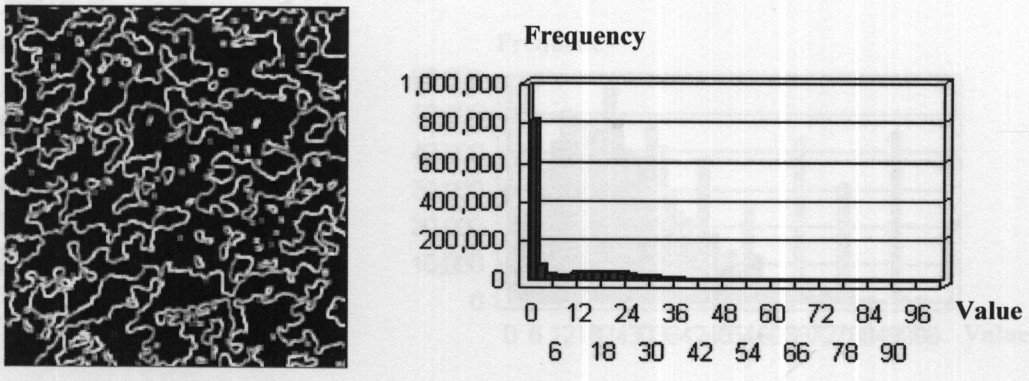

Figure 4.9 Variance texture and histogram profile

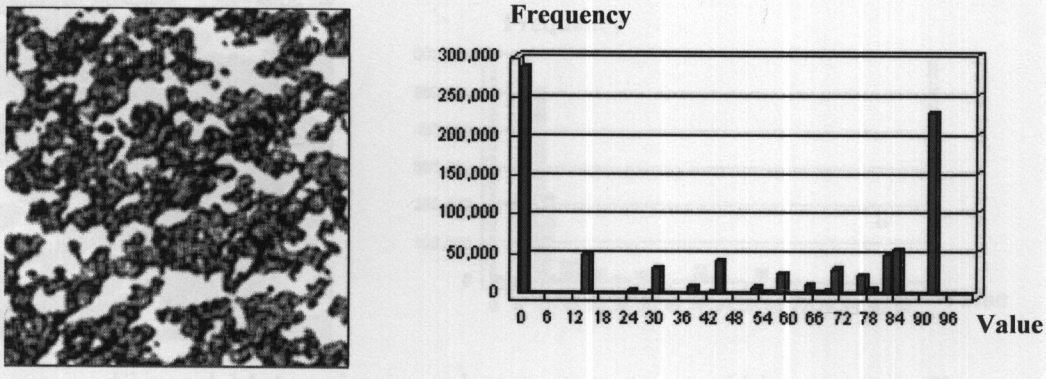

Figure 4.10 Entropy texture and histogram profile

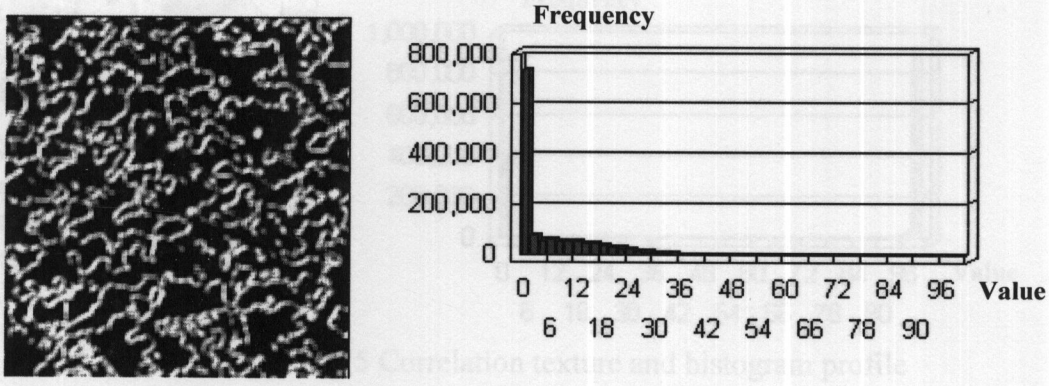

Figure 4.11 Contrast texture and histogram profile

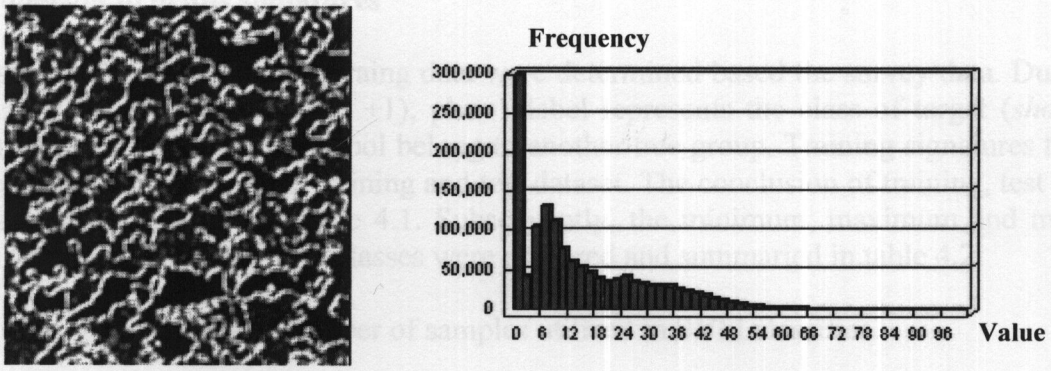

Figure 4.12 Dissimilarity texture and histogram profile

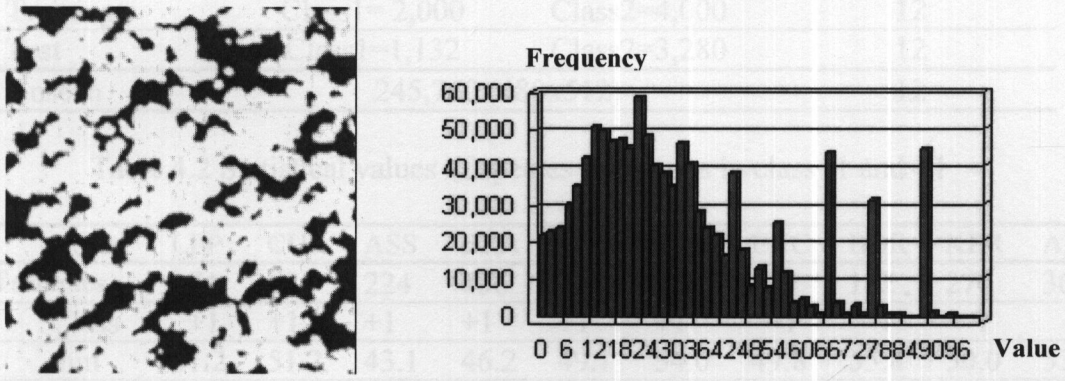

Figure 4.13 Homogeneity texture and histogram profile

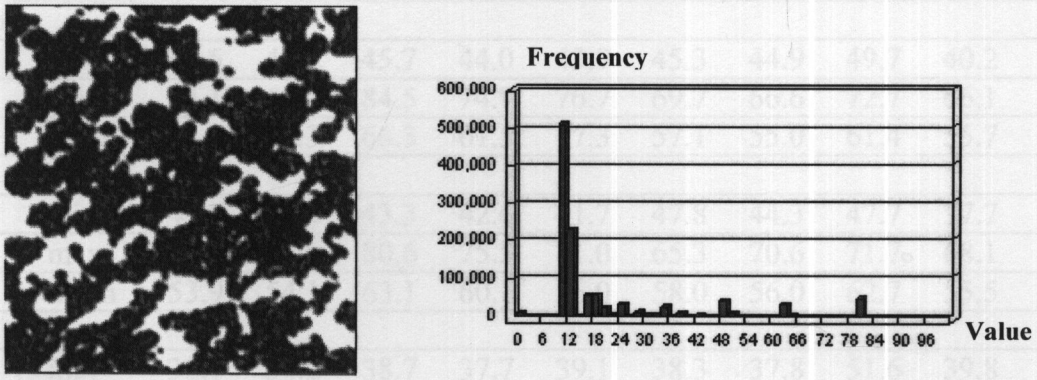

Figure 4.14 Angular second moment texture and histogram profile

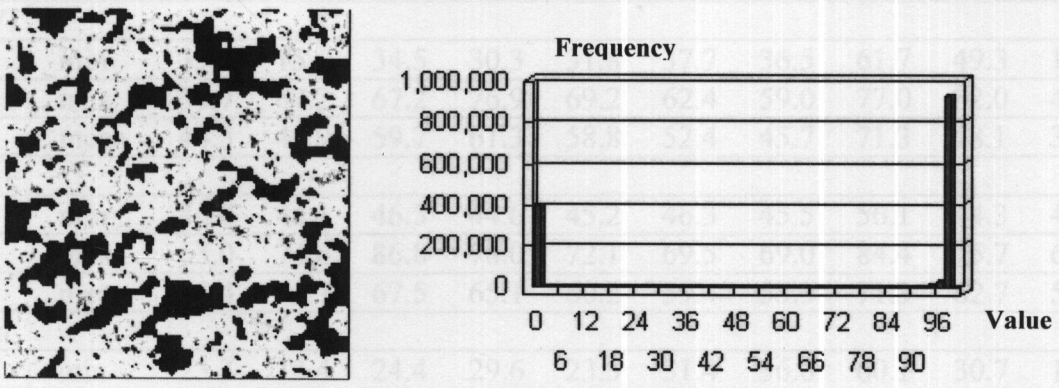

Figure 4.15 Correlation texture and histogram profile

4.4 Properties of genus signatures

Total six thousand examples of traing data were determined based the survey data. Due to the banary classification (-1 and +1), plus 1 label represents the class of target (*shorea* genus). In contrast, Minus 1 symbol belong to another tree group. Training signatures then were classified to two groups: training and test dataset. The conclusion of training, test and live data were illustrated in table 4.1. Subsequently, the minimum, maximum and mean values for each member of both classes were explored and summaried in table 4.2.

Table 4.1 Number of samples utilized in SVM classifier

Dataset	No. of samples		Data Dimensions
Training	Class1= 2,000	Class2=4,000	12
Test	Class1=1,132	Class2=3,280	12
Unseen	245,760 (480x512)		12

Table 4.2 Statistical values of species signatures in class -1 and +1

Band	Stat	LEP	CUR	ASS	BRA	PAR	STE	EXC	BOR	KER	ANI
NO.of samples		374	621	224	456	330	182	224	182	270	361
	Class	+1	+1	+1	+1	+1	+1	-1	-1	-1	-1
Blue	min	51.2	51.2	43.1	46.2	49.1	54.0	49.8	55.8	50.0	53.3
	max	73.7	88.3	82.1	84.2	86.4	77.2	74.3	77.2	73.3	69.1
	mean	62.0	64.9	66.3	66.3	64.9	64.9	62.6	67.9	63.3	59.0
Green											
	min	46.5	43.5	45.7	44.0	43.9	45.3	44.9	49.7	40.2	46.0
	max	64.1	69.2	84.5	74.9	76.7	69.7	66.6	72.7	66.1	59.8
	mean	54.0	54.3	66.3	61.5	57.3	57.1	55.0	61.4	55.7	51.1
RED											
	min	45.0	41.4	43.3	42.6	41.7	47.8	44.3	47.7	37.7	47.5
	max	63.4	76.5	80.6	75.5	71.0	65.3	70.6	71.7	68.1	62.7
	mean	53.9	54.1	63.1	60.1	56.0	58.0	56.0	62.7	55.5	53.6
NIR											
	min	32.1	34.2	38.7	37.7	39.1	38.3	37.8	51.6	39.8	34.6
	max	54.0	63.6	79.6	73.5	67.0	63.2	59.9	82.4	73.6	51.0
	mean	44.3	47.3	60.7	59.0	53.4	51.7	46.6	68.3	58.5	40.8
NDVI											
	min	33.2	15.5	34.5	30.3	31.8	37.7	36.5	61.7	49.3	18.5
	max	59.7	67.2	67.2	76.9	69.2	62.4	59.0	77.0	82.0	47.8
	mean	44.5	49.9	59.7	61.3	58.8	52.4	45.7	71.3	68.1	35.9
PCA1											
	min	46.0	44.1	46.3	44.6	45.2	46.3	45.5	56.1	44.3	44.2
	max	63.0	74.6	86.8	78.0	72.1	69.5	69.0	84.4	75.7	60.7
	mean	53.4	55.7	67.5	65.1	60.2	59.4	55.3	71.3	62.7	50.1
Mean											
	min	23.3	13.4	24.4	29.6	23.5	31.4	36.0	60.1	30.7	15.6
	max	62.1	68.9	81.6	78.1	67.6	64.7	65.8	82.7	73.2	53.1
	mean	48.6	45.3	65.7	62.8	56.4	54.9	52.8	70.9	61.5	45.5

Band	Stat	LEP	CUR	ASS	BRA	PAR	STE	EXC	BOR	KER	ANI
VAR	min	0.1	0.1	0.3	0.0	0.2	0.1	0.1	0.0	0.1	0.1
	max	33.1	35.9	54.6	46.8	40.4	28.9	30.7	2.8	22.3	26.6
	mean	5.4	11.8	11.1	5.2	7.2	3.9	3.0	1.0	1.8	4.0
HOM											
	min	3.6	0.4	0.5	3.1	0.8	4.7	3.1	3.1	2.2	9.5
	max	65.6	67.3	49.3	74.4	46.2	53.3	41.0	63.3	58.9	71.1
	mean	34.7	27.3	14.9	26.0	20.7	25.7	20.5	26.0	25.2	34.2
CON											
	min	0.1	0.1	0.3	0.0	0.2	0.1	0.2	0.1	0.1	0.0
	max	26.1	32.6	42.1	38.3	32.1	26.3	23.4	2.9	24.7	23.1
	mean	4.8	9.4	8.9	4.3	6.6	4.9	2.7	1.0	2.2	4.5
DIS											
	min	2.0	2.5	5.6	1.4	3.7	2.8	4.0	2.0	2.5	1.7
	max	40.4	57.6	57.1	53.7	46.0	48.0	34.2	15.5	47.7	41.0
	mean	12.5	21.5	23.0	13.3	16.9	13.6	11.9	8.7	10.5	11.5
ENT											
	min	64.9	59.3	76.3	57.9	83.3	76.3	66.7	76.3	79.0	64.9
	max	100	100	100	100	100	100	100	100	100	100
	mean	92.2	92.3	98.6	94.9	96.5	96.7	97.0	95.9	97.6	91.5
ASM											
	min	11.1	11.1	11.1	11.1	11.1	11.1	11.1	11.1	11.1	11.1
	max	28.4	35.8	21.0	30.9	18.5	21.0	25.9	21.0	18.5	28.4
	mean	14.1	14.3	11.6	13.1	12.4	12.3	12.3	12.6	12.0	14.3
COR											
	min	87.3	92.3	96.2	83.7	97.4	95.5	96.9	71.7	91.5	93.3
	max	100	100	100	100	100	100	100	100	100	100
	mean	99.6	99.9	99.8	99.5	99.8	99.4	99.6	98.9	99.2	99.7

LEP: *Shorea leprosura* CUR: *Shorea curtisii* ASS: *Shorea assamica* BRA: *Shorea bracteolate*
PAR: *Shorea parvifolia* STE: *Parashorea stelata* EXC: *Koompassia excelsa*
BOR: *Scorodocarpus borneensis* KER: *Dipterocarpus kerrii* ANI: *Anisoptera costata*

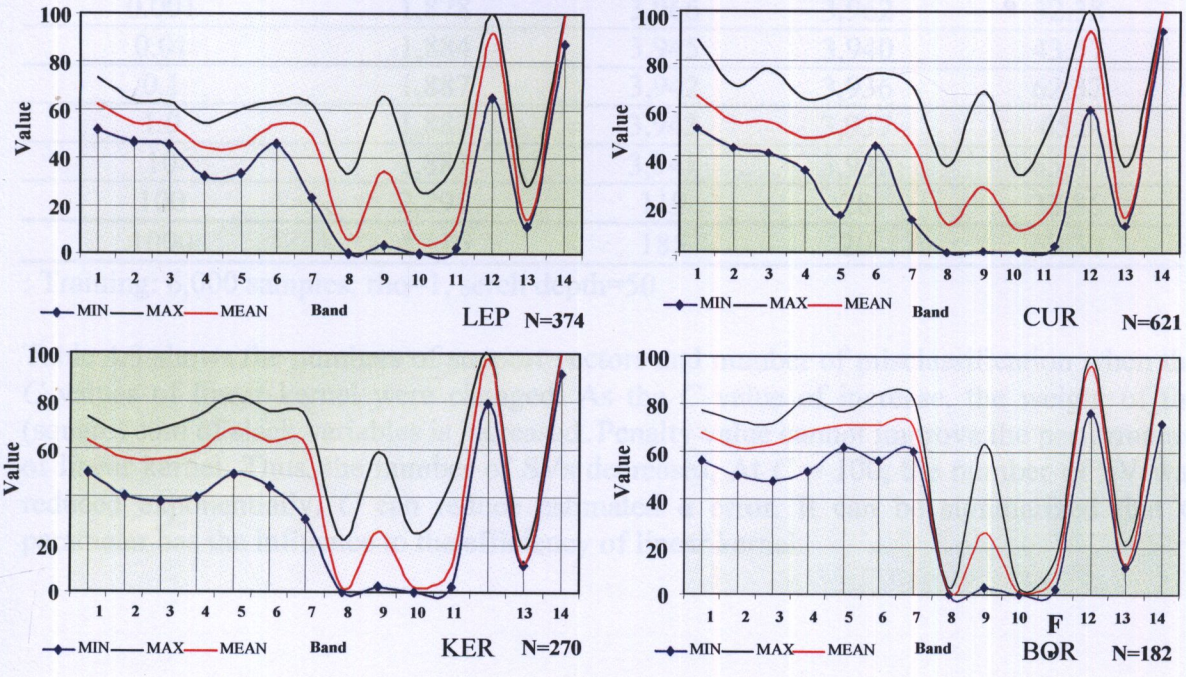

Figure 4.16 Comparison of test species responding to the DN value

Figure 4.16 displays the DN curve displaying the minimum, maximum and mean value in each channel. The representatives of *shorea* genus, *leprosura* (1) *and curtissi* (2), give the DN profile that a look similar. On the other hand, *Dipterocarpus kerrii*and (3) *Scorodocarpus borneensis* (4) representatives of another genus, have the different curve in band 8-11. With these dissimilarity made it possible to discriminate them.

4.5 Tree Genus Classification by SVM classifier

4.5.1 The first scenario: Classification based on the spectral information

For the first section of this experiment, only four spectral data were evaluated. Generalizaion performances of SVM were tested with the three different kernel functions. The combinations of kernel configuration (C, γ, d, r, s) were determined. Available options that can be setup for SVM code loosely separated into 4 groups: learning, performance estimations, kernels and output options. (See in appendix)

(1) Model performance estimation based on the soft margin SVM

To generate the optimal hyperplane, training data were transformed to the higher dimensional feature space via the kernel functions. SVM try to create the hyperplane that can separate the data with the maximum margin between two classes. The effects of kernel parameters and the margin parameter on the number of support vectors and Xi α error were compared following.

• Linear Kernel

The simplest kernel type requires only the marginal parameter (C). To find out the best parameter value, the linear kernel with the increase of penalty parameter value (C) was evaluated with the training dataset. A high value of error penalty will force the SVM training to avoid classification errors. A large value of this parameter will result in a larger search space for the QP optimizer and also time consumer.

Table 4.3 The effects of the penalty parameter to linear kernel

Penalty value (-C)	No.of misclassification	Total SVs	SVs at upper bound	Xi α error (%)
0.001	1,878	3,966	3,962	32.38
0.01	1,884	3,945	3,940	43.57
0.1	1,887	3,942	3,936	62.37
1.0	1,887	3,943	3,937	65.5
10	1,887	3,941	3,937	65.67
100	2,291	119	28	38.85
1000	4,116	185	20	69.30

: Training: 6,000 samples, rho=1, serch depth=50

Table 4.3 shows the numbers of support vectors and number of misclassification when the C values of linear kernel were changed. As the C value of increase, the weight of the (square) sum of slack variables is increased. Penalty value cannot improve the performance of linear kernel. Thus, the number of SVs decreases. At C = 100, the number of SV was reduced exponentially. C can reduce estimated α error. It can be summarized that C parameter has the influence to the efficiency of linear kernel.

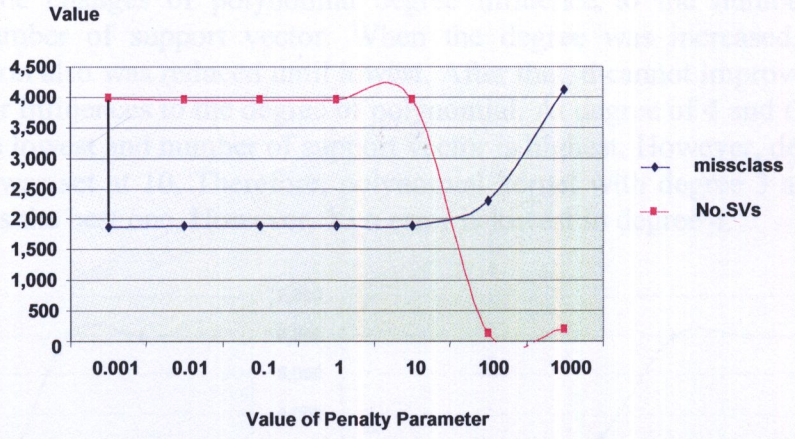

Figure 4.17 Influence of penalty value to the performance of linear kernel

Chart in figure 4.17 indicates the change pattern of number of misclassification and number of support vector. At penalty value 0.001, it should be considered as the best one due the the lowest value in the first field and highest in the second field.

• Polynomial Kernel

The degree of polynomial and marginal parameter were examined. Optionally, γ, r and s parameter can be also defined for the SVM model. Initially, the penalty value was fixed at 1.0 and 10 repsectively. In each level, polynomial degree were raised from degree 1 to degree 7. Then, the number of mixclassification, total SVs, Svs at upper bound and XiAlpha errors for each of model were observed.

Table 4.4 The effects of degree parameter to the polynomial performance *C* 1

Polynomial Degree (d)	No.of misclassification	Total SVs	SVs at upper bound	Xi α error (%)
1	3,990	789	198	67.72
2	2,000	685	0	34.2
3	2,238	521	0	37.90
4	2,000	1,381	0	33.73
5	6,000	0	0	100
6	6,000	0	0	100
7	6,000	0	0	100

: Training: 6,000 samples, Fixing $C = 1.0$, γ=1, r=1, rho=1, serch depth=50

Table 4.5 The effects of degree parameter to the polynomial performance *C* 10

Polynomial Degree (d)	No.of misclassification	Total SVs	SVs at upper bound	Xi α error (%)
1	2,838	490	8	56.05
2	3,143	664	0	58.95
3	2,261	540	0	53.51
4	3,391	1183	0	48.29
5	6,000	0	0	100
6	6,000	0	0	100
7	6,000	0	0	100

: Training: 6,000 samples, Fixing $C = 10$, γ=1, r=1, rho=1, serch depth=50

Figure 4.18 illustrates the changes of polynomial degree influence to the number of misclassification and number of support vector. When the degree was increased, the number of misclassification also was reduced until lowest. After that, d cannot improve the performance. C parameter influences to the degree of polynomial. At degree of 4 and C =1, the number of misclass is lowest and number of support vector is highest. However, degree of 3 is the best when C was set at 10. Therefore, polynomial kernel with degree 3 and 4 should be also accepted as the best one. However, Xi α error is lowest in degree 4.

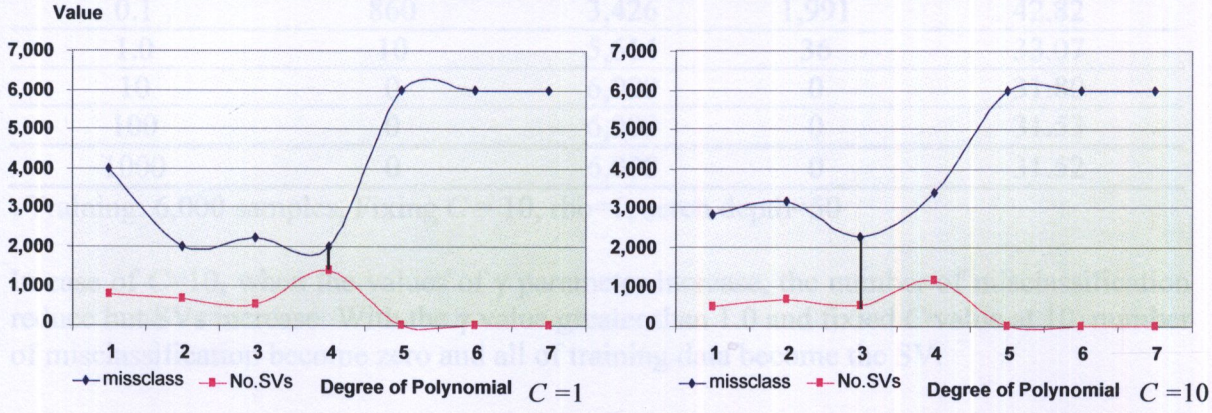

Figure 4.18 Influence of degree to the performance of polynomial kernel

Polinomial with degree 5-7 return the poor performance without support vector. It can not classify all training data correctly and estimated Xi α error equal 100%. Therefore, the maximum degree of kernel is degree 4.

• Radius Basis Function (RBF) kernel

For the last kernel, parameter C and γ were required. The various levels of gamma were investigated. C was fixed at 1.0 and 10 and gamma value was changed from 0.001 to 1000. When the γ value was reduced, the number of misclassification also was redued until equal zero. The number of SVs was increase continuously. In case of C=1, γ=0.1 give the lowest α error about 28.28%.

Table 4.6 The effects of γ parameter to the efficiency of RBF kernel, C 1

Gamma (-γ)	No.of misclassification	Total SVs	SVs at upper bound	Xi α error (%)
0.001	1,783	3,853	6,050	31.05
0.01	1,185	3,855	2,833	28.28
0.1	1,575	3,592	3,473	29.97
1.0	257	5816	1,974	30.23
10	7	5,991	1,975	32.80
100	0	5,991	1,970	32.83
1000	0	5,991	1,973	32.83

: Training: 6,000 samples, Fixing C = 1.0, rho=1, serch depth=50

Table 4.7 The effects of γ parameter to the efficiency of RBF kernel, *C* 10

Gamma (-γ)	No.of misclassification	Total SVs	SVs at upper bound	Xi α error (%)
0.001	1,696	3,745	3,712	34.03
0.01	1,482	3,443	3,241	41.82
0.1	860	3,426	1,991	42.82
1.0	10	5,614	36	33.07
10	0	6,000	0	31.80
100	0	6,000	0	31.53
1000	0	6,000	0	31.52

: Training: 6,000 samples, Fixing $C = 10$, rho=1, serch depth=50

In case of C=10, when the values of γ parameter increase, the number of misclassification reduce but SVs increase. With the γ value greater than 1.0 and fixied C value at 10, number of misclassification become zero and all of training data become the SV.

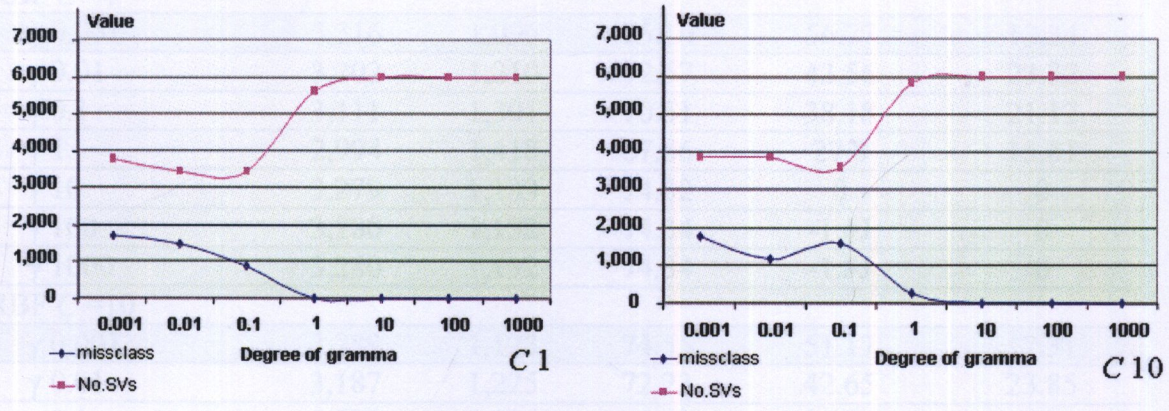

Figure 4.19 Influence of γ parameter to the performance of RBF kernel

(2) Model vadiation

The goal of model selection is to identify the model that will give the best genearization performance when appling to the test data and actual data. To validate the accuracy of SVM model, they must be applied to the test dataset. 4,312 samples were classified by the SVM model. The accuracy of each one was summarized in table 4.8.

Table 4.8 model validation performance trade-off

Model	No.of correct	No. of incorrect	Accuracy (%)	ξα-estimator of precision	ξα-estimator of recall
Linear kernel					
C 0.001	3,404	1,008	77.15	62.60	27.21
C 0.01	3,373	1,039	76.45	58.38	28.62
C 0.1	3,367	1,045	76.31	57.67	28.89
C 1	3,368	1,044	76.34	57.77	28.89
C 10	3,368	1,044	76.34	57.77	28.89
C 100	2,648	1,764	60.02	36.68	76.86
C 1000	1,275	3,137	28.90	18.66	52.74

Model	No.of correct	No. of incorrect	Accuracy (%)	ξα-estimator of precision	ξα-estimator of recall
Polynomial C =1					
degree 1	1,137	3,275	25.77	25.69	100
degree 2	3,280	1,132	74.34	-1.#J	0
degree 3	2,970	1,442	67.32	40.11	55.57
degree 4	3,280	1,132	74.34	-1.#J	0
Polynomial C =10					
degree 1	1,891	2,521	42.86	29.51	88.34
degree 2	2,285	2,127	51.79	21.06	61.98
degree 3	2,694	1,718	61.06	69.17	36.38
degree 4	1,812	2,600	41.07	17.64	35.34
Polynomial C =100					
degree 1	1,775	2,637	40.23	27.18	79.15
degree 2	2,285	2,127	51.79	21.06	31.98
degree 3	2,694	1,718	61.06	69.17	36.38
degree 4	1,812	2,600	41.07	17.64	35.34
RBF C =1					
γ 0.001	3,316	1,096	75.16	56.77	13.34
γ 0.01	3,202	1,210	72.57	43.56	23.32
γ 0.1	3,111	1,301	70.51	38.18	21.12
γ 1	2,994	1,418	67.86	27.8	15.81
γ 10	3,279	1,133	74.32	0	0
γ 100	3,280	1,132	74.34	-1.#J	0
γ 1000	3,280	1,132	74.34	-1.#J	0
RBF C =10					
γ 0.001	3,289	1,123	74.55	51.17	17.31
γ 0.01	3,187	1,225	72.23	42.65	23.85
γ 0.1	3,028	1,384	68.63	34.75	25.35
γ 1	2,994	1,418	67.86	27.80	15.81
γ 10	3,268	1,144	74.07	16.67	0.27
γ 100	3,280	1,132	74.34	-1.#J	0
γ 1000	3,280	1,132	74.34	-1.#J	0

According to the estimated accuracy, linear and RBF kernel function give comparable accuracy. But polynomial shows the poor performance. Linear kernel with C 0.001 providedsthe best accuracy score and lowest ξα-estimator of recall. The scatter plot of SVs in the figure 4.20 displays the probability score in x axis and number of pixel in y axis. It show the position of SV by utilizaing the value $\alpha^*\gamma$ derived from the SVM model calculation. The SVs that placed closed to the target line (-1, +1) have the probability to classify belonging to the class (-1 or +1). While the SVs that were plotted around the zero axis possible identifying as the case of unclassify. In the case of polynomial, degree 2 and 4 (C=1) returns the best. In RBF kernel, $\gamma = 0.001$ is the best parameter both in C=1 and 10.

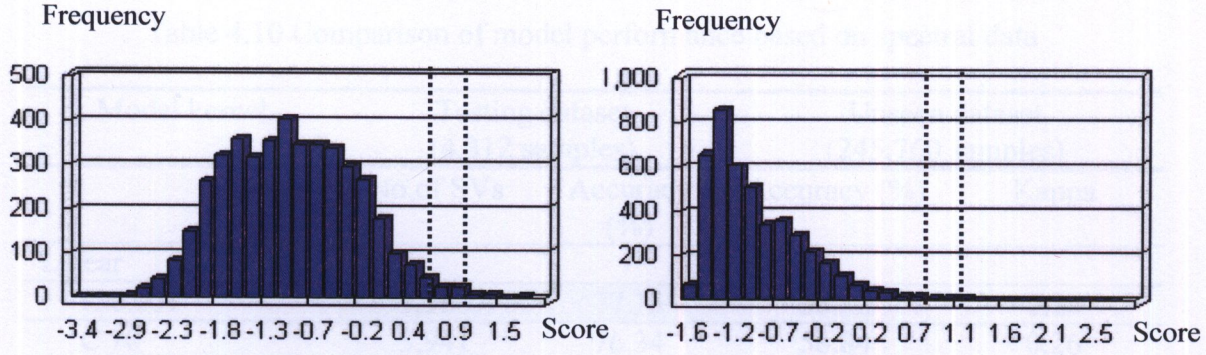

Figure 4.20 Frequency distribution of probability score (left) linear *C* 0.001, (right) RBF *C* 10 γ 0.001

(3) Apply the best model to the actual dataset

Referring to the results of above table, the eleven candidate models were adopted to analyze the unseen data. For the linear kernel, model with the *C* value equal 0.001, 1, 10 and 1,000 were selected. While the polynomial models with degree 2, 3, 4 at *C*= 10 were promoted. For the last group, RBF model with γ 0.001, 10, 100 at *C*= 10 and γ 0.001at *C*= 100 were considered.

As the results of SVM classify, the several hyperplanes were constructed to separate the data into two classes based on the probability value which class it belong to. Therefore, to achieve only two class results, the range of each class must be carefully considered. Some frequency distribution charts shown in below must be concerned (See appendix for full version).

Table 4.9 Statistics of probability scores in different types of SVM model

Kernel Model	Maximum Score	Minimum Score	Mean Score	Std Score	Pixels Class+1	Pixels Class-1
Linear kernel						
C 0.001	-3.81	4.83	0.052	0.73	51,156	245,760
C 10	-3.95	5.22	0.10	0.78	42,688	245,760
C 100	-1.23	2.63	0.27	0.38	66,146	245,760
C 1000	-3.14	2.47	-0.21	0.50	15,848	245,760
Polynomial*C*=10						
degree 2	-5.11	1.81	-2.16	2.34	11,601	234,159
degree 3	-22.86	1.99	-0.45	1.27	62,653	183,107
degree 4	-6.40	1.50	-2.73	2.64	18,660	227,100
RBF *C* =10						
γ 0.001	-3.97	6.38	-0.56	1.23	34,485	211,275
γ 10	-1.0	0.88	-0.58	0.32	0	245,760
γ 100	-1.0	0.18	-0.58	0.32	102	245,658
RBF *C* =10*0*						
γ 0.001	-9.3	6.25	-2.37	3.22	37,445	208,315

Table 4.10 Comparison of model performance based on spectral data

Model kernel	Testing dataset (4,312 samples)		Unseen dataset (245,760 samples)	
	No.of SVs	Accuracy (%)	Accuracy (%)	Kappa
Linear				
C 0.001	3,966	77.15	56.32	0.26
C 10	3,941	76.34	56.84	0.26
C 100	119	60.02	60.63	0.30
C 1000	185	28.90	22	-0.51
Polynomial *C* =10				
degree 2	664	51.79	42.44	-0.06
degree 3	540	61.06	56.56	0.18
degree 4	1183	41.07	34.22	-0.23
RBF *C* =10				
γ 0.001	3,745	74.55	57.89	0.22
γ 10	6,000	74.07	-	-
γ 100	6,000	74.34	-	-
RBF *C* =100				
γ 0.001	3,854	65.46	57.667	0.22

Table 4.10 refers the differences of SVM capacity when applying to the testing dataset and unseen dataset. Classification accuracy decrease in almost kernel models when were applying to the actual data. The large numbers of support vectors were not garuntee that the classification performance must be perfect. The $\alpha*\gamma$ value derived from SVM algorithm is the critical value of support vector. For instance, 664 support vectors of polynomial degree 2 respond the accuracy less than degree3 which has only 540. The overall performances of SVM when analyzing to the spectral data were not quite well. The maximum accuracy retieved by spectral data classification is approximately 60.63% (linear kernel with *C*=100).

4.2.2 The second scenario: Classification with inclusion of texture data

Due to the poor performances of SVM models in the previous sections, texture data were inclused into the classification procedure. Then the comparisons of classification accuracy between spectral data only and integration of spectral and textures were performed.

(1) SVM Model evaluation

Candidate eleven models were considered in this part. The combinations of four channels of spectral data and one texture resulting in five dimension input data were conducted. Eight integrated dataset were transformed to the high dimensional feature space via the three kernel functions. The numbers of support vectors which play the significant role to determine the optimum hyperplane were summarized in each combined dataset.

Table 4.11 Conclusion of number of SVs of each combined dataset

	No.of SVs								
Kernel	SPEC	Mean	VAR	HOM	CON	DIS	ENT	ASM	COR
Linear									
C 0.001	3,966	3,944	3,952	3,969	3,943	3,937	3,958	3,968	3,960
C 10	3,941	3,924	3,929	407	3,921	3,919	276	3,935	3,933
C 100	119	238	209	66	37	62	52	176	193
C 1000	185	42	56	66	39	0	51	48	154
Polynomial *C* =10									
degree 2	664	820	1,064	1,267	993	984	779	3,019	839
degree 3	540	827	741	1, 242	854	1,091	542	971	1,160
degree 4	1183	1,580	1,919	1,796	1,805	1,340	905	691	1,072
RBF *C* =10									
γ 0.001	3,745	3,635	3,666	3,688	3,668	3,308	3,729	3,739	3,745
γ 10	6,000	5,991	5,992	5,992	5,990	5,991	5,991	5,987	5,990
γ 100	6,000	5,991	5,992	5,991	5,991	5,991	5,991	5,987	5,991
RBF*C*=10*0*									
γ 0.001	3,854	3,512	3,345	3,558	3,555	3,533	3,478	3,634	3,649

Training data = 6,000 samples

(2) SVM model validation

Investigated models were verified by applying to the testing data. The numbers of correct and incorrect based on the model function were estimated. The classification accuracy (% of pixls classified in the correct class) was summarized. In table 4.12, estimated accuracy for each combined dataset was reviewed. After included the texture feature, the overall performance of SVM algorithm were lightly adjusted. The combination of four spectral bands and contrast texture returns the best accuracy score with 77.61% (77.15% only spectral).

Table 4.12 Comparison of accuracy percentage of testing dataset

	Accuracy Percentage (test data)							
Kernel	Mean	VAR	HOM	CON	DIS	ENT	ASM	COR
Linear kernel								
C 0.001	77.49	70.14	75.18	77.61	63.21	76.99	77.11	77.43
C 10	77.02	65.23	60.29	77.45	63.79	31.14	76.52	76.98
C 100	22.64	56.88	66.58	75.41	45.52	28.60	56.53	28.81
C 1000	23.73	34.76	44.64	25.75	54.30	42.32	28.65	30.44
Polynomial *C* =10								
degree 2	74.07	65.76	58.76	34.02	63.79	67.97	53.56	71.60
degree 3	74.34	64.87	61.73	57.16	47.74	62.19	53.13	74.54
degree 4	64.19	61.33	51.39	48.07	63.18	41.48	63.83	39.55
RBF								
C =10 γ 0.001	75.23	71.35	71.31	75.41	66.55	74.57	77.19	74.55
C =100 γ 0.001	74.23	72.54	71.04	74.37	64.07	74.14	74.34	73.82

(3) SVM model assessment

To trade off the performance of texture, one texture was integrated with four spectral bands. In this experiment, nine models with the differences of kernel functions and value parameters were tested. The probability scores were considered to determaine the possible range of each class (-1 or +1). Figure 4.21 illustrates the frequency distribution of probability scores along x-y axis. The highest histogram displays the scores that the large numbers of pixels that belong to. The dot line represents the boundary of the target class (+1).

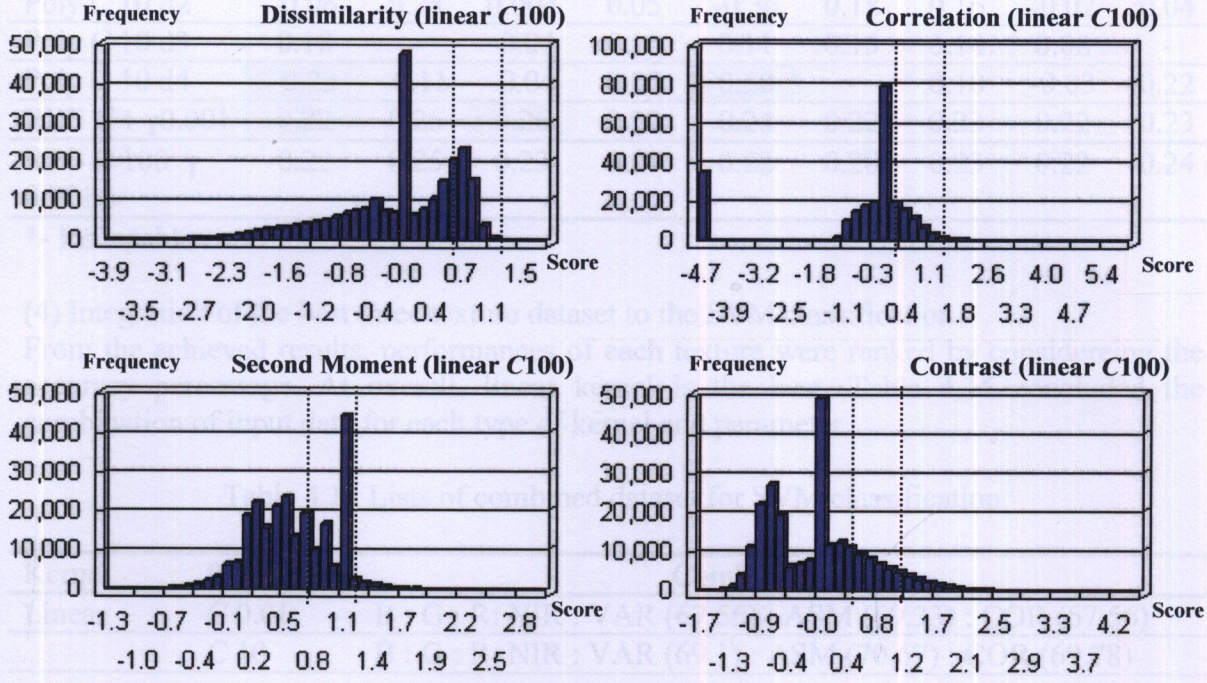

Figure 4.21 Comparison the frequency distribution of probability score

Table 4.13 Comparison of classification accuracy when including texture data

	Accuracy Percentage (actual data)								
Kernel	SPE	MEA	VAR	HOM	CON	DIS	ENT	ASM	COR
Linear *C* 0.01	56.315	64.00	67.56	69.22	64.89	64.33	67.89	69.33	67.56
Linear *C* 10	56.84	66.89	69.11	49.44	67.11	64.78	32.77	70.67	69.78
Linear *C* 100	60.63	20.78	50.44	46.11	47.22	47.00	22.00	64.56	31.67
Linear *C* 1000	22.00	21.44	46.11	46.44	45.11	45.44	25.44	22.00	29.33
Poly *C* 10 d2	42.44	61.56	44.67	47.78	31.78	55.89	54.67	44.22	47.00
Poly *C* 10 d3	56.56	-	44.67	55.33	52.89	58.0	53.78	50.00	-
Poly *C* 10 d4	34.22	39.11	44.22	67.11	63.00	-	52.11	47.78	60.22
RBF *C* 1γ0.001	57.89	60.00	60.67	58.11	59.22	57.78	58.44	57.89	58.33
RBF *C* 100 γ 0.001	57.66	60.22	58.33	57.33	57.89	56.67	58.44	58.22	58.89

*- Inseapable case

The best combinated dataset that return the best performance in linear is the integration of spectral ans second moment with 70.67%, in polynomial is spectral and contrast with 63% and in RBF is spectral and variance with 60.67%.

Table 4.14 Comparison of kappa coefficient in texture data

	Kappa Coefficience (actual data)								
Kernel	SPE	MEA	VAR	HOM	CON	DIS	ENT	ASM	COR
Linear *C* 0.01	0.26	0.33	0.38	0.41	0.34	0.33	0.40	0.42	0.39
Linear *C* 10	0.26	0.38	0.41	0.07	0.37	0.34	-0.31	0.44	0.42
Linear *C* 100	0.30	-0.53	-0.52	0.02	0.04	-0.09	-0.51	0.32	-0.34
Linear *C* 1000	-0.51	-0.54	0.02	0.02	-0.16	0.004	-0.42	-0.50	-0.37
Poly *C* 10 d2	-0.06	0.28	0.004	0.05	-0.30	0.18	0.16	-0.02	0.04
Poly *C* 10 d3	0.18	-	-0.04	0.16	0.11	0.15	0.14	0.08	-
Poly *C* 10 d4	-0.23	-0.11	-0.04	0.37	0.30	-	0.10	-0.03	0.22
RBF *C* 1 γ0.001	0.22	0.25	0.26	0.22	0.24	0.22	0.23	0.22	0.23
RBF *C* 100 γ 0.001	0.22	0.25	0.23	0.21	0.22	0.20	0.23	0.22	0.24

*- Inseapable case

(4) Integration of the best three texture dataset to the SVM classification
From the achieved results, performances of each texture were ranked by considereing the accuracy percentage. At overall, linear kernel is the best. Table 4.15 concluded the combination of input data for each type of kernel and parameter.

Table 4.15 Lists of combined dataset for SVM classification

Kernel	Parameter	Combined dataset
Linear	*C* 0.01	B : G : R: NIR : VAR (67.56) : ASM (69.33) : COR (67.56)
	C 10	B : G : R: NIR : VAR (69.1) : ASM (70.67) : COR (69.78)
Polynomial	degree 3	B : G : R: NIR : DIS (58.00) : HOM (55.33) : CON (52.89)
	degree 4	B : G : R: NIR : CON (63.00) : COR (60.22) : HOM (67.00)
RBF *C* 10	γ 0.001	B : G : R: NIR : VAR (60.67) : CON (59.22) : MEAN (60.00)
C 100	γ 0.001	B : G : R: NIR : COR (58.89) : HOM (57.33) : MEAN (60.22)

Table 4.16 Comparison of the accuracy of classification of the combined dataset

Kernel	Parameter	Spectral		Texture	
		Accuracy	Kappa	Accuracy	Kappa
Linear	*C* 0.01	56.32	0.26	58.00	0.27
	C 10	56.84	0.26	43.11	-0.49
Polynomial	degree 3	56.56	0.18	44.00	-0.01
	degree 4	34.22	-0.23	48.44	0.06
RBF *C* 10	γ 0.001	57.89	0.22	59.88	0.25
C 100	γ 0.001	57.67	0.22	59.56	0.25

After increase texture feature in the SVM classification, the classifier performances were improved lightly. Linear and RBF kernel function return the better results when comparing to that of pure spectral analaysis. However, the classification accuracy was degraded in some cases of polynomial and linear.

(5) Noise reduction and map results

In general, the results from the image classification include some noise by the effects of the similarity of DN values. Filtering technice based on the majority value was applied to the results to achieve the sound maps. The results of SVM classification based on the spectral value show in figure 4.22. Results of SVM classification based on the combination of spectral and one texture illustrate in figure 4.23 and three textures in 4.24.

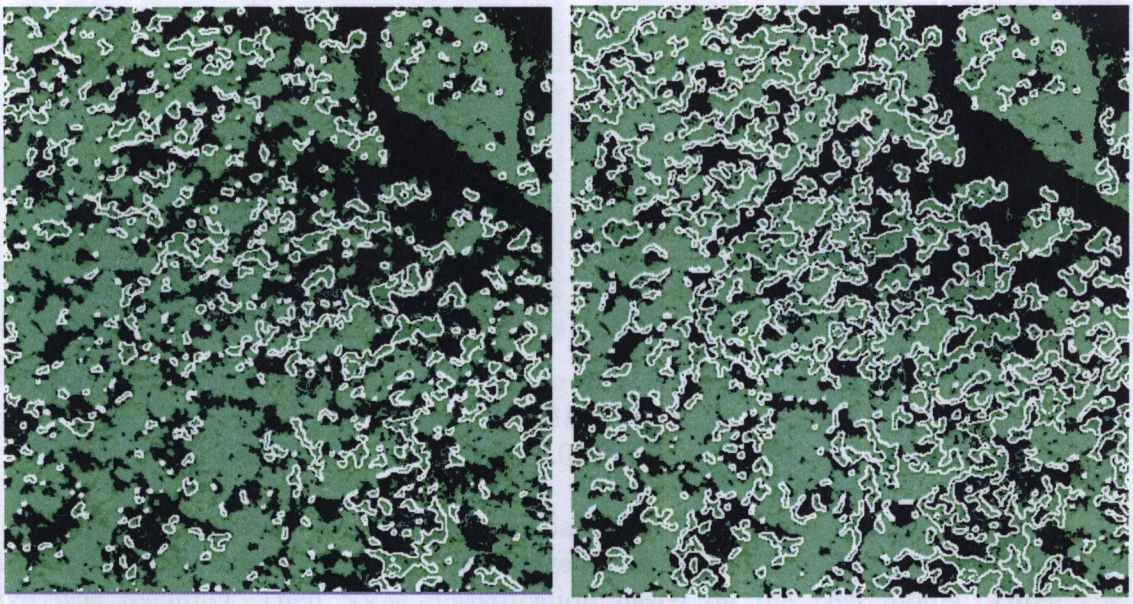

Figure 4.22 Tree crown map by spectral data classification, (left) results of linear kernel with *C* 10 (638 tree crowns) and (right) results of kernel with *C* 100 (507

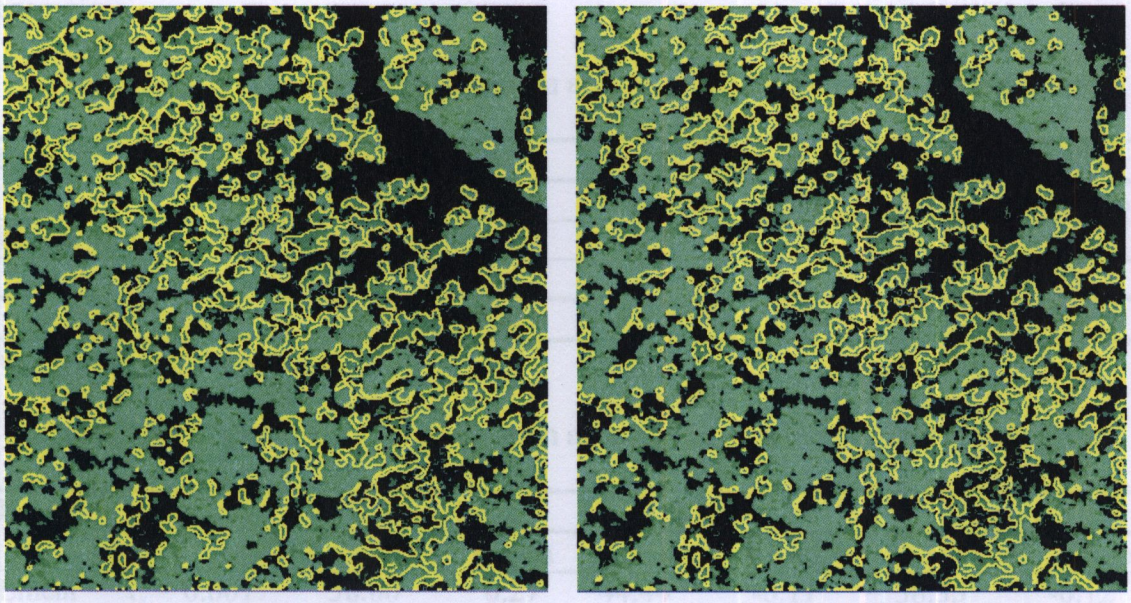

Figure 4.23 Tree crown map by including texture (left) spectral and second moment by Linear *C*10 (601 crowns) and (right) spectral and correlation by Linear *C*10 (657 crowns)

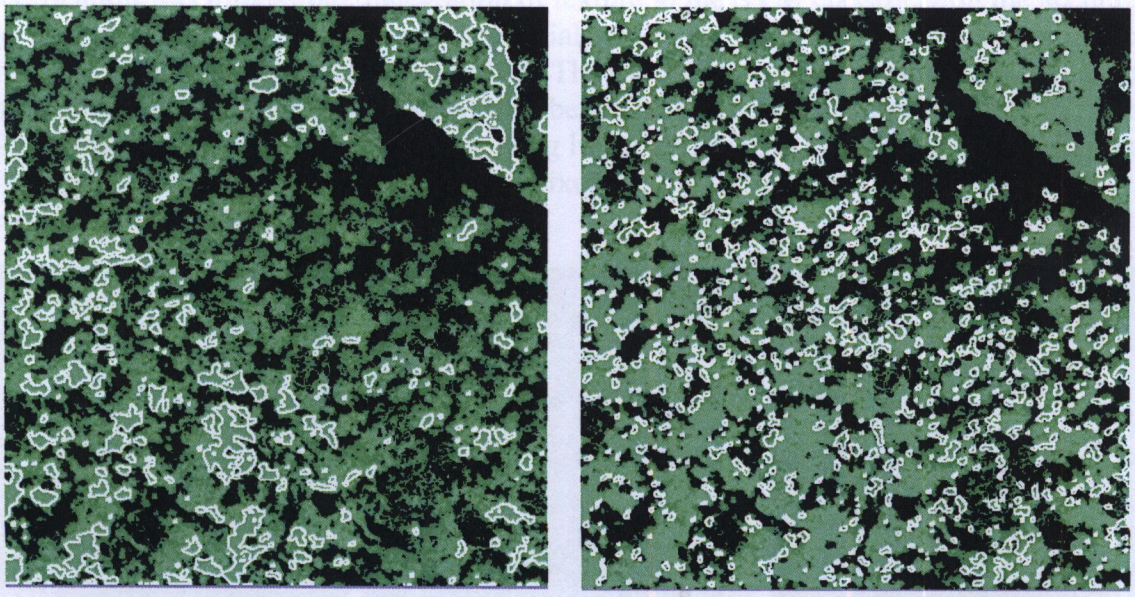

Figure 4.24 Tree crown map by including three texture data (left) spectral and VAR ASM COR by Linear *C*10 (387 crowns) and (right) spectral and VAR CON MEAN by RBF C10 γ 0.001 (1,034 crowns)

4.2.3 The third scenario: The minimum spatial resolution for tree crown delineation

Another parameter evaluated was the image spatial resolution. The original image pixel size was regarded. Then SVM classification based on the best model. Three spatial resolution levels were investigated the capacities to discriminate tree genus. Linear kernel with penalty 0.001 and 10 were tested. The combination of spectral data and three textures including variance, second moment and correlation become the input data for this secenario.

Table 4.17 Comparison of classification accuracy in 3 different spatial resolutions

Kernel	Parameter	0.6 pixel size		1.2 pixel size		1.8 pixel size	
		Accuracy	Kappa	Accuracy	Kappa	Accuracy	Kappa
Linear	$C = 0.001$	56.315	0.26	21.11	-0.5	-	-
	$C = 10$	56.84	0.26	52.22	0.04	50.55	0.01

*using only 4 spectral bands

Table 4.18 Comparison of classification accuracy in 3 different spatial resolutions

Kernel	Parameter	0.6 pixel size		1.2 pixel size		1.8 pixel size	
		Accuracy	Kappa	Accuracy	Kappa	Accuracy	Kappa
Linear	$C = 0.001$	58.00	0.27	44.44	-0.11	38.33	-0.12
	$C = 10$	43.11	-0.49	35.55	-0.15	38.33	-0.12

*combining spectral and variance, second moment and correlation texture

According to the result in table 4.17 and 4.18, spatial resolution greatly influences to the model performances. When utilizing only spectral data, with 1.8 m pixel size, crown

classification was impossible. Ingegration of texture to the SVM classification the accuracy was degraded. So, texture not plays the crutial role to improve the classification accuracy when the spatial resolution is regraded. The minimum spatial resolution for genus classification must be equal to the 0.6 m or better. The examples of results show in figure 4.25. Three results were obtained by applying linear kernel with *C* equal 0.001.The number of tree crown for spectral classification at pixel 0.6 m, 1.2 m and 1.8 m is 608, 324, 111 tree crowns respectively.

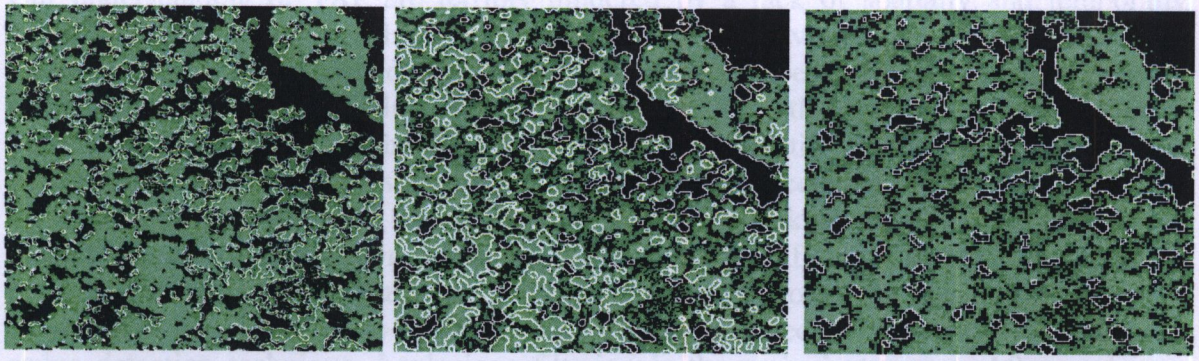

Figure 4.25 Comparison of results from the different spatial resolutions. 0.6 m (left), 1.2 m (middle) and 1.8 m (right)

4.2.4 Spcies Classification

Due to the poor performance of genus classification, species classification cannot be done. Training data of each species in the study plot must be re-collected as much as possible to create the more reliable training model.

CHAPTER V

CONCLUSIONS AND RECOMMENDATIONS

5.1 Conclusion

Our understanding of TRF are terribly hindered by a lack of spatially and temporally extensinve information tree. How does the boundary of individual tree crown in the dense forest can be segmented and delineatated to genus or species? Does Remote Sensing technology can be served? It's the challenging task. So, this thesis was carried out to persuit the possibilities for the tree crown image classification in the tropical rain forest which comprises of the diversity of flora. Well, with the procedured proposed in this paper, the applicabilities of Remote Sensing to this demanding task are fessible. The assumption that the center of tree crown is brighter than the edge of the crown or the boundary between crowns is very useful when applying to segment crown patches. Intillay, non-tree crown must be eliminated to avoid misclassification and reduce the noices. To do forth, eadge detection technique, Laplaciane filtering is the main instrument. Afterward, tree crown regions were derived. The critical problem in the dense forest is the combination of tree crowns. In this viewpoint, lower edge threshold filtering is adopted as the effective approach to separate the joined crown. However, the large size of crown is impossible to disconnect without the changes of crown shapes. So, it's accepted as the limitations.

For image classification results, at first, SVM source code, namely SVM^{light} was used because it's available on the Internet, and is the powerful learning machine. Only spectral data was utilized in the first scenario. Various transformed models constructed by the kernel functions and marginal parameter were validated to find out the optimal separable hyperplane. In this experiment, linear kernel provides the best proformance when considereing the precision rate and error assessment. Linear kernel with the penalty parameter (C 100) gives the accuracy rate 60.63 % and kappa coefficience 0.3. The numbers of support vector and their status determined by the value of alpha * gamma play the considerable role to the SVM performances.

Next, the texture features were included in the analysis. The overall accuracy of SVM algorithm were slightly adjusted. The combination of four spectral bands and argument second moment texture by applying linear kernel returns the best probability score with accuracy 70.67% and kappa coefficient 0.44. Variance, second moment and correlation texture were ranked the best in the linear kernel. Homogeneity, correlation and contrast return the sound performance for polynomial kernel. On the other hand, mean, contrast and variance are the best for RBF kernel. However, the integration of spectral and groups of the following best texture could not improve the classification accuracy. Considereing the discussion, linear kernel with spectral and ASM texture was concluded to be the best combination for genus classificatuion classification.

Although the spatial resolution of QB is much larger than the basic of each tree such as the size of leaf, as desribed above, incorpolation of texture data gave some improvement of chassificatin performance. As expected, texture data with 1.2, 1.8 m spatial resolution showed degraded performance. Considering the new satellite program like Geoeye with the higher quality, the method prepared in this papere will be more useful and practical.

5.2 Recommendation for the futher works

- To adjust the classification accuracy, the higher resolution satellite image or aerial photo must be available in the study site such as Worldview, Geoeye
- Texture features created by GLCM technique with other options such as differtent window size (5x5, 7x7) or different direction should be considered.
- Another technique for texture extraction may be alternative way to improve the classification accuracy such as wavelet analysis, Markov Random Fields, Fast Fourier Transform
- Hyperspectral image with the high spatial and spectral resolution has great possible to improve the performance
- *Other information should be included into the classification procedure: digital* elevation medel, vegetation indics, image hue, image saturation, image intensity.
- Each tree speices in the nature is varied in ages, abundances, location, etc. So, training area must be re-collected as much as possible to cover the various properties of target class.

References

Abe, S. (2005). Support Vector Machines for Pattern Classification: Advances in Pattern Recognition. Kobe University, Kobe, Japan. Springer-Verlag London Limited.

Asner, G. P. (1998). Biophysical and biochemical sources of variability in canopy reflectance. *Remote Sensing of Environment*, 64(3), 234-253.

Bahlmann, C.; Haasdonk, B.; Burkhardt, H. (2002). On-line hand writing recognition using support vector machines – a kernel approach. Int. Workshop on Frontiers in Handwriting Recognition (IWFHR), Niagara-on-the-Lake.

Bharrati, M. H.; Liu, J. J.; MacGregor, J. F. (2004). Image texture analysis: methods and comparisons. Chemometrics and Intelligent Laboratory System 72 pp.57-71.

BIOTEC, (2006). Database and Geographic Information System–GIS Development on Biodiversity in the Hala-Bala Forest in Southern Thailand. Final Report, National Center for Genetic Engineering and Biotechnology.

Burges, C.J.C. (1998). A tutorial on support vector machines for pattern recognition, Data Mining and Knowledge Discovery 2(2) pp. 121-167.

Campbell, G.S.; Norman, J.M. (1989). The description and measurement of plant canopy structure. p. 1-19. In G. Russell et al. (ed.) Plant canopies: Their growth, form and function. Soc. Exp. Biol., Seminar Series 31, Cambridge University Press, New York.

Chan, J.C.-W.; Laporte, N.; Defries, R.S. (2003). Texture classification of logged forests in tropical Africa using machine-learning algorithms. *International of Remote Sensing*, Vol. 24, No.6, 1401-1407.

Chapman, S. (2004). Support Vector Machine. February 13.

Christopherson, R. W. (1994). Geosystems: an introduction to physical geography. Second edition. Macmillan College Publishing Company, New York, pp.617-649.

Christoulas, G.; Tsagaris, V.; Anastassopoulos, V. (2007). Textural characterization from various representations of MERIS data. *International Journal of Remote Sensing*, Vol.28, Nos. 3-4, February, pp. 675-692.

Clark, M.L.; Roberts, D.A.; Clark, D.B. (2005). Hyperspectral discrimination of tropical rain forest tree species at leaf to crown scales. *Remote Sensing of Environment.*

Cochrane, M. A. (2000). Using Vegetation reflectance variability for species level classification of hyperspectral data. *International Journal of Remote Sensing*, 21(10), 2075-2087.

Cortes, C.; Vapnik, V. (1995). Support-vector networks, *Machine Learning* 20 (3) (1995) pp. 273-297.

Cristianini, N.; Taylor, J.S. (2000). Support Vector Machines and Other Kernel-based Learning Algorithms. Cambridge, UK: Cambridge University Press

Culvenor. D.S, (2003). Extracting individual tree information: A survey of techniques for high spatial resolution imagery. *Remote Sensing of forest Environments*: concepts and case studies. Kluwer Academic Publishers, Boston/Dordrecht/London, pp. 255-277.

Czaplewski, R.L. (1994). Variance approximations for assessments of classification accuracy. Research paper RM-316. Fort Collins, CO: U.S. Department of Agriculture, Forest Service, Rocky Mountain Research Station.

Darius S. Culvenor, 2001. Evaluation of the Tree Identification and Delineation Algorithm (TIDA) using a forest canopy simulation model. *International Journal of Remote Sensing*, pp. 777-779.

Dikshit, O. (1996). Textural classification for ecological research using ATM images. *International Journal of Remote Sensing*, 17, 887-915.

Dube, P.; Hay, G., & Marceau, D. (1999). Voronoi diagrams, extended area stealing interpolation, and tree crown recognition: a fuzzy approach. *Proceedings Automated Interpretation of High Spatial Resolution Digital Imagery for Forestry*, 115-126. Victoria, British Columbia.

Durbha, S. S.; King, R. L.; Younan,; N. H. (2007). Support Vector Machines regression for retrieval of leaf area index from multi-angle imaging spectroradiometer. *Remote Sensing of Environment* 107 pp.348-361.

Erikson, M., (2003a). Segmentation of individual tree crowns in colour aerial photography using region growing supported by fuzzy rules. *Canadian Journal of Forest Research* 33 8, pp. 1557-1563.

Erikson, M., (2003b). Species classification of individually segmented tree crowns in high-resolution aerial images using radiometric and morphologic image measures. *Remote Sensing of Environment*, Volume 91, Issues 3-4, 30 June 2004, Pages 469-477

Fournier, R. A.; Maily, D.; Walter, J-M.N.; Soudani, K. (2003). Indirect measurement of forest canopy structure from *in situ* optical sensors. *Remote Sensing of forest Environments*: concepts and case studies. Kluwer Academic Publishers, Boston/Dordrecht/London, pp. 77-113.

Franz, E.; Gebhardt, M.R.; Unklesbay, K.B. (1991). The use of local spectral properties of leaves as an aid for identifying weed seedlings in digital image, *Transactions of the ASAE* 34 (2) 682-687.

Gemmell, F. (1998). An investigation of terrain effects on the inversion of a forest reflectance model. *Remote Sensing of Environment*, 65 155-169.

Golley, F.B. (1983). Tropical rain forest ecosystems: structure and function. Amsterdam-Oxford-New York. Amsterdam, Elsevier Scientific.

Gougeon, F.A. (1995a). Comparison of possible multi-spectral classification schemes for tree crowns individually delineated on high spatial resolution MEIS images. *Canadian Journal of Remote Sensing* 21(1): 1-9.

Gougeon, F.A. (1995b). A crown-following approach to the automatic delineation of individual tree crowns in high spatial resolution aerial images. *Canadian Journal of Remote Sensing* 21(3): 274-284.

Grant, L. (1987). Diffuse and specular characteristics of leaf reflectance. *Remote Sensing of Environment*, 22, 309-322.

Groesz, F.J.; Kastdalen, L. (2007). Mapping trees and thicket with optical image. Testing the use of high resolution image data for mapping moose winter food resources. Norwegian Space Centre and Hedmark University College, pp 1-36.

Hall, R. J. (2003). The roles of aerial photographs in forestry remote sensing image analysis. *Remote Sensing of Forest Environments*: Concepts and Case studies, Chapter3, Kluwer Academic Publishers, Boston/Dordrecht/London, pp. 47-75.

Haralick, R.M.; Shanmugam, K.; Dinstein, I.(1973). Texture feature for image classification. *IEEE Transactions on Systems*, Man, and Cybernetics 3, 610-21.

Hemery, G.E.; Savill, P.S.; Pryor, S.N. (2005). Applications of the crown diameter–stem diameter relationship for different species of broadleaved trees. *Forest Ecology and Management*, Volume 215, Issues 1-3, 25 August, Pages 285-294.

Hsu, C-C.; Chang; Lin, C-J. (2004). A practical guide to support vector classification. Technical Report, Department of computer science, National Taiwan University. Taipei

Huang, C.; Davis, L.S.; Townshend, J. R. G., (2000). An Assessment of Support Vector Machines for land cover classification. *International Journal of Remote Sensing*, Vol. 23, No. 4, pp.725-749.

Komura, R.; Kubo, M.; Kamata, N.; Muramoto, K. (2003). Analysis of size of tree crown on aerial image using circle unitfication. SICE Annual Conference in Fukui, August 4-6, Fukui University, Japan.

Kulikova, M. S.; Mani, M.; Srivastava, A.; Descombes, X.; Zerubia, J. (2007). Tree Species classification using Radiometry, Texture and Shape based features. *In Proceeding of European Signal Processing Conference* (EUSIPCO).

Lafarge, F.; Descombes, X.; Zerubia, J. (2004). Textural kernel for SVM classification in Remote Sensing: Application to forest fire detection and urban area extraction.

Larsen, M.; Rudemo, M. (1998). Optimizing templates for finding trees in aerial photographs, *Pattern Recognition Lett.* 19, 1153-1162.

Leckie, D.; Gougeon, F.A.; Tinis, S.; Nelson, T.; Burnett, C.N., Paradine, D. (2005). Automated tree recognition in old growth conifer stands with high resolution digital imagery. *Remote Sensing of Environment*, 94, pp.311-326.

Leckie, D. G.; Yaun, X.; Ostaff, X.; Piene, D. P.; MacLean, D. A. (1992). Analysis of high spatial resolution multispectral MEIS imagery for Spruce Budworm damage assessment on a single tree basis. *Remote Sensing of Environment*, 40, 125-136.

Lillesand, T.M.; Kiefer, R.W. (2000). Remote sensing and image interpretation, Fourth Edition, University of Madison.

Lin, C., (2001). The dependence of reflected radiance and reflectance of the forest vegetation- A case study of CYCLOBANOPSIS GLAUCA. *In proceedings the Asian Conference on Remote Sensing*, 5-9 November, Singapore.

Li, X.; Strahler, A. H. (1992). Geometric-optical bidirectional reflectance modeling of the discrete crown vegetation canopy: effect of crown shape on mutual shadowing. *IEEE Transactions on Geo-science and Remote Sensing*, 62, 285-291.

Lillesand, T. M.; Kiefer, R. W. (1994). Remote sensing and image interpretation (3rd ed). John Wiley & Sons, Inc., New York, N. Y.

Ma, C.; Randolph, M.A.; Drish, J. (2001). A support vector machines-based rejection technique for speech recognition. Acoustics, Speech, and Signal Processing, Proceedings. (ICASSP '01). *IEEE International Conference on Publication Date*: Volume: 1, on page(s): 381-384.

Moe, T. A, (1998). Algorithm Development for Identifying Tree Crown in Tea Bearing Forest with the Use of Potential High Spatial Resolution Satellite Data. Master Thesis, Asian Institute of Technology, Bangkok, Thailand.

Muniz, R.; Corrales, J.A. (2006). Novel Techniques for Color Texture Classification. In IPCV 2006, pages 114-120.

Niyomtam, C. (2000). Flora in the Hala-Bala. The natural and wildlife conservation project. Royal Department of forestry.

Parker, G.G. (1995). Structure and microclimate of forest canopies. In "Foest Canopies" (M.D. Lowman and N. M. Nadkarni, Eds.), pp. 73-106. Academic Press, San Diego.

Orka, H.O.; Naesset, E.; Bollandsas, M., (2007). Utilizing airborne laser intensity for tree species classification. ISPRS Workshop on Laser Scanning 2007 and SilviLaser, Espoo, September 12-14, Finland.

Pinz, A.J. (1991). A computer vision system for the recognition of trees in aerial photographs.. Pages 111-124 in T. Tilton, (ed.) Multi-source Data Integration in Remote Sensing. Proceedings of a workshop held at the University of Maryland, College Park, Maryland, June 14-15. NASA Conf. Pub. 3099.

Pollock, R.J. (1996). The automatic recognition of individual trees in aerial images of forests based on a synthetic tree crown image model. Ph.D. dissertation, University of British Columibia, Vancouver, Canada.

Poopath, (2007). Studies on species diversity of Dipterocarpaceae in Hala-bala forest, Yala and Narathiwat province. Master thesis of science (Forest), Kasetsart University, Bangkok, Thailand.

Poorter, L., Oberbauer, S. F., & Clark, D. B. (1995). Leaf optical-properties along a vertical gradient in a tropical rain-forest canopy in Costa-Rica. *American Journal of Botany*, 82(10), 1257-1263.

Pouliot, D.A., King D.J., Bell F.W., Pitt D.G., (2002). Automated tree crown detection and delineation in high-resolution digital camera imagery of coniferous forest regeneration. *Remote Sensing of Environment* 82: 322-334.

Rees, W. G. (2001). Physical principles of remote sensing. Second edition, Scott Polar Research Institute, University of Cambridge, pp.300-309.

Richards, P.W. (1954). The Tropical Rain forest. Cambridge University Press, Cambridge.

Roberts, D. A., Ustin, S.L., Qgybhenutim, S., Greenbert. J., Dobrowski, S. Z., Chen, J., et al. (2004). Spectral and structural measures of Northwest forest vegetation at leaf to landscape scales. *Ecosystems*, 7(5), 545-562.

Sebald, D.J.; Bucklew, J.A. (2000). Support Vector Machine Techniques for Nonlinear Equalization. Signal Processing, *International of Remote Sensing*, Volume: 48, Issue: 11on page(s): 3217-3226.

Sherrod, P. H. (2003-2007). DTREG Predictive Modeling Software. The tutorial for modeling software, DTREG. This document available at www.dtreg.com.

Thomas, C.D., Cameron, A.; Green, R.E.; Bakkenes, M.; Beaumont, L.J.; Collingham, Y.C. (2004). *Extinction risk from climate change*. Nature, 427(6970), 145-148.

Townshend, J.; Justice, C. (1981). Information extraction from remotely sensed data: a user view. *International Journal of Remote Sensing*, 2, 313-329.

Tso, B.; Mather, P.M. (2001). Classification Methods for Remotely Sensed Data. Taylor & Francis London and New Yourk.

Uuttera, J.; Haara, A.; Tokola, T.; Maltamo, M. (1998). Determination of the spatial distribution of trees from digital aerial photography. *Forest Ecology and Management* 110; 275-282.

Woodcock, C. E.; Strahler, A. H. (1987). The factor of scale in remote sensing. *Remote Sensing of Environment*, 21, 311-332.

Wu, L.; Zhang, Y.; Gao, Y.; Zhang, Y. (2004). Tree crown detection and delineation in high resolution RS image: A texture approach discussion. *International Journal of Remote Sensing*, 3841-3844.

Wulder, M. A.; Franklin, S. E. (2003). Remote sensing of forest environments, Introduction. The transition from theory to information. *Remote Sensing of forest Environments*: concepts and case studies. Kluwer Academic Publishers, Boston/Dordrecht/London, 3-12.

Zien, Ratsch, Mika, Scholkopf, Lengauer and Muller, (2000). Engineering support vector machine kernels that recognize translation initiation sites, BIOINF: *Bioinformatics*, 16.

APPENDIX A

TREE LOCATION IN THE STUDY PLOT

ID	Easting	Northing	Accuracy (m)	DBH (cm)	Crown width (m)	Species Name
1	813464	641402	7	94	15.00	*faguetiana*
2	813622	641516	5	74	7.50	*guiso*
3	813602	641500	5	44	6.00	*leprosura*
4	813784	641398	6	58	7.50	*leprosura*
5	813796	641406	6	50	7.50	*leprosura*
6	813773	641457	7	88	7.00	*stelata*
7	813755	641488	6	108	8.00	*borneensis*
8	813771	641445	6	89	8.00	*kerrii*
9	813456	641386	7	100	10.00	*excelsa*
10	813502	641386	6	130	16.00	*faguetiana*
11	813264	641396	6	68	14.00	*leprosura*
12	813432	641383	7	90	18.00	*leprosura*
13	813737	641890	7	86	9.00	*leprosura*
14	813713	641748	7	95	12.00	*leprosura*
15	813750	641710	6	89	13.00	*stelata*
16	813686	641521	5	79	9.00	*bracteolata*
17	813620	641515	6	89	12.00	*guiso*
18	813757	641417	6	83	11.00	*leprosura*
19	813694	641651	6	87	11.00	*assamica*
20	813685	641650	5	105	15.00	*costata*
21	813667	641538	5	88	13.00	*bracteolata*
22	813495	641529	5	84	13.00	*faguetiana*
23	813454	641627	6	95	16.00	*parvifolia*
24	813459	641663	6	94	14.00	*parvifolia*
25	813410	641684	6	87	12.00	*faguetiana*
26	813434	641689	5	85	12.00	*faguetiana*
27	813413	641705	5	86	14.00	*faguetiana*
28	813395	641713	5	79	14.50	*leprosura*
29	813464	641402	5	94	16.00	*leprosura*
30	813324	641715	5	95	15.00	*assamica*
31	813345	641739	5	101	17.00	*faguetiana*
32	813341	641745	6	89	12.00	*faguetiana*
33	813288	641734	6	93	14.00	*stelata*
34	813263	641709	6	99	15.00	*parvifolia*
35	813251	641733	6	88	13.00	*stelata*
36	813297	641766	6	87	18.00	*stelata*
37	813283	641782	7	79	16.00	*assamica*
38	813280	641767	7	87	17.00	*stelata*
39	813245	641769	7	99	13.00	*curtisii*
40	813241	641774	6	87	12.00	*leprosura*

ID	Easting	Northing	Accuracy (m)	DBH (cm)	Crown width (m)	Name
41	813231	641818	6	89	12.00	*leprosura*
42	813217	641814	6	94	16.00	*leprosura*
43	813215	641803	6	93	17.00	*assamica*
44	813208	641821	7	86	11.00	*stelata*
45	813195	641835	7	89	11.00	*assamica*
46	813185	641846	7	83	10.00	*curtisii*
47	813141	641780	7	87	11.00	*assamica*
48	813180	641788	8	105	14.00	*assamica*
49	813149	641802	8	89	13.00	*leprosura*
50	813149	641769	9	90	16.50	*curtisii*
51	813152	641767	8	87	12.00	*leprosura*
52	813122	641758	6	79	14.00	*leprosura*
53	813126	641753	6	87	12.00	*curtisii*
54	813116	641800	6	99	18.00	*curtisii*
55	813114	641817	6	89	16.00	*curtisii*
56	813131	641816	5	93	17.00	*curtisii*
57	813108	641854	6	78	11.00	*leprosura*
58	813074	641844	5	93	11.00	*leprosura*
59	813039	641842	5	80	11.00	*leprosura*
60	813025	641816	5	85	12.50	*curtisii*
61	812975	641821	5	94	12.00	*curtisii*
62	813412	641644	6	92	13.00	*curtisii*
63	813828	641726	6	89	11.00	*ochrophloia*

APPENDIX B

OPTIONAL PARAMETERS FOR SVM

- Parameter for SVM learn module

General options:

-?	- this help
-v [0..3]	- verbosity level (default 1)

Learning options:

-z {c,r,p}	- select between classification (c), regression (r), and preference ranking (p) (default classification)
-c float	- C: trade-off between training error and margin (default [avg. x*x]^-1)
-w [0..]	- epsilon width of tube for regression (default 0.1)
-j float	- Cost: cost-factor, by which training errors on positive examples outweight errors on negative examples (default 1)
-b [0,1]	- use biased hyperplane (i.e. x*w+b0) instead of unbiased hyperplane (i.e. x*w0) (default 1)
-i [0,1]	- remove inconsistent training examples and retrain (default 0)

Performance estimation options:

-x [0,1]	- compute leave-one-out estimates (default 0)
-o]0..2]	- value of rho for XiAlpha-estimator and for pruning leave-one-out computation (default 1.0)
-k [0..100]	- search depth for extended XiAlpha-estimator (default 0)

Transduction options

-p [0..1]	- fraction of unlabeled examples to be classified into the positive class (default is the ratio of positive and negative examples in the training data)

Kernel options:

-t int	- type of kernel function: 0: linear (default) 1: polynomial (s a*b+c)^d 2: radial basis function exp(-gamma ||a-b||^2) 3: sigmoid tanh(s a*b + c) 4: user defined kernel from kernel.h
-d int	- parameter d in polynomial kernel
-g float	- parameter gamma in rbf kernel
-s float	- parameter s in sigmoid/poly kernel
-r float	- parameter c in sigmoid/poly kernel
-u string	- parameter of user defined kernel

Optimization options (see [Joachims, 1999a], [Joachims, 2002a]):

-q [2..]	- maximum size of QP-subproblems (default 10)
-n [2..q]	- number of new variables entering the working set in each iteration (default n = q). Set n<q to prevent zig-zagging.
-m [5..]	- size of cache for kernel evaluations in MB (default 40)

The larger the faster...

-e float - eps: Allow that error for termination criterion [y [w*x+b] - 1] = eps (default 0.001)

-h [5..] - number of iterations a variable needs to be optimal before considered for shrinking (default 100)

-f [0,1] - do final optimality check for variables removed by shrinking. Although this test is usually positive, there is no guarantee that the optimum was found if the test is omitted. (default 1)

-y string - if option is given, reads alphas from file with given and uses them as starting point. (default 'disabled')

-# int - terminate optimization, if no progress after this number of iterations. (default 100000)

Output options:

-l char - file to write predicted labels of unlabeled examples into after transductive learning

-a char - write all alphas to this file after learning (in the same order as in the training set)

svm_learn is called with the following parameters:

svm_learn [options] example_file model_file

- Parameter for SVM classify module

-h Help.

-v [0..3] Verbosity level (default 2).

-f [0,1] 0: old output format of V1.0
1: output the value of decision function (default)

svm_classify is called with the following parameters:

svm_classify [options] example_file model_file output_file

APPENDIX C

FREQUENCY DISTRIBUTION PROBABILITY SCORE OF SVM RESULTS

(1) Four bands of spectral data

- Linear kernel: C = 0.001, 10, 100 and 1000

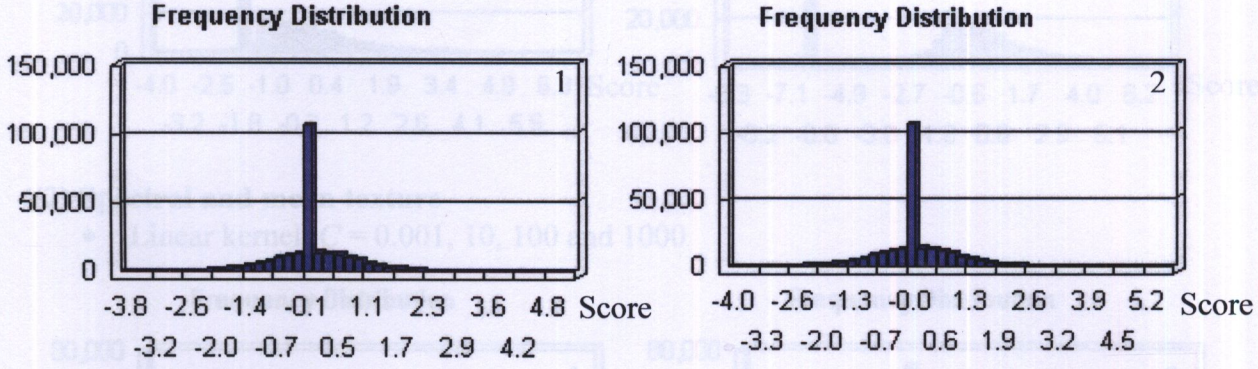

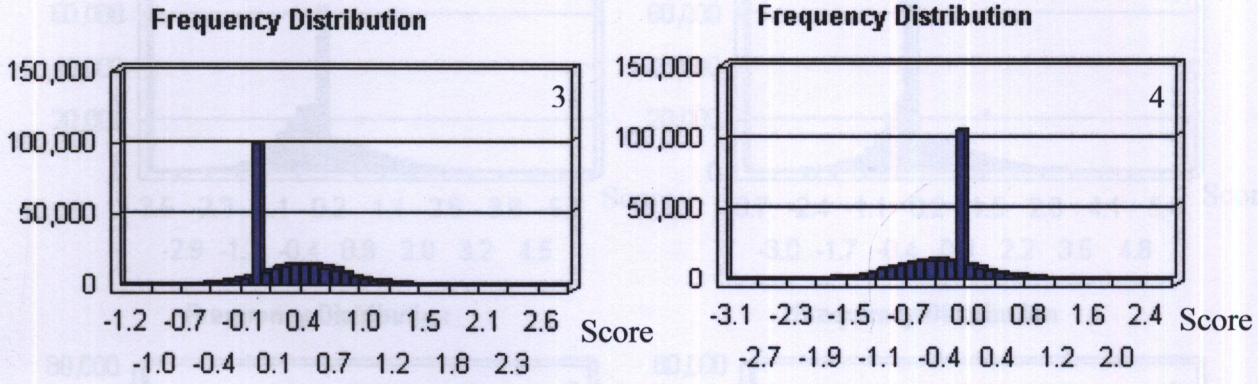

- Polynomial kernel: C =10, d= 2, 3, 4

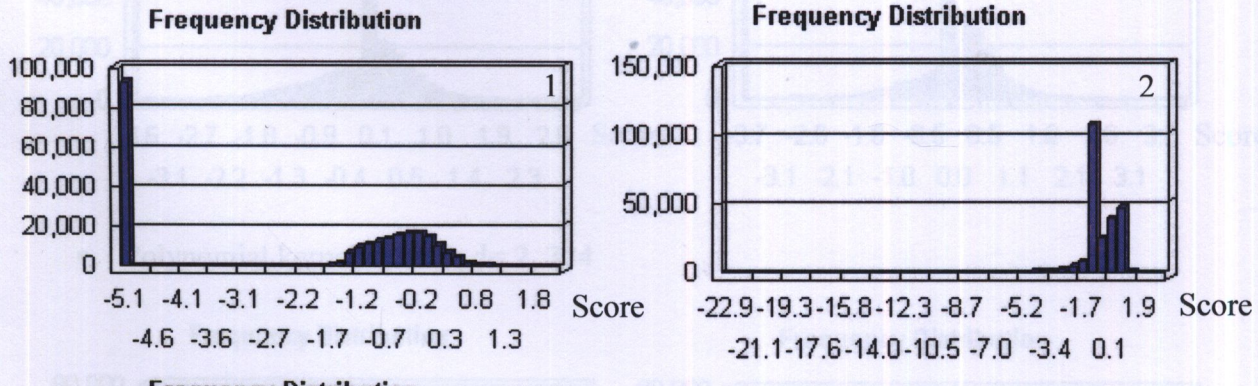

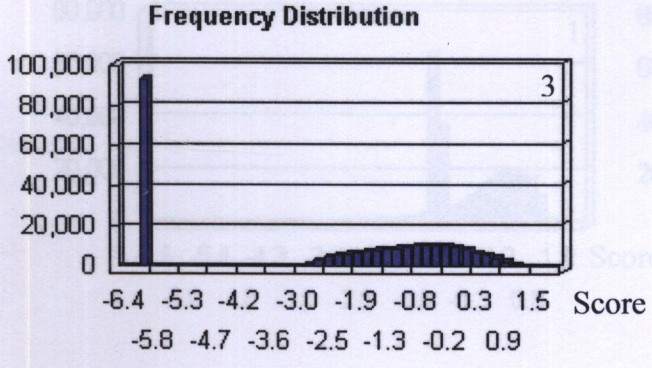

- RBF kernel γ 0.001, C =10, 100

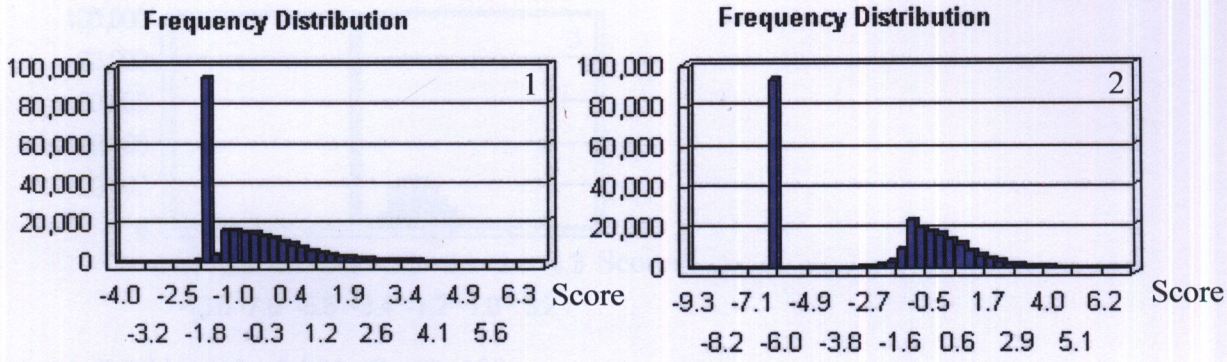

(2) Spectral and mean texture

- Linear kernel: C = 0.001, 10, 100 and 1000

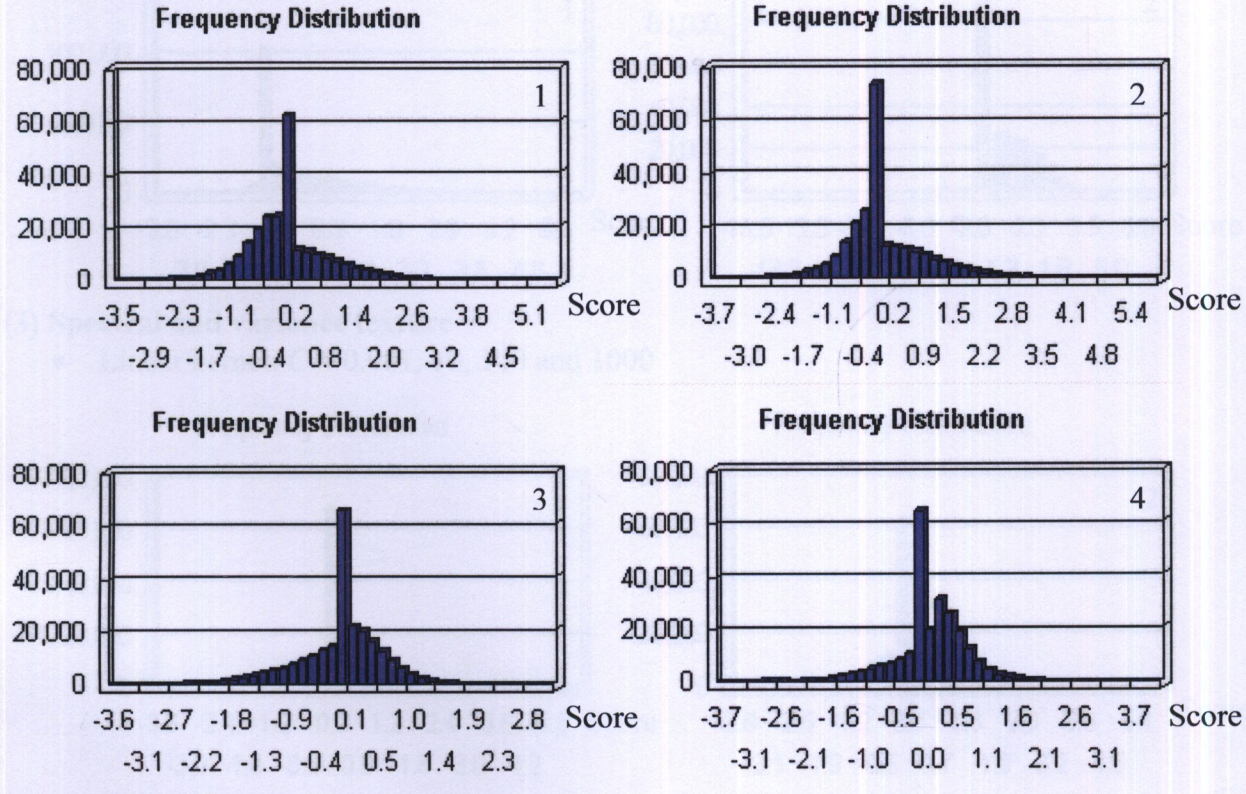

- Polynomial kernel: C =10, d= 2, 3, 4

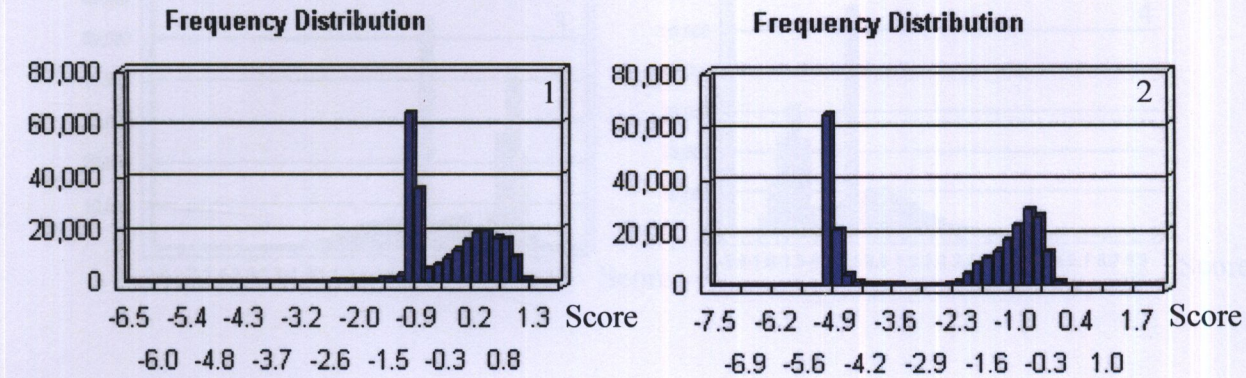

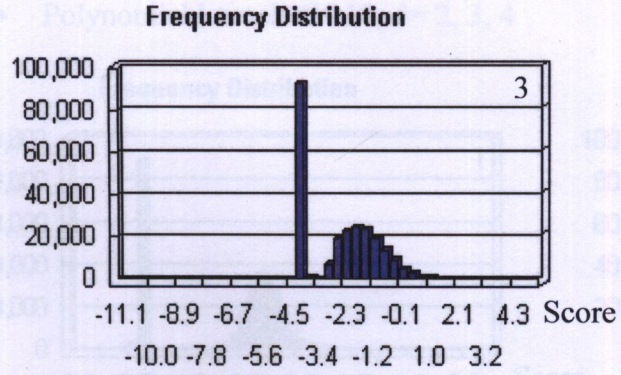

- RBF kernel γ 0.001, C =10, 100

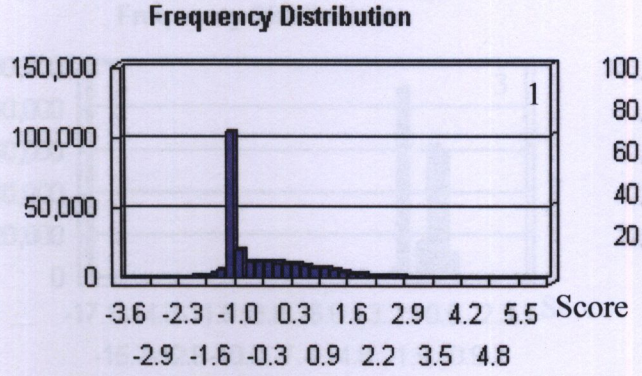

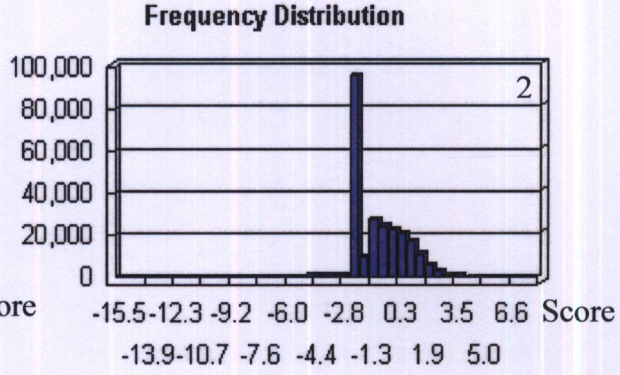

(3) Spectral and variance texture

- Linear kernel: C = 0.001, 10, 100 and 1000

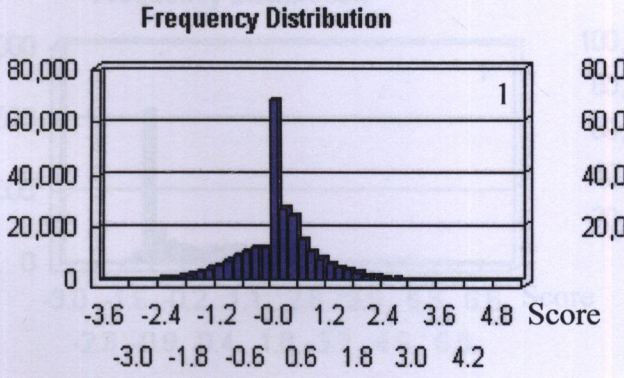

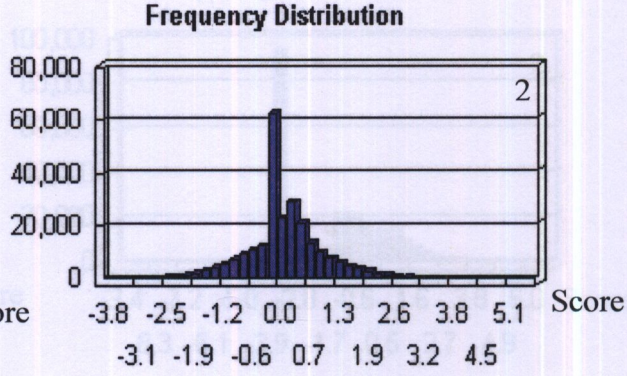

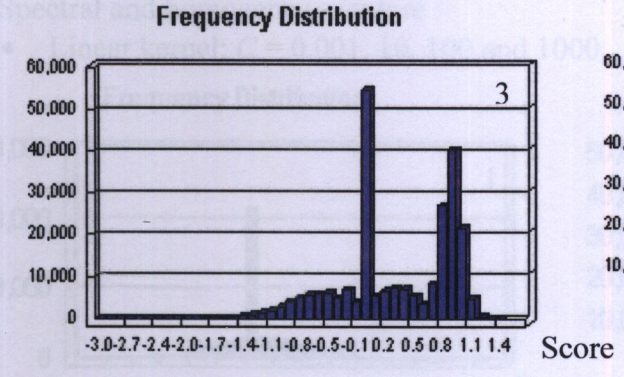

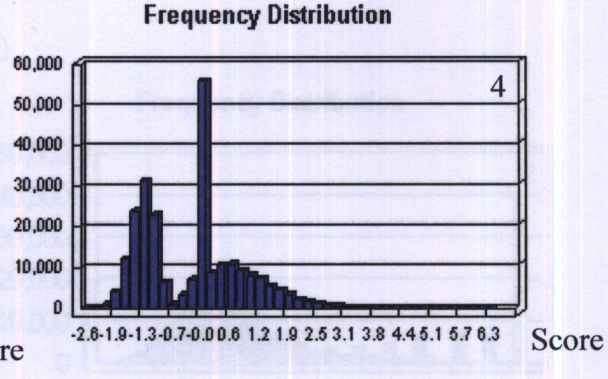

- Polynomial kernel: C =10, d= 2, 3, 4

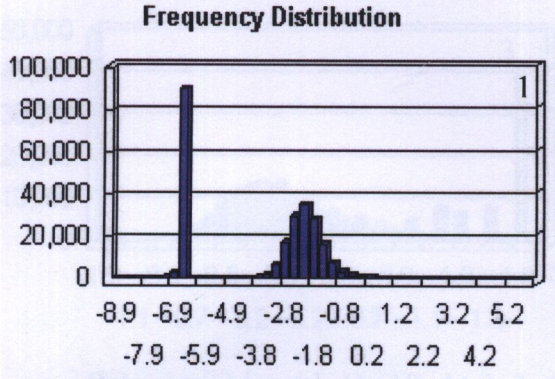

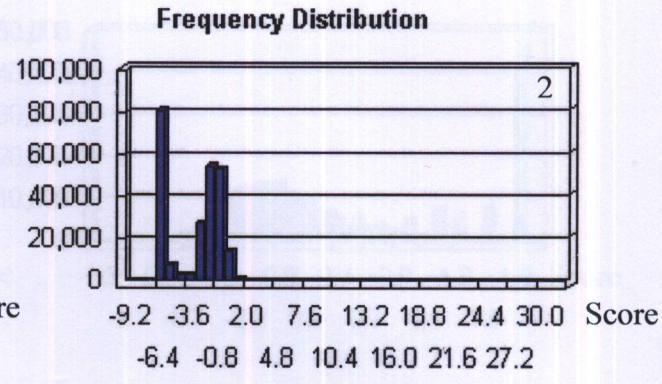

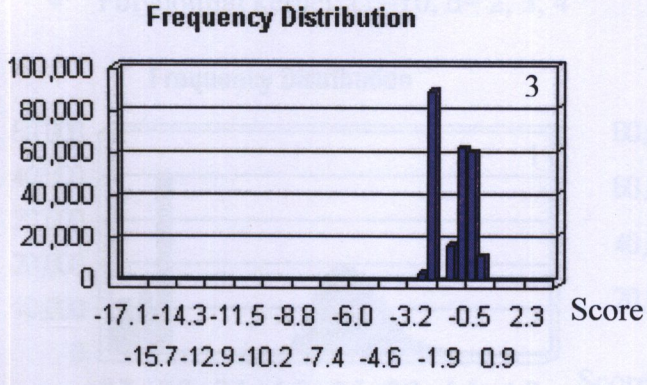

- RBF kernel γ 0.001, C =10, 100

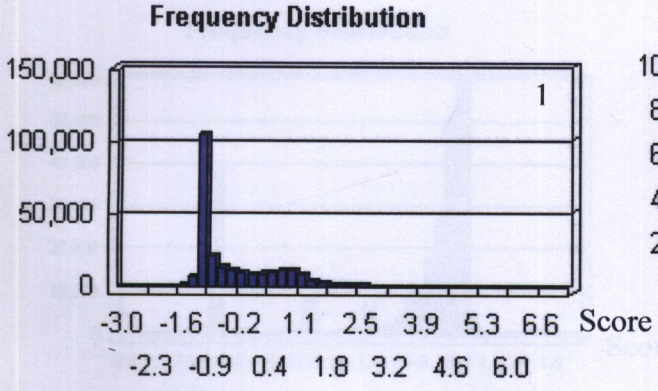

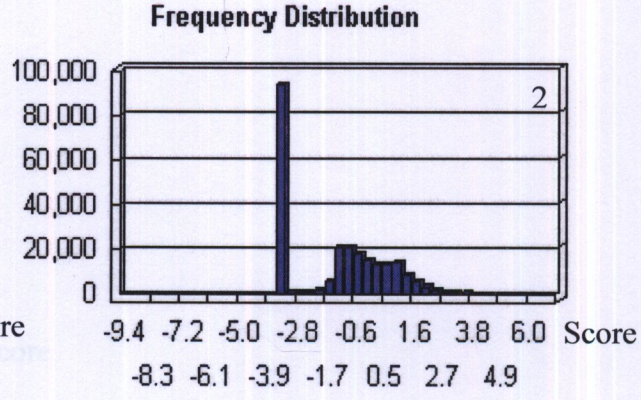

(4) Spectral and homogeneity texture

- Linear kernel: C = 0.001, 10, 100 and 1000

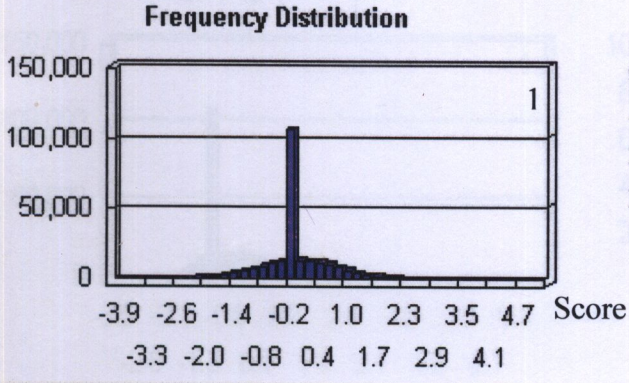

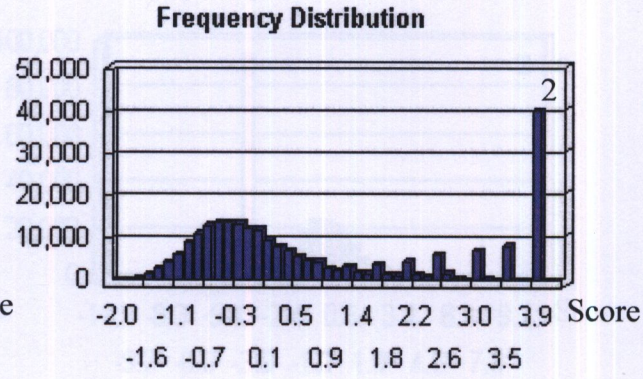

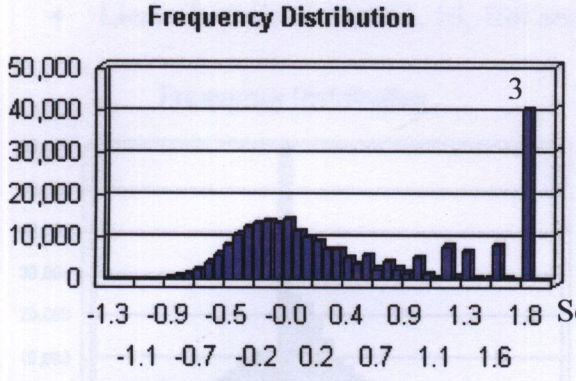

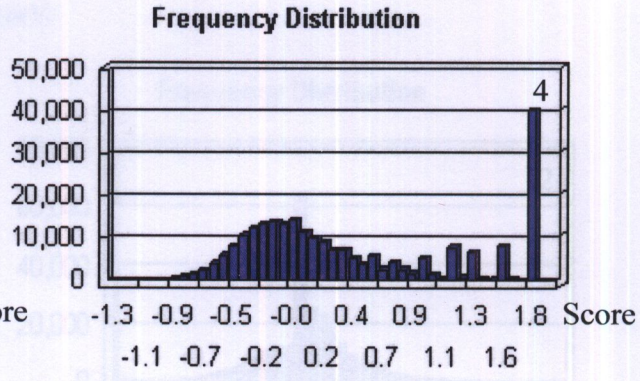

- Polynomial kernel: C =10, d= 2, 3, 4

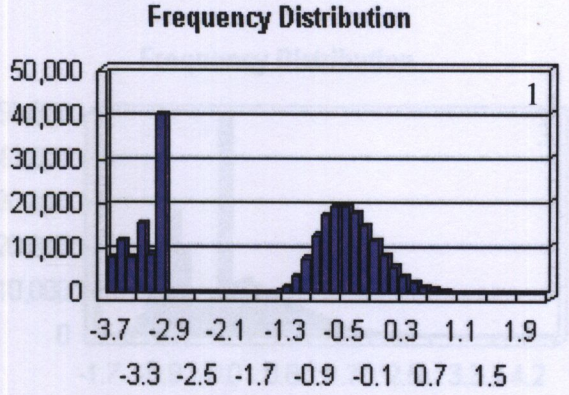

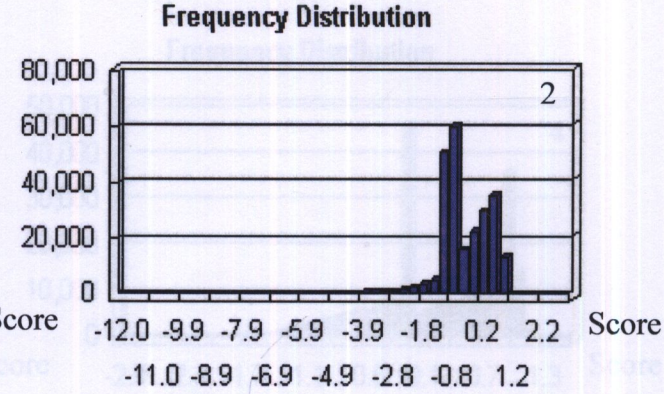

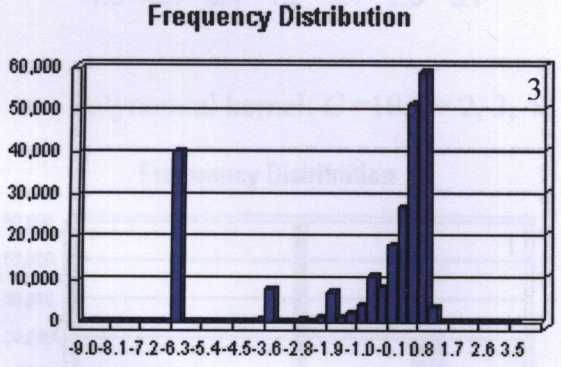

- RBF kernel γ 0.001, C =10, 100

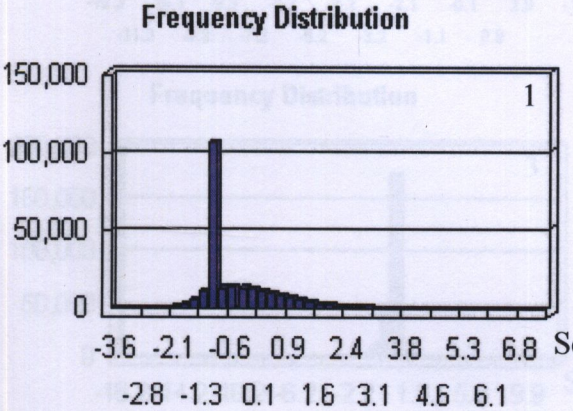

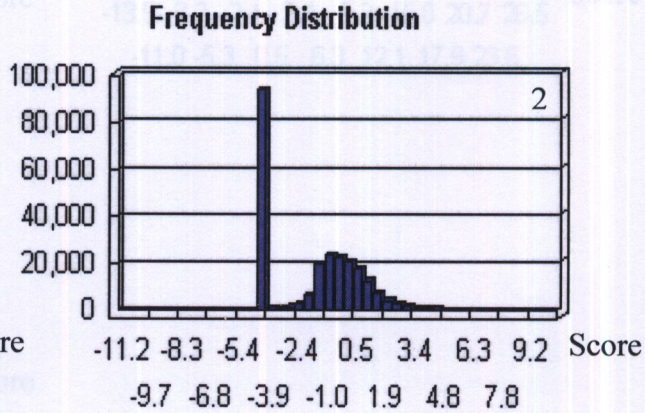

(5) Spectral and contrast texture

- Linear kernel: $C = 0.001$, 10, 100 and 1000

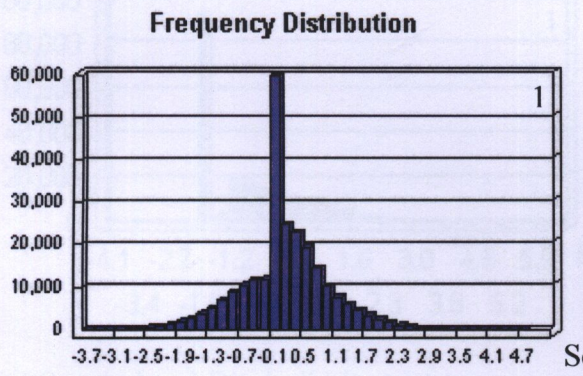

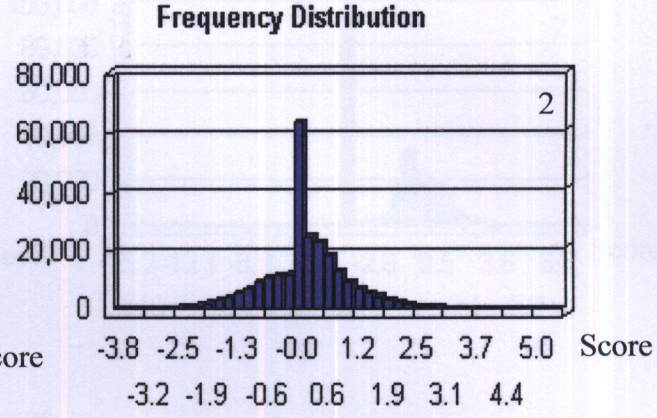

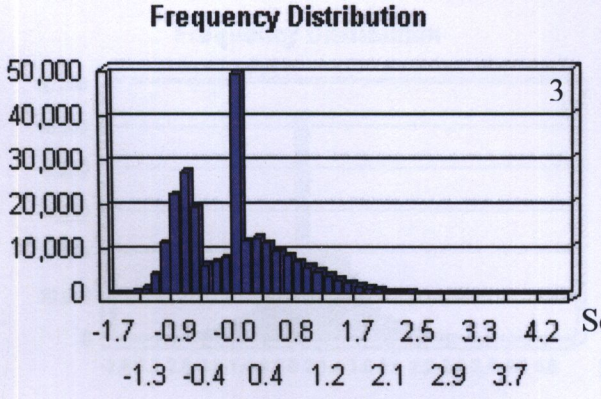

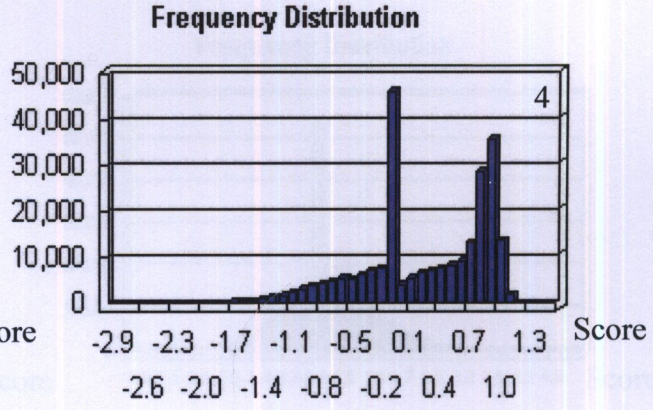

- Polynomial kernel: C =10, d= 2, 3, 4

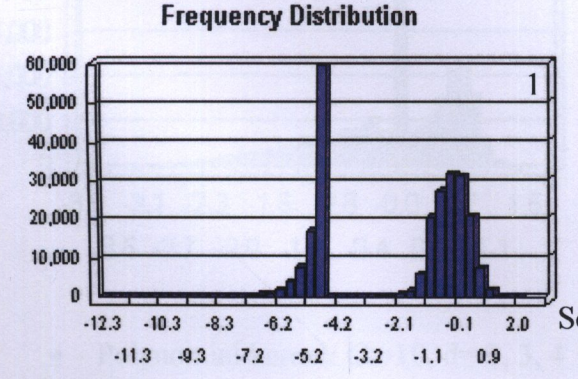

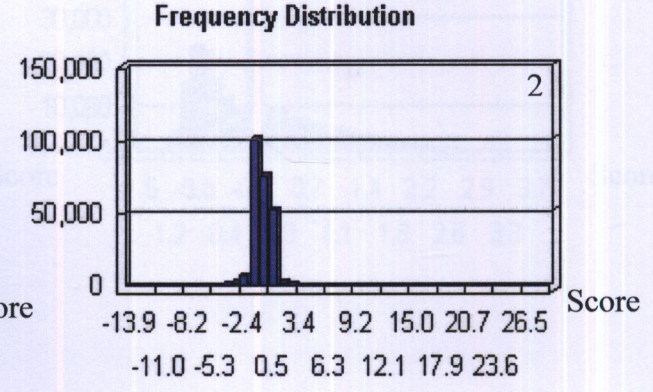

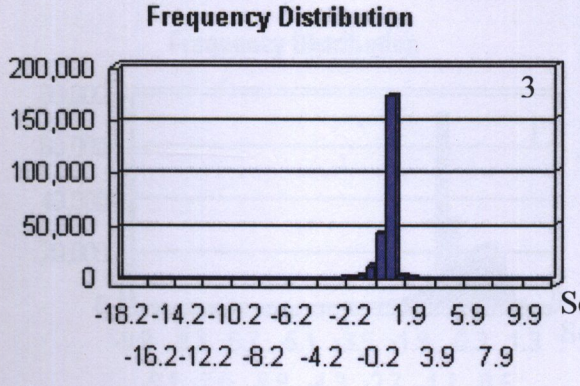

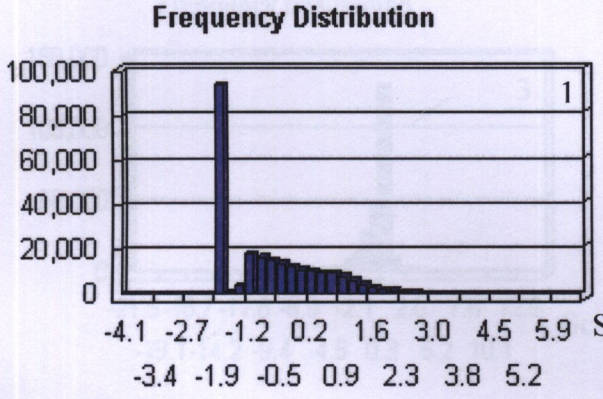

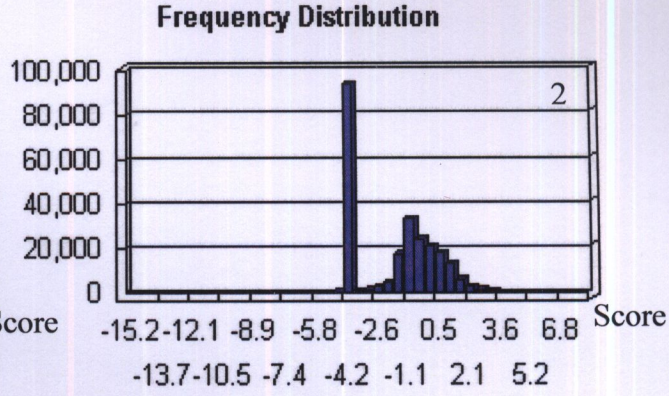

(6) Spectral and Dissimilarity texture

- Linear kernel: C = 0.001, 10, 100 and 1000

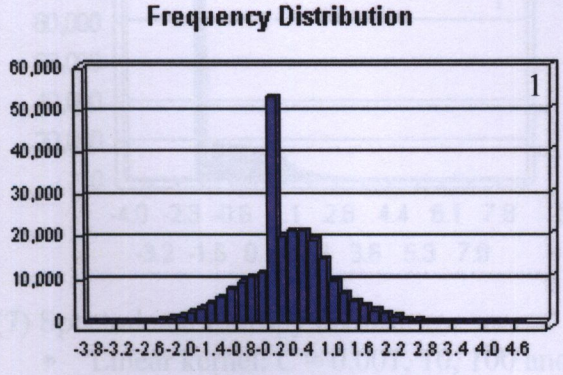

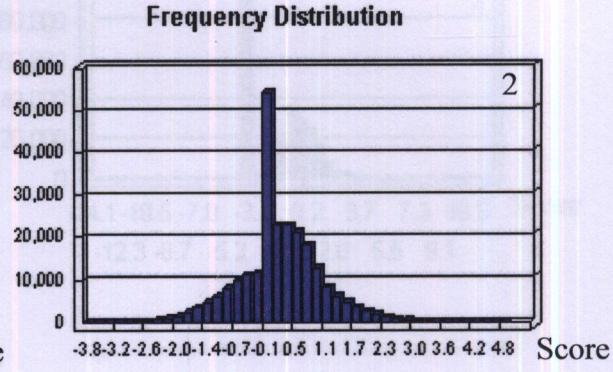

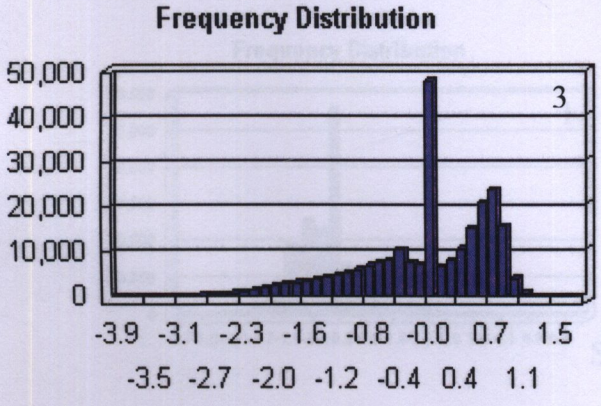

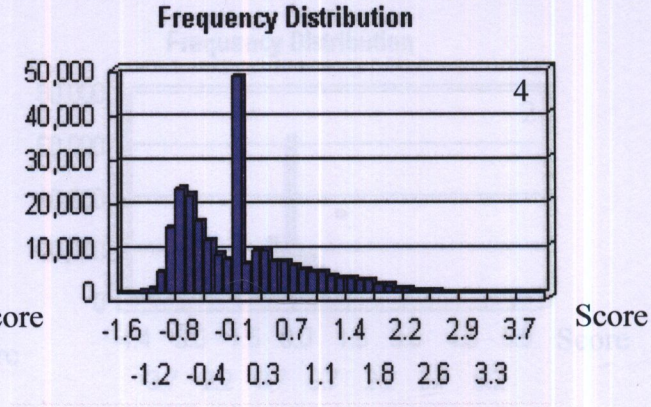

- Polynomial kernel: C =10, d= 2, 3, 4

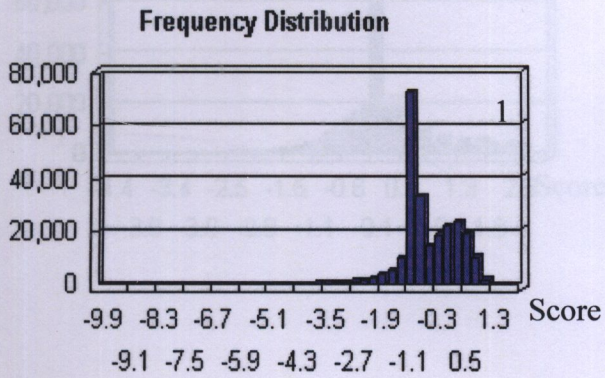

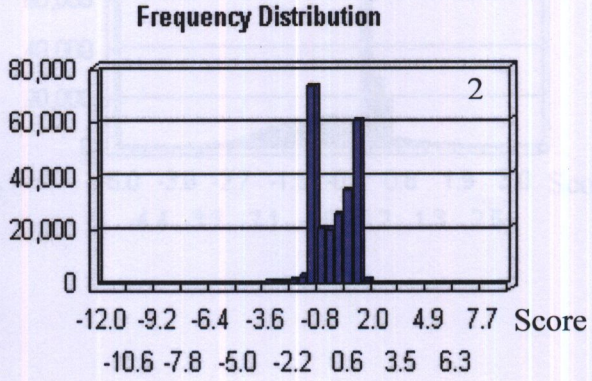

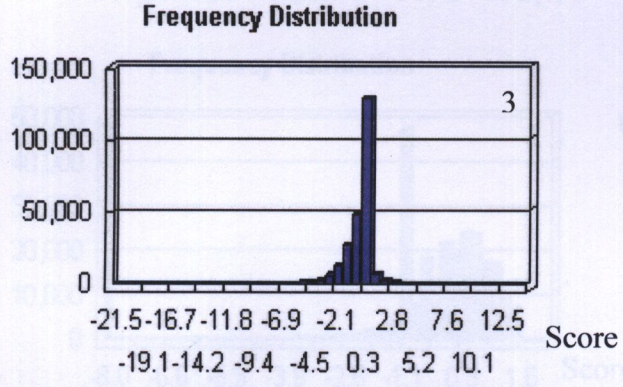

- RBF kernel γ 0.001, C =10, 100

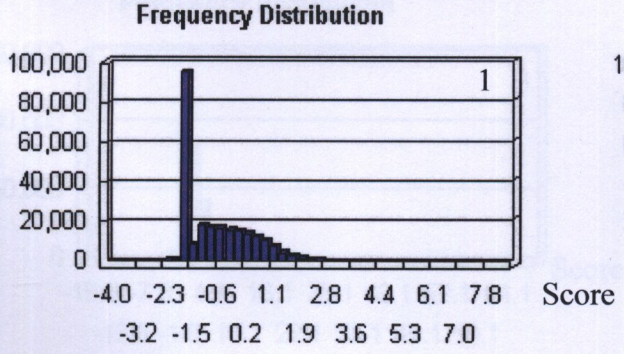

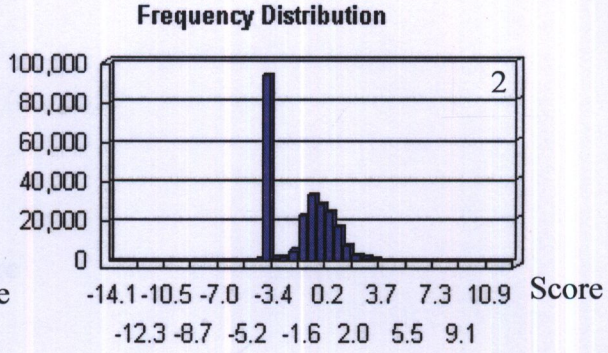

(7) Spectral and Entropy texture

- Linear kernel: C = 0.001, 10, 100 and 1000

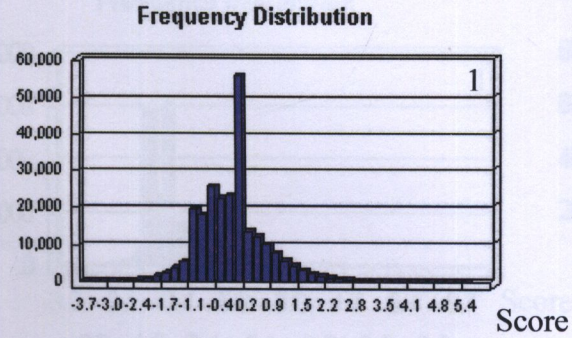

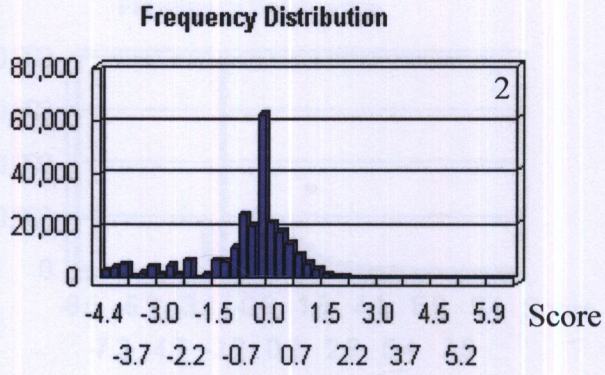

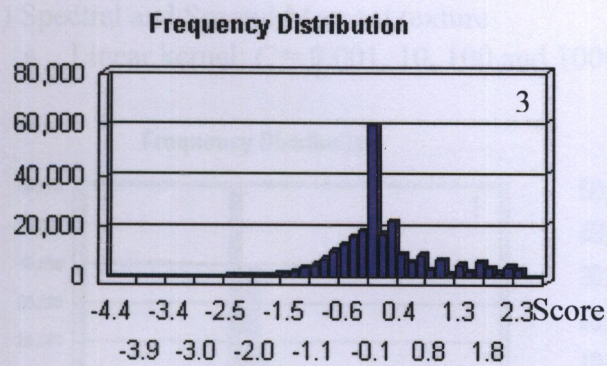

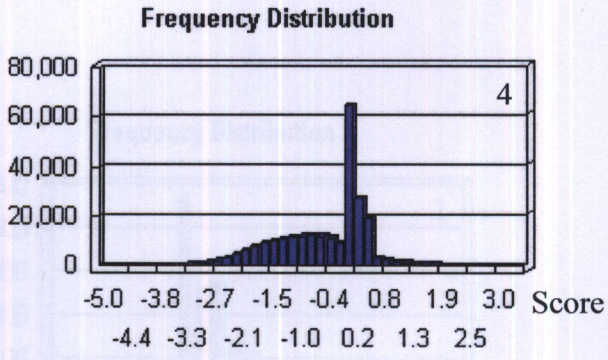

- Polynomial kernel: C =10, d= 2, 3, 4

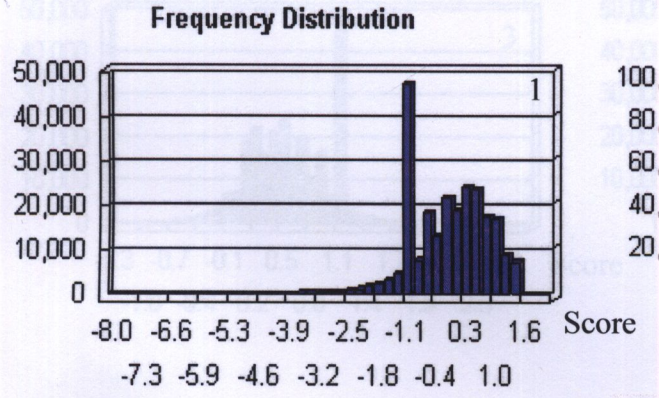

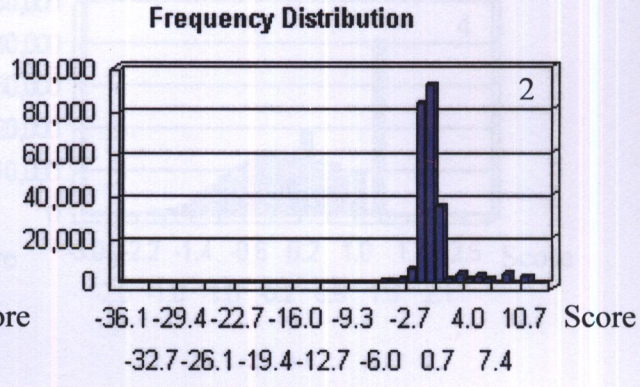

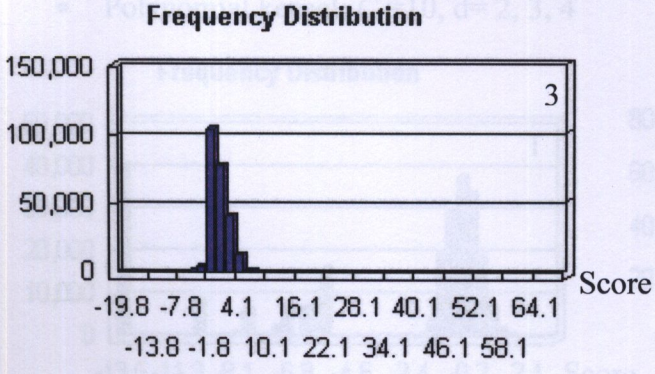

- RBF kernel γ 0.001, C =10, 100

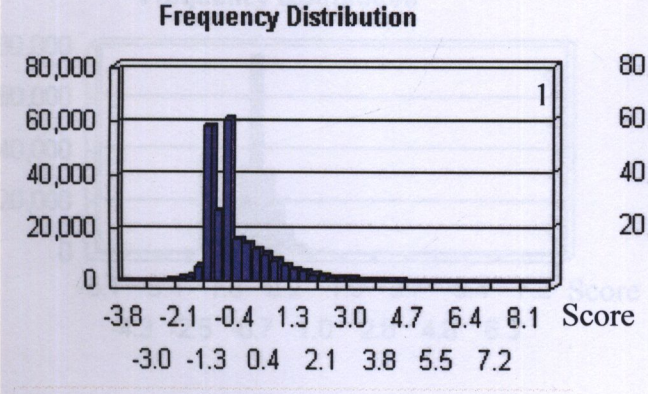

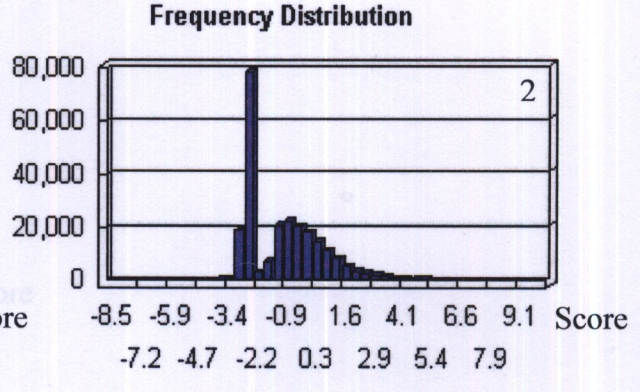

(8) Spectral and Second Moment texture

- Linear kernel: C = 0.001, 10, 100 and 1000

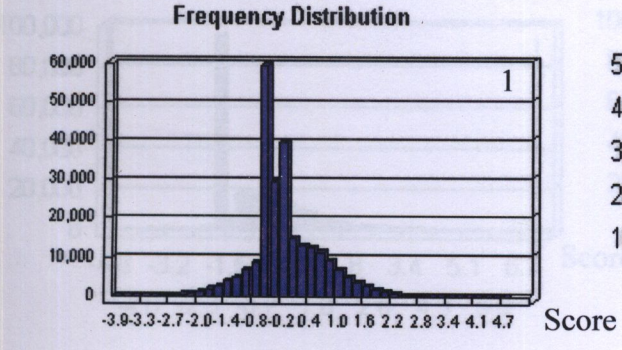

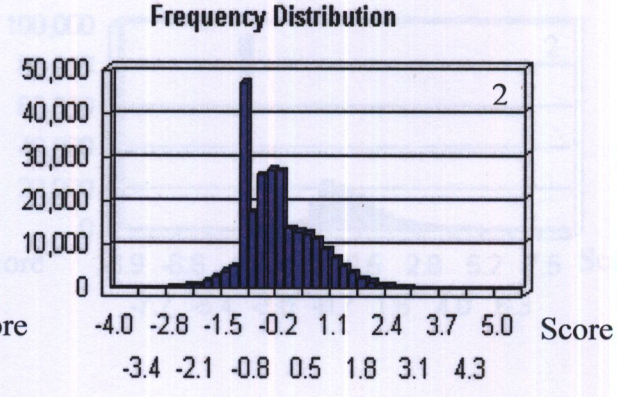

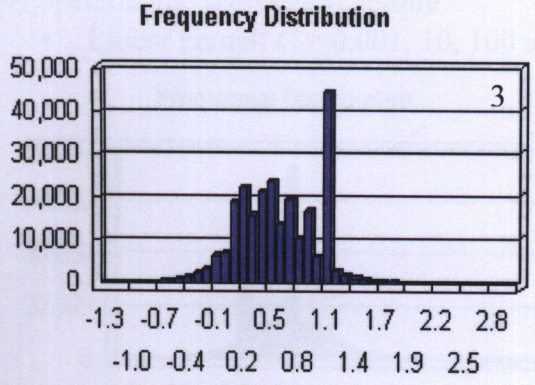

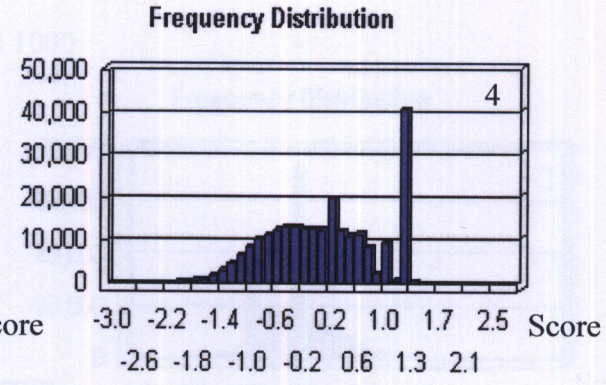

- Polynomial kernel: C =10, d= 2, 3, 4

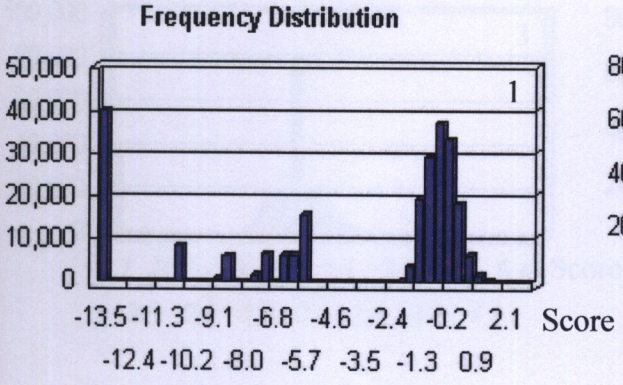

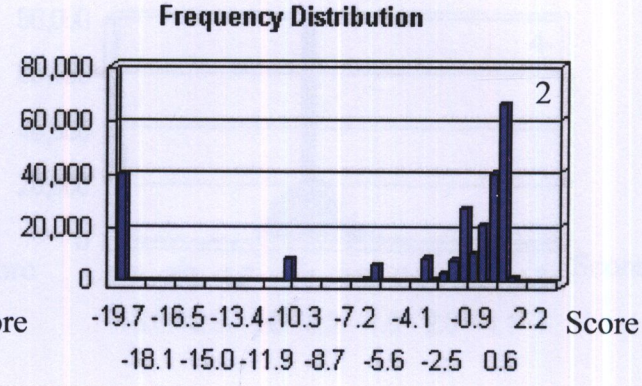

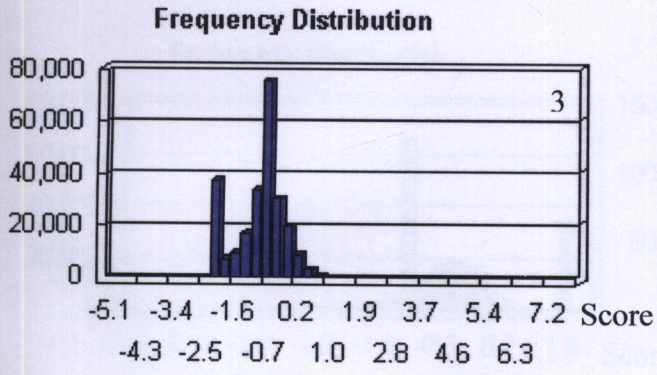

- RBF kernel γ 0.001, C =10, 100

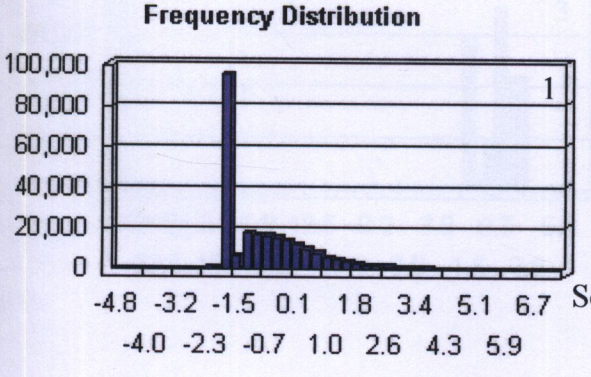

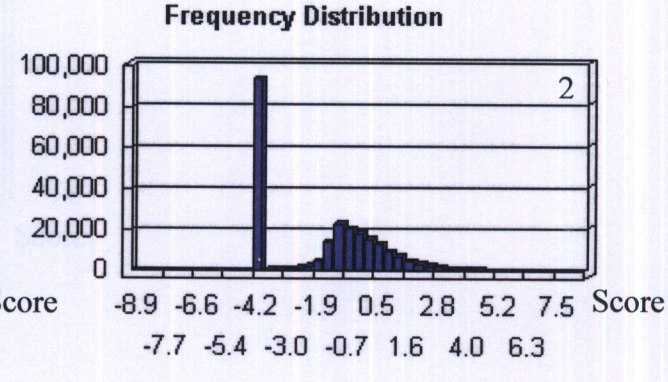

(9) Spectral and correlation texture

- Linear kernel: $C = 0.001$, 10, 100 and 1000

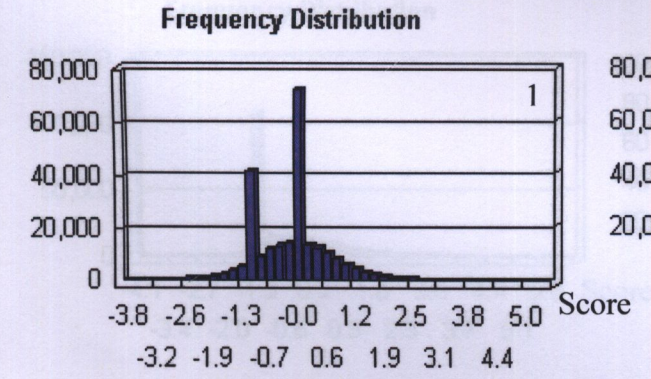

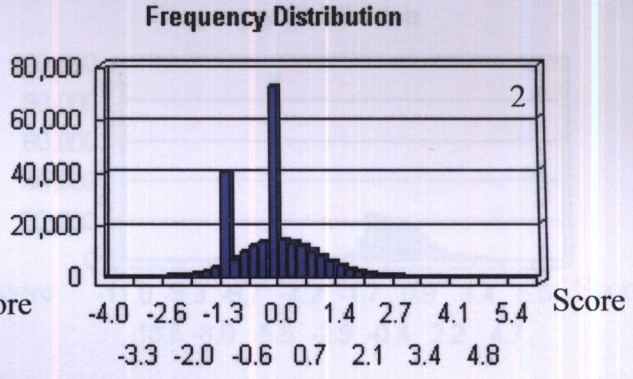

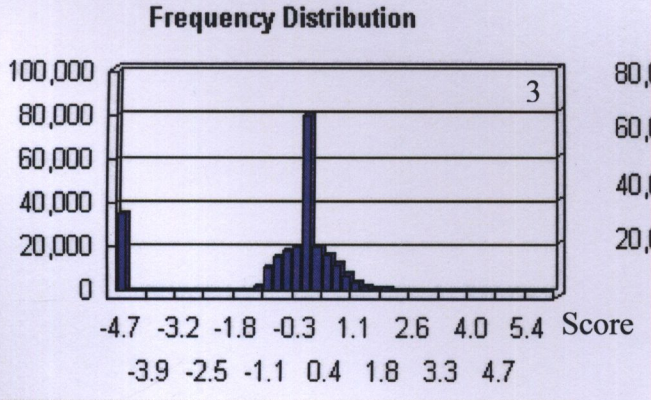

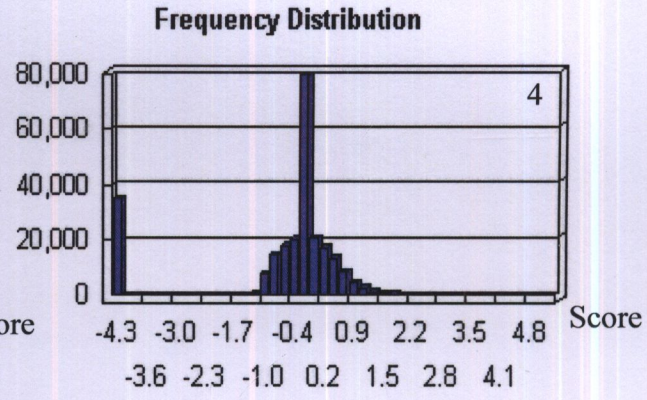

- Polynomial kernel: C =10, d= 2, 3, 4

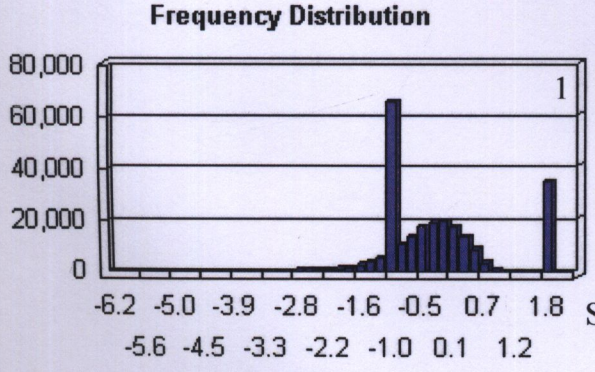

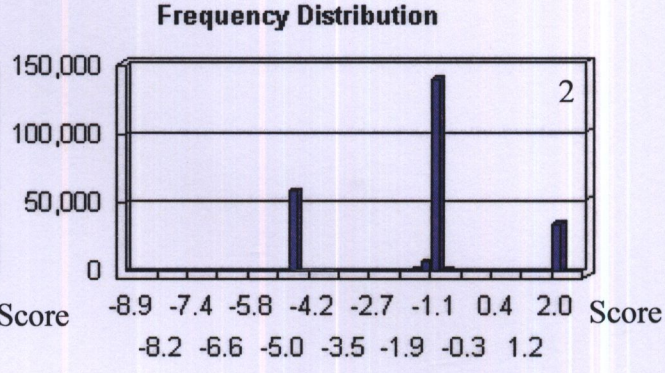

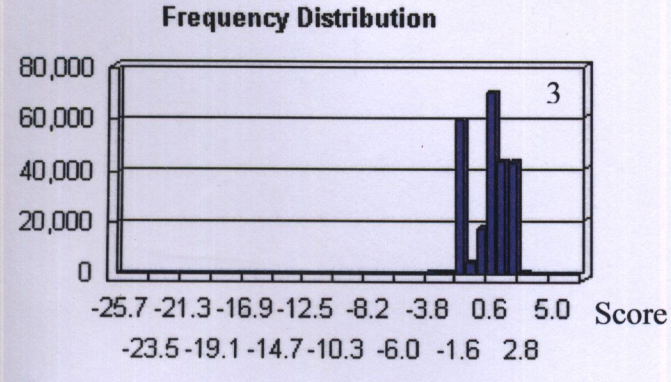

- RBF kernel γ 0.001, C =10, 100